COMPARISON OF PRECIPITATING CUMULUS CELLS:
MODEL-GENERATED VERSUS RADAR-OBSERVED

by

JUDSON EDWARD STAILEY

B.S.C.E., The Ohio State University
(1971)

SUBMITTED IN
PARTIAL FULFILLMENT
OF THE REQUIREMENTS FOR THE
DEGREE OF MASTER OF SCIENCE
at the
MASSACHUSETTS INSTITUTE OF TECHNOLOGY
May, 1978

Signature of Author...
Department of Meteorology; May 24, 1978.

Certified by...
Thesis Supervisor.

Accepted by...
Chairman, Departmental Committee
on Graduate Students.

COMPARISON OF PRECIPITATING CUMULUS CELLS: MODEL-GENERATED VERSUS RADAR-OBSERVED

by
JUDSON EDWARD STAILEY

Submitted to the Department of Meteorology on 24 May 1978
in Partial Fulfillment of the Requirements for
the Degree of Master of Science

ABSTRACT

The purpose of this study was twofold: to evaluate the ability of a circularly symmetric two-cylinder model of a precipitating cumulus cell to simulate radar-observed cells, and to ascertain to what accuracy the model input variables need to be known to obtain realistic results.

Data from GATE were employed because of their availability and coverage and because the tropical atmosphere during the experiment contained relatively little vertical wind shear. Cells organized into two types of mesoscale features, a line and a cluster, were simulated. Because of the variability observed in the cell characteristics, the mesoscale features were idealized into geometrically simple configurations of "representative" cells. The representative cells were geometrically compatible with the model and had dimensions based on the average sizes of observed cells. The size of the model inner cylinder, assumed to be the region of active convection, was estimated from the areas of observed reflectivity cores. The size of the outer cylinder, analogous to the environment of the cells, was estimated from distances between cells in the mesoscale features. This idealization process produced what appeared to be realistic dimensions.

Vertical profiles of temperature and relative humidity were also needed for initialization. A large sample of observed profiles was idealized by a method which retained the main characteristics of the profiles while smoothing the minor variations. The idealized relative humidity profiles fell into three distinct types, the distribution of which varied with the synoptic situation. Variations in the idealized temperature profiles were small and not systematic.

The effectiveness of the model in simulating observed cells was investigated by comparing observed with model cell heights, maximum reflectivities, and heights of the reflectivity maxima. When initialized appropriately, the model produced cells which appeared to be remarkably similar to observed cells. Although cell dimensions were not unimportant, the relative humidity profile exerted the greatest influence on model cell growth, Open-atmosphere humidity profiles were found to be too dry to support vigorous convection. Realistic cells were generated when the humidity was increased under the assumption that the cells were growing in a mesoscale region which was more moist than the open atmosphere. Calculations showed that convective activity could contribute to the humidification of the open atmosphere, but this contribution was not sufficient to alter the relative humidity profile to the point where realistic cells could be simulated. Further humidification via mesoscale ascent was necessary.

The need for taking into account the effects of mesoscale processes is discussed, and methods for doing so are suggested. The need for the addition of a realistic boundary layer is discussed. The further addition of a less artificial initiating impulse coupled with the structure and properties of the boundary layer is suggested.

ACKNOWLEDGEMENTS

The author would like to express his sincere gratitude to Dr. Peter Yau, who designed the model tested in this thesis, took time to acquaint the author with the model, and endorsed this study. Appreciation is also expressed to Dr. Pauline M. Austin, who supervised the research and writing of this thesis. Without her patience, encouragement, and expert advice, this thesis would not have been written.

Mr. Frank Marks and Dr. Speed Geotis made themselves available for numerous discussions related to tropical meteorology, the GATE program, and the radar data. Mr. William Silver and Mr. Alan Siggia assisted in computer programming.

The author also thanks his wife, Laura, for proofreading the thesis and for the continued love and understanding she has provided.

Finally, the author is indebted to the Air Force Institute of Technology, which made this research possible, and to Capt. Harry Hughes, program manager, for his support.

TABLE OF CONTENTS

LIST OF TABLES

LIST OF FIGURES

CHAPTER ONE

INTRODUCTION

1.1 Background

It is generally recognized that moist convection plays an important role in vertical heat and moisture transport. Through this role, it is believed to have far-reaching effects on synoptic and global circulations (see, e.g. Charney and Eliassen, 1964; Gray, 1973). These effects cannot be completely understood, however, until the nature and magnitude of cumulus transports can be determined with a reasonable degree of accuracy. Because of the small scale of cumulus cells and their complexity, it is extremely difficult to measure directly their transport of heat, moisture, and other qualities. Indirect methods of determining cumulus transports using radar data (Austin and Houze, 1973) or diagnostic studies of large-scale variables (Arakawa and Schubert, 1974) have been devised, but they provide only crude estimates.

One tool which can aid the meteorologist in investigating cumulus transports is the cumulus cell model. Cell models have been designed to serve a number of purposes (investigation of microphysical or dynamical processes, aids in weather modification experiments, etc.). Some of these models might be suitable for use in cumulus transport studies provided that they are capable of simulating observed cells with a sufficient degree of detail. Comparisons of cells generated by the more theoretically oriented models with observed cells have usually been made in the most general way, involving only the concern that the model cell resemble a (i.e. any) cumulus cell (see, e.g. Orville and Sloan, 1970, who considered the configuration of orographically induced cells). In other studies (e.g. Weinstein, 1970), in which particular observed cells were modeled, qualitative comparisons have been made between the general appearance of major features in the modeled and observed cells. The quantitative comparisons that have been made (e.g. Sax, 1969, who compared computed with observed cell heights) were not made in sufficient detail to elicit confidence in the models' ability to simulate important cumulus processes.

The main difficulty in making comparisons has stemmed from the lack of important processes or properties which could be both observed in a real cell and calculated in a model with sufficient accuracy and resolution to allow a reasonably accurate comparison. Yau (1977) has contributed to the solution of this problem by devising a microphysical parameterization which allows for the natural development of drop size spectra and thus the calculation of realistic radar reflectivities. These reflectivities can be compared with reflectivities observed within real cells by radar. Yau incorporated his microphysical parameterization into a fairly sophisticated two-cylinder model in which an inner cylinder represents a cumulus cell and a surrounding outer cylinder represents the environment of the cell. This type of formulation, while being reasonably well suited for investigating cumulus transports, requires less computation than the more complex two-dimensional models of, for example, Soong and Ogura (1976). This computational simplicity permits relatively extensive experimentation to be carried out.

1.2 Statement of Problem

In spite of the advantages of Yau's model, it is, compared to the real world, highly simplified. In order to assess its usefulness for computing vertical transports, it is desirable to determine how well it simulates real cells. Toward this objective, this study will compare cells generated by the model with cells observed by radar. A secondary objective is to determine specifically what characteristics of cells and the atmosphere in which they are occurring need to be known, and to what accuracy they need to be known, in order to achieve realistic simulations from the model.

The model will be initialized with horizontal cell dimensions estimated from radar data and with environmental temperature and relative humidity profiles determined from rawinsonde soundings. Comparisons will be made between radar reflectivities generated by the model and those observed by radar. The data will be drawn from the GARP* Atlantic Tropical Experiment (GATE). This data set was chosen for its availability and excellent coverage and because the tropical atmosphere has relatively little vertical wind shear, a property which cannot be taken into account by the axisymmetric cell model.

In Chapter 2, the model microphysics, dynamics, and general formulation are briefly described. The input variables are discussed and the results of Yau's sensitivity tests on those variables are presented. Values of input variables which will remain constant throughout this study and the rationale behind their choice will be given.

---

*Global Atmospheric Research Project

The data are discussed in Chapter 3. A brief description of GATE is given after which the sources, handling, and analysis of the data are described. The need for idealizing the data to provide "representative" cell dimensions and soundings is discussed and the idealization process is described. Methods for comparison of model-generated with radar-observed cells are presented.

Two types of situations are considered. One is a well-organized and well-developed line of convective cells, a configuration which is typical of tropical disturbances. Experiments and comparisons for this situation are presented in Chapter 4. The second type of situation, a cluster of cells which occurred during a relatively undisturbed period, is considered in Chapter 5.

Conclusions drawn from the experiments and recommendations for future use of the model are presented in Chapter 6.

CHAPTER TWO

DESCRIPTION OF MODEL

The model being evaluated in this thesis was designed by M.K. Yau (1977) to allow investigation of the interaction of dynamical and microphysical processes in precipitating cumulus clouds. In this chapter, a brief description of the important characteristics and properties of the model is given.

2.1 Microphysical Processes

The microphysical processes were designed to be a compromise between the explicit calculation of diffusional growth of drops and of stochastic collection processes and the simplified parameterization scheme proposed by Kessler (1969), in which interaction between cloud and rain is formulated on the concept of autoconversion and in which precipitation particles always assume the Marshall-Palmer distribution and fall within a single effective velocity at a given level. As in the Kessler parameterization, Yau bypassed growth of cloud droplets and diffusional growth of precipitation particles by employing an autoconversion scheme and allowing for accretion of cloud water onto precipitation particles. However, he grouped precipitation particles into ten size categories, each with a representative fall velocity, and required that autoconverted water be added only to the smallest size category. The drop-size distribution was then built through accretion of cloud and interaction between precipitation particles. The efficiency for the collection of cloud droplets by precipitation particles was assumed to by 0.8. The collection efficiency for raindrops was based on a collision efficiency of one and the coalescence efficiency given by Brazier-Smith et al. (1973). Breakup processes included were impaction (in which each collision produces a main drop and three satellite drops) and instantaneous breakup (in which drops larger than those in the largest size category spontaneously break into a number of drops distributed over a pre-determined spectrum). Finally, cloud existing in subsaturated air was assumed to evaporate instantaneously to the point of saturation. If the cloud water was insufficient to saturate the air, rain water was evaporated using the microphysical diffusion equation.

Yau tested his microphysical parameterization against the stochastic scheme, comparing the initiation of warm rain in a one-dimensional updraft. Comparisions between liquid water content and radar reflectivity at two heights in the updraft and of surface rainfall intensity showed no significant differences between the two schemes. Comparisons of the evolution of raindrop size spectra showed a few minor differences of questionable significance.

2.2 Model Formulation and Dynamics

The model was designed to employ the anelastic pressure equation (Ogura and Phillips, 1962) in such a way as to allow explicit calculation of the perturbation pressure. Geometrically, the model is composed of two concentric cylinders whose radii are constant with height and time. The inner column is the cloud region which comprises the area of active convection. Compensatory currents occur in the outer column to satisfy the requirement of continuity. Horizontally averaged equations were developed in the manner described by Asai and Kasahara (1967), in which the cloud is assumed to be axisymmetric and the properties at a given level are averaged across each cylinder. Exchange of properties between cylinders is accomplished by dynamic entrainment and detrainment (i.e. one-way advection by horizontal flow between cylinders) and turbulent entrainment, a two-way exchange of properties, which is a function of the difference of those properties and the difference of the vertical motion across the interface. Aside from this type of turbulent exchange, vertical and horizontal eddy fluxes are neglected. Boundary conditions specify no flow through the top or bottom of the cylinders or through the outer vertical boundary of the outer cylinder. The outer cylinder thus becomes the "environment" and is isolated from interactions with larger scale effects.

The model uses specifications of initial temperature and relative humidity versus height to define a pressure-versus-height profile which results in a hydrostatic atmosphere. Convection is then initiated by imposing a vertical velocity and moisture impulse on the bottom of the inner cylinder. The velocity impulse takes the form of a $\sin^2$ function of height while the moisture impulse saturates part or all of the region of velocity impulse.

2.3 Model Input Variables

The model allows the specification of a number of variables of meteorological and numerical significance in order to simulate cells under different conditions and handle the calculations in an appropriate way. The meteorological variables specify the size of the cell, the characteristics of the atmosphere in which it is occurring, the nature of the initiating impulse, and a microphysical property related to the conversion of cloud water to precipitation. The numerical variables deal with the numerical space and time resolution, the precision of calculations, and the time limit of integration. In this section, the variables will be described, their significance will be discussed, the results of Yau's sensitivity tests on them will be summarized, and, when possible, the values to be used in this study and the reason for their choice will be given.

2.3.1 Meteorological Variables

The first set of meteorological variables, specifying the size of the cell to be modeled and the size of its environment, includes the radius of the inner cylinder and the ratio of the inner to outer cylinder radii. The radius of the inner cylinder defines the area of the initiating updraft and hence the region of active convection. The ratio of the inner to outer cylinder radii (designated σ) defines the radius of the outer cylinder given the radius of the inner cylinder. According to the dynamics of the model, changes in the inner cylinder radius (without changing σ) affect the strength of the perturbation pressure force and the entrainment process. Both the dynamic and turbulent entrainment bear an inverse relation to the inner radius. The perturbation pressure force, on the other hand, increases as the radius of the inner cylinder increases. Yau conducted experiments using inner cylinder radii of 1.0, 1.5, and 2.0 km. The vigor of the cell increased dramatically as the radius was increased from 1.0 to 1.5 km, but more slowly as the radius was further increased to 2.0 km. These results seem to indicate that entrainment is an important dissipative process for the smaller cells while the pressure force takes on more importance in the larger cells. The ratio of the radii defines the ratio of the areas of the cylinders. This ratio plays an important role in the averaging of properties over the cylinders and in continuity considerations. Proceeding on the hypothesis of Asai and Kasahara (1967) that convection will maximize vertical heat transport, Yau calculated vertical heat transports for reasonable combinations of the inner cylinder radius and the lapse rate while varying σ. The results indicated that σ should be between 0.3 and 0.4 (depending on the situation) to maximize vertical heat transport. In all his experiments except one, Yau used a σ of 0.32. The test case used a σ of 0.16 and yielded a much stronger cell. The reasons for this are as follows. Continuity requires that the updraft that occurs in the inner cylinder during the development of the cell be compensated by a downdraft in the outer cylinder. Because the area of the outer cylinder is smaller for the larger σ, the compensatory downdraft must be stronger. This affects the growth of the cell in two ways. First, the mixing of downward momentum by entrainment reduces the strength of the updraft and hence the rate of condensation. Secondly, adiabatic warming and drying of the air in the outer cylinder and its subsequent mixing inside the cloud reduces the amount of vapor that can be condensed. The result is a weaker updraft and less condensation for a larger σ. In this study, the values of the inner cylinder radius and σ will be based on radar data.

The second set of meteorological variables describes the atmosphere in which the convection is taking place. The height of the model is specified in such a way that the top of the model, where vertical motion is constrained to cease, provides as little interference as possible with the growth of the cell. This depends, of course, on the nature of the cell being modeled, but for cells which are not expected to penetrate the tropopause it is reasonable to place the top of the model near the tropopause. Yau used 15 km for the model height in his tests and did not test the model's sensitivity to this variable (probably because none of his cells reached over 10 km in height). This study will also use 15 km for the model height since that is the approximate height of the tropopause and since no cells were observed to reach that height in the situations being tested.

The model allows the assumption of an idealized atmosphere or the input of an observed atmosphere. For an idealized atmosphere, the vertical profiles of temperature and relative humidity are constructed from given lapse rates. Describing an actual atmosphere requires designating a surface pressure and temperature and relative humidities at 500 m increments from the surface to 15 km. The sensitivity of the model to these variables is rather obvious -- stronger lapse rates and higher relative humidities result in more vigorous cells. In this study, the surface pressure will be determined from nearby surface observations and the vertical profiles of temperature and relative humidity will be determined from observed soundings.

The third set of meteorological variables describes the initiating impulse. These variables are the height of the impulse, the strength of the velocity impulse, and the degree of saturation of the impulse. The velocity profile in the impulse is given by $w = w_0 \sin^2 (\frac{\pi Z}{H_0})$ for $Z \leq H_0$, where H_0 is the height of the impulse and w_0 is its maximum. Yau used an H_0 of 2 km in all his experiments and got reasonable results. Since this impulse scheme is rather artificial, no attempt will be made to determine a more appropriate height. Yau used a w_0 of 1 m sec^{-1} in all his experiments except one, in which 0.2 m sec^{-1} was used. The resulting cell in the test case was nearly identical to the "control" storm except that it took slightly longer (about 5 minutes) to develop. Since timing is not critical in this study (indeed, the time interval at which radar data were available makes such a time lag insignificant), a w_0 of 1 m sec^{-1} will be used. The impulse may be saturated over its entire height or only above the cloud base. Yau did not test these alternatives in his thesis. He did, however, test a cell saturated above the cloud base against a cell with no humidity impulse. The development of the latter cell was delayed, but otherwise it did not differ significantly from the cell saturated above the cloud base. Since timing is not important, this study will use an impulse which is saturated over its entire depth.

The last meteorological variable is the autoconversion threshold. When the amount of cloud water exceeds this value, autoconversion takes place. Yau tested autoconversion thresholds for cloud water mixing ratios between 0.0 and 0.001 in a kinematic updraft and compared rainfall intensity as a function of time. This test demonstrated that precipitation was relatively insensitive to changes in autoconversion threshold. For simplicity, Yau used 0.001 g g^{-1} in his study. The same value will be used here.

2.3.2 Numerical Variables

The first numerical variable prescribes the vertical resolution of the model. The gridpoints in a 15 km high model may be 500 m or 250 m apart. Yau used 250 m in all his experiments except one, in which he used 500 m. This test showed that the larger grid spacing slightly decreased the amplitude of most cloud variables. Since the decrease was not significant, a grid spacing of 500 m will be used in this study to save computation time.

The second numerical variable prescribes the time step. Yau used 10 seconds in all his experiments except two, in which he tested 5 sec and 20 sec. The results demonstrated that the model is not sensitive to changes in the time step within this range. A time step of 20 sec will be used here to save computation time.

The third numerical variable prescribes the number of Fourier modes used in calculating the perturbation pressure. Yau used ten modes in all experiments except one, in which he tested twenty modes and found no significant change. Again, to save time, this study will use ten modes.

The last numerical variable prescribes the time of integration. This should be long enough to allow the cell to complete most of its life cycle, but not so long as to waste computation time. Experience from Yau's experiments and general knowledge of thunderstorms indicate that an hour should be a sufficiently long time to integrate the model.

2.4 Model Output Variables

A myriad of quantities related to dynamic, thermodynamic, and microphysical processes may be output for each model level at given times during the course of the integration. The output variables used for comparing model cells to observed cells will be discussed in Chapter Three.

CHAPTER THREE

SOURCES OF DATA AND METHODS OF ANALYSIS

3.1 The Source of the Data

In order to make the type of comparison attempted in this thesis, a reasonably complete data set -- composed of surface, upper air, and radar observations -- was needed. Routine operational data would not have provided the needed detail; a comprehensive data set from a special research project was required. Such a data set was available from the GARP Atlantic Tropical Experiment (GATE). GATE was conducted in the equatorial region from West Africa to the western Atlantic Ocean during the summer of 1974. To meet the general objective of investigating the mechanisms by which tropical heating drives the global circulation of the atmosphere, 70 nations participated, providing 40 ships, 13 aircraft, and several satellites to serve as observational platforms. Meteorological phenomena were investigated on a number of scales from synoptic to cumulus. The scale of greatest interest in this thesis is the "cloud-cluster" scale, referred to as the B-scale, which encompassed a range of 10^2 to 10^3 km. Data for investigating phenomena of the cloud-cluster scale were gathered primarily by an array of seven ships, referred to as the B-scale array. In this array, centered at 8.5°N, 23.5°W, the seven ships formed a hexagon with one ship in the center (see Figure 3.1). A variety of surface and oceanic data was recorded at each of the ships and sondes were released every three hours (1-1/2 hours in especially interesting situations). Four of the ships carried quantitative weather radars with digital recording systems.

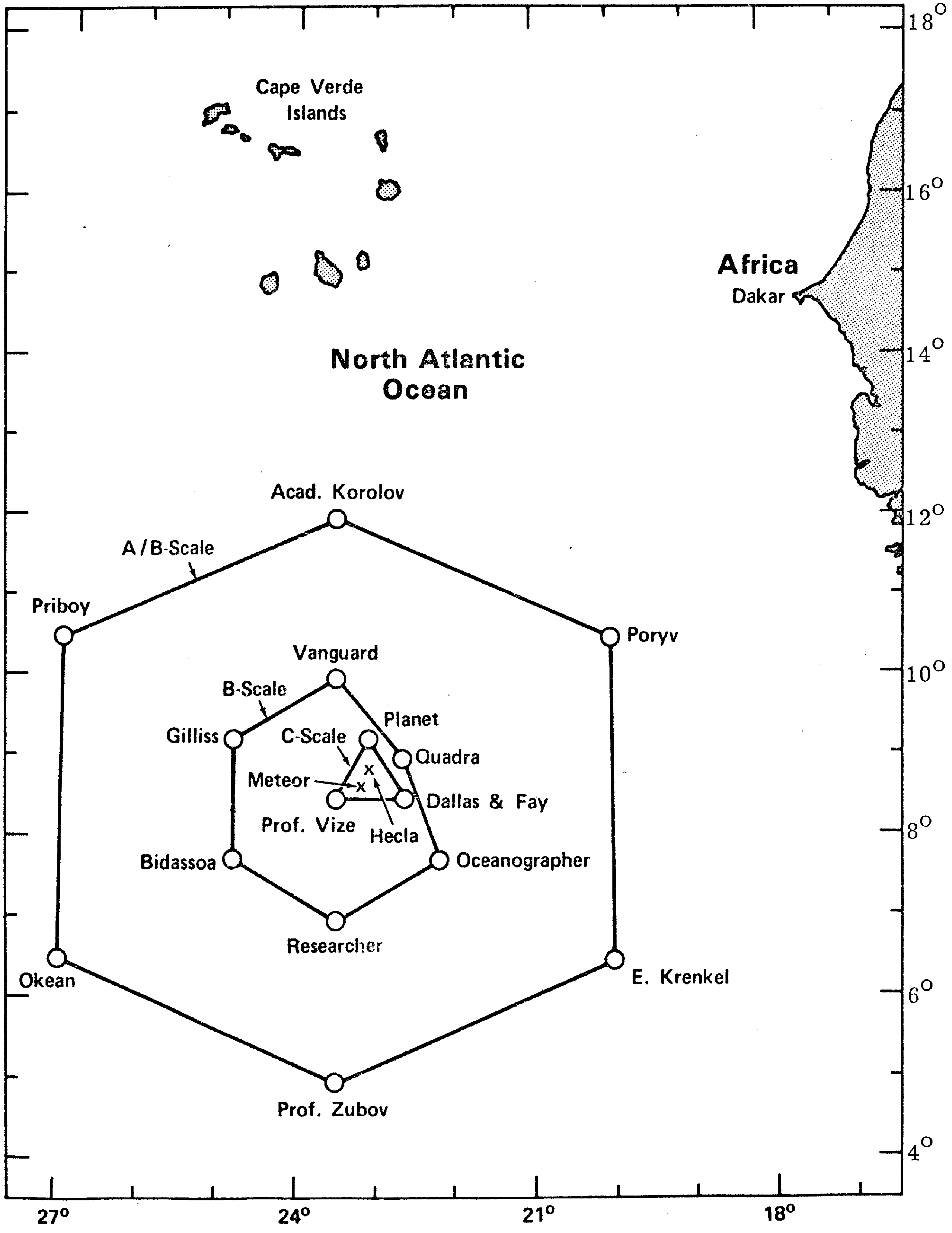

Figure 3.1. The GATE ship arrays during Phase III. The inner hexagon is the B-scale array.

The experiment was composed of three 21-day observational phases. Data from the third phase, which took place in September, were used in this thesis. A more complete description of GATE is available in Kuettner _et al_. (1974).

3.2 Analysis of Synoptic-Scale Data

Detailed analysis of the synoptic-scale phenomena in which the cells being modeled occurred is beyond the scope of this thesis. It is sufficient to categorize the general synoptic conditions under which the cells occurred. Reed _et al_. (1977) developed a useful categorization scheme by applying composite analysis techniques to the eight wave disturbances that crossed western Africa and the eastern Atlantic during phase III and the preceding interphase period of GATE (23 August - 19 September). They divided each of these easterly waves into eight north-south bands (see Figure 3.2). The second band was centered on the region of maximum northerly wind component west of the trough; the fourth, on the trough; the sixth, on the region of maximum southerly wind component east of the trough; and the eighth, on the following ridge. Bands 1, 3, 5, and 7 occupied intermediate positions. The positions were based on the 700-mb flow along the path of the wave disturbance center (defined as the position of the maximum vorticity). Reed _et al_. referred to these bands as categories or phases, but in this thesis they will be referred to as sectors. The sectors were divided into seven east-west rows, 4° of latitude deep with the center of the disturbance at the midpoint of the middle row. Figure 3.2 shows how this process was accomplished for one of the waves.

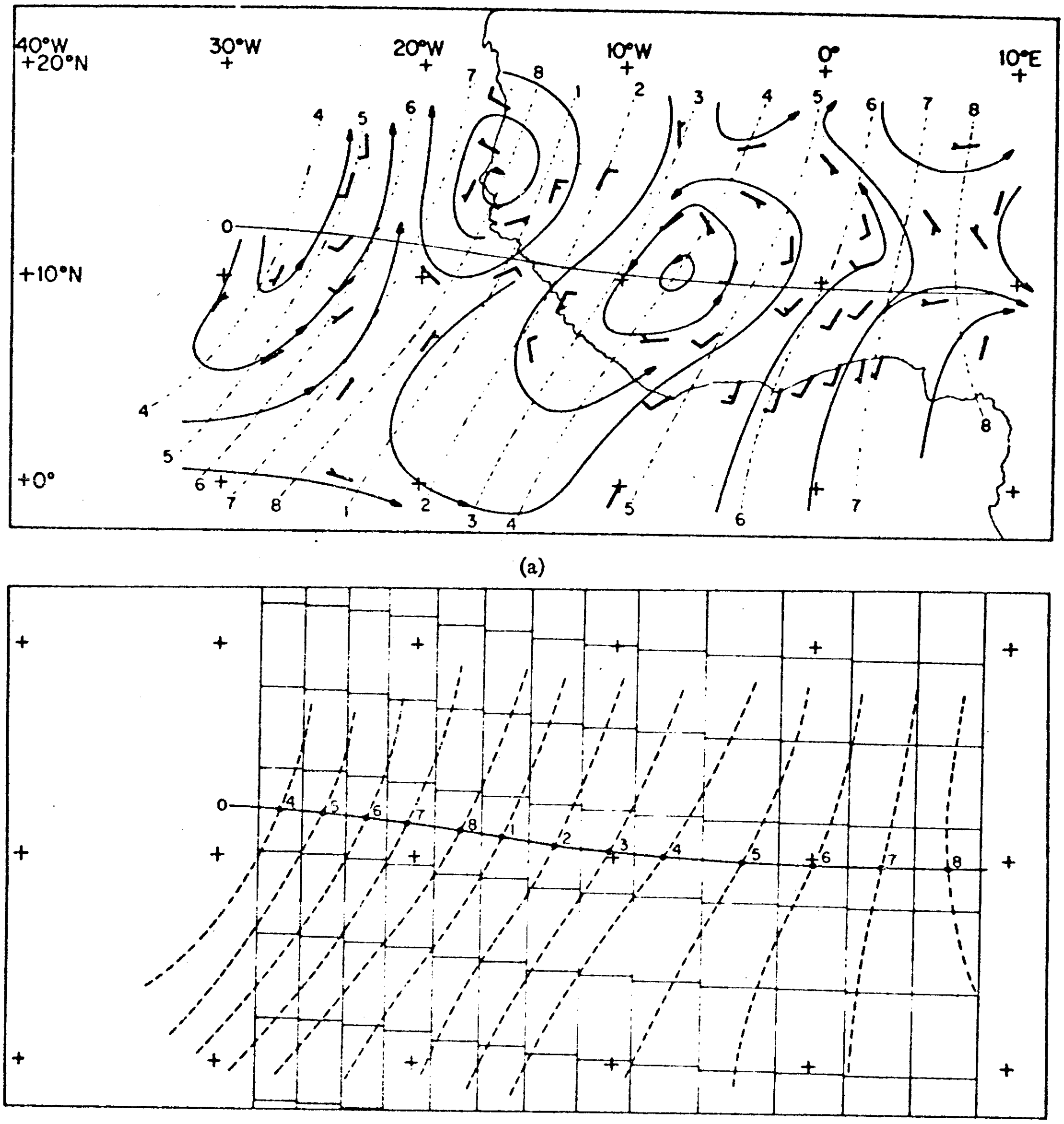

(a)

(b)

Figure 3. 2. Illustration of a GATE wave and its division into sectors. The streamline analysis in (a) was accomplished on filtered 700-mb winds. Orientation of the features defining the sectors is shown as slanting, dashed lines. The sectors are oriented N-S as shown in (b), centered on the points where the defining features cross the path of the disturbance center, the E-W line marked with a zero. (from Reed, et. al., 1977)

The streamline analysis was based on winds which had been band-pass filtered to reduce waves of shorter than two days and longer than six days to less than half-amplitude, while retaining almost fully waves of three to four day period. The east-west line marked with a zero delineates the path of the disturbance center. Each wave was divided into 56 boxes in the manner shown and the observations were averaged in each box to produce the composite wave.

Reed and his colleagues found that the waves propagated westward at an average speed of 8 m sec^{-1} in the zone of cyclonic shear to the south of the 700-mb easterly jet. The mean latitude of the disturbance paths was 12°N, the mean wavelength was about 2500 km, and the mean period was about 3.5 days. The maximum low-level convergence and upward vertical motion occurred just ahead of the trough. The maximum cloudiness and precipitation was found just south of the disturbance center in sectors 2 and 3 near the position of maximum convergence and upward motion.

The paths of the centers of the disturbance were at a fairly constant latitude. Thus, the B-scale array was usually located in the row of boxes immediately south of the row in which the disturbance paths were centered. Since the waves were usually tilted on NE-SW axes, the wave features generally passed over the array a few hours before the wave sector indicated that they did (e.g. the troughs usually passed over the array a few hours before the array was located at the midpoint of wave sector 4). This effect may be seen in the wave depicted in Figure 3.2.

The wave sectors discussed in this section will be referred to in Chapters 4 and 5 in order to describe the general synoptic situations under which the cells being modeled occurred.

3.3 Radar Data

3.3.1 Source

The general approach to the collection of radar data during GATE is described by Hudlow (1975). The radar data used in this thesis were collected with the WR73 radar belonging to the M.I.T. Weather Radar Research Project. This 5.7-cm radar was located aboard the Gilliss, one of the ships in the B-scale array (see Figure 3.1). The radar generally sampled once every 15 minutes, occasionally less often when significant convection was not present. Each sampling was an elevation step sequence in which 360° of azimuth were scanned at a number of elevation angles. This provided three-dimensional data for constant altitude displays, vertical cross-sections, etc. Weather echoes were averaged to eliminate frequency fluctuations, range-normalized, and recorded digitally in 512 range bins along each azimuth. The range bins were set up to cover the 256 km range of the radar in such a way as to provide finer range resolution near the radar. This method gave the reflectivity data finer resolution where they were more reliable and made the range resolution more consistent with the vertical and azimuthal resolutions. A complete description of the processed radar data from the Gilliss may be found in Austin (1976).

3.3.2 Handling

Most of the analysis of radar data in this study involved the use of three-dimensional (3-D) radar maps. These maps were constructed from the polar data described in the previous section by superimposing a three-dimensional rectangular box over the area of interest, dividing that box horizontally and vertically into a grid of smaller boxes, and averaging the reflectivity data observed within each small box. The result was a "stack" of constant-altitude plan position indicator (CAPPI) maps, each of which was a horizontal cut through the region at a given level showing equivalent radar reflectivity factor (Z) in dBZ organized on a cartesian plane. Figure 3.3 is an example of a CAPPI radar map. The horizontal resolution of the CAPPI's was 1 km for both the line considered in Chapter 4 and the cluster considered in Chapter 5. The 3-D radar maps for the line were composed of seven layers, each 2 km deep, so that the maps covered a vertical depth of 14 km. The 3-D maps for the cluster had a vertical resolution of 1 km and were composed of from seven to ten layers.

Maximum-tops radar charts were used to compare model cells to observed cells. These "max-tops" charts were generated by determining geometrically the maximum height at which precipitation was detected above each cartesian grid box. This was accomplished by searching through polar data from progressively higher elevation angles. The max-tops charts for the line had a horizontal resolution of 4 km while the charts for the cluster had a 2-km resolution. The tops in both sets of charts were recorded to the nearest kilometer.

3.3.3 Analysis

[NOTE ON TERMINOLOGY: In this thesis the terms updraft and downdraft, when applied to the model, will refer to the inner and outer cylinders, respectively, of the model. When applied to radar data, the term updraft will refer to the intense reflectivity core of a cell wherein active convection is presumed to be taking place and will be understood

```
                                                Block 815 IV
                                                  MIT GATE  5 Sept 1974 (248)

  ·  ·  ·  ·  ·  ·  ·  ·  ·  ·  ·  ·  ·  ·  · 27    41 36 24 24 25 18 15 19 15 20 18
  ·  ·  ·  ·  ·  ·  ·  ·  ·  ·  ·  ·  ·  ·  · 18 34 30 42 39 22 16 11 11 15 18    17
     ·  ·  ·  ·  ·  ·  ·  ·  ·  8  7  ·  · 16    22 26 40    39 18  ·    16 15 19 23
  ·  ·  ·  ·  ·  ·  ·  ·  · 13 17 12  ·  ·  9 23 26 29 23 44 37 27 11     ·    19 21
  ·  ·  ·  ·  ·  ·  ·  ·  · 13 19 24  9  ·  · 20 24 24  · 22 43 20     ·  · 16 19 23
  ·  ·  ·  ·  ·  ·  ·     ·  6 18 19 21  7  · 24 23 29 21 15 44 41 12  ·  · 16 18 23
  ·  ·  ·  ·  ·  ·  ·  ·  ·  · 11 18 15 19  7  · 28 29 27 26 26 16 27  ·  · 13 22 16
  ·  ·  ·  ·  ·  ·  ·  ·  ·  ·  8 11 15 12  · 13 16 31    33 33 35 12  ·    17 24 22
  2  ·  ·  ·  ·  ·  ·  ·  ·  ·  ·  6 14 12 18 15 19 34 34 37 34    19 13 18 21 23 22
  1  ·  ·  ·  ·  ·  ·  ·  ·  ·  ·  · 13 12 15 21 26 37 38 39 33 21  · 17    23 24 21
  ·  ·  ·  ·  ·  ·  ·  ·  ·  ·  ·  ·  9  9    15 25 37 39 35 30    14 19 21 23 25 26
  ·  ·  ·  ·  ·  ·  ·  ·  · 10  ·  ·  7 10 11 16 23 35 42 36 26 21 18 20    24 23 28
  ·  ·  ·  ·  ·  ·  ·  ·  ·  · 10  ·  8  9  8  9 12 30 42 36 31 31 21 20 22 22 24 25
  ·  ·  ·  ·  ·  ·  ·  ·  ·  ·  5  ·  ·  9  5  ·    33 35 39 25 22 23 24    23    22
  ·  ·  ·  ·  ·  ·  ·  ·  ·  ·  ·  7  5  ·  7  ·  · 15 36 32 26 23 24 25 24 22 23 22
  ·  ·  ·  ·  ·  ·  ·  ·  ·  ·  4  6  7 16 23 12  ·  · 18 38 31 25 25 23 20 22 15 23
  ·  ·  ·  ·  ·  ·  ·  ·  ·  ·  ·  3 12 20 27 36 24  · 19 35 30 25 26 24 17 17 24 25
  ·  ·  ·  ·  ·  ·  ·  ·  ·  ·  ·  ·  3 24 34 37 31  ·  9 14 23 25 23 21 13 21 28 27
  2  ·  ·  ·  ·  3  ·  ·  ·  ·  ·  · 14 30 37 39 37 25     9 12 21 23 16  ·  · 28 33
  ·  ·  ·  ·  3  ·  ·  ·  ·  ·  ·  · 14 33 41 42 34 20  ·  7 15 13 20 19 17 20 28 33
  ·  ·  3  ·  ·  ·  ·  ·  ·  ·  ·  · 31 36 42 42 44 40 38  · 15 13 17 19 17 21 26 33
  ·  2  3  ·  2  ·  ·  ·  ·  ·  ·  ·  · 32 39 41 41 44 40 12 16 18 18 19 22 22 26 24
  1  ·  2  ·  1  ·  ·  ·  ·  ·  · 12 12 21 33 36 38 30 15 14 20 24 21 16 17 23 21 28
  4  ·  ·  ·  ·  ·  ·  ·  4  ·  9 18 15 18 13 36 42 32 14  · 16 19 21 15 16 19 19 25
  3  ·  ·  ·  ·  ·  ·  ·  ·  ·  ·  5  7 14 18 41 47 22  ·  · 15 18 19 15 14 16 18 21
  5  ·     ·  2  ·  ·  ·  ·  ·  ·  · 22 20 22 29 47 11  ·  · 12 12 16 14 12 16 19 20
 12  5  ·     ·  ·  7  ·  ·  ·  · 17 22 33 32 19 39 16  ·  ·  ·  ·  8 13  9 13 18 20
 13  7  3  3     ·  9  ·  ·  ·  ·  6 32 27 35 37 29 12  ·  ·  ·  ·  ·  ·  · 12 23 28
 13 12 10 11 11     4 11  7  ·  · 12 35 33 39 38 35 18  ·  ·  ·  ·  ·  ·  · 18 28 29
 17 15 13 18 12  8  6 11 10  ·  ·  2 28 29 37 38 35 28  ·  ·  ·  ·  ·  ·  · 23 26 29
 20 15 14 16 13 11  7 13 13  ·  ·  2  3 17 23 34 35 25  ·  ·  ·  ·  ·  9 11 21 29 27
 21 17 20 20 24 23 14 30 14 11 14 15 13 19 37 33 31 20  ·  6  4  ·  4 10 17 24 24 27

Cursor position
Lat= 9.39 N, Lon=24.66 W, slice(#  7)=   0.0-   2.0 km
```

Figure 3.3. Example of a CAPPI radar map. This map shows part of the line considered in Chapter 4. The reflectivities, given in dBZ for 1X1 km grid points, were determined by averaging over the layer from 0-2 km. The 3-D map from which this CAPPI was made extended to a height of 14 km and was composed of seven of these CAPPIs.

to be analogous to the inner cylinder of the model. The term downdraft, when applied to radar data, will refer to the region surrounding the active convection wherein compensatory vertical motions are taking place, and will be understood to be analogous to the outer cylinder of the model. These terms will be used to describe regions, not vertical motions, with full awareness of the fact that descent may sometimes occur in the "updraft" and ascent may sometimes occur in the "downdraft".]

It was necessary during the course of this study to inspect an area or line of convective activity to identify individual cells and determine the size of their updrafts. The precipitation in these areas and lines was nearly always spatially continuous. Thus, it was difficult to determine the boundaries between cells. Since the nature of the model requires that each cell be a separate entity, cells and updrafts had to be defined in such a way that individual cells would be separated from each other.

CAPPI radar maps, similar to the example in Figure 3.3, were used to identify cells and determine their updraft areas. If one assumes that a peak reflecticity marks the center of a cell, a reasonable way to determine the extent of its updraft is to search outward from the peak until a sudden, strong decrease, say 3 dB (representing a reduction by half), in the reflectivity is encountered. This point would mark the outer edge of the updraft. Unfortunately, such a sharp reflectivity gradient was often absent from the data, and, when present, often delineated unrealistically large updrafts. In order to avoid these problems, it was necessary to adopt somewhat less logical but more broadly applicable rules for defining the limits of an updraft. To separate cores of maximum reflectivity into individual cells, it was assumed that the reflectivity between cells must at some point be less than or equal to half the maximum reflectivity. Thus, a reflectivity core was identified as a cell if its point of maximum reflectivity could not be connected to any other cell without crossing a point where the reflectivity was three or more decibels less than its (own) maximum. This left some flexibility in defining the extent of the updraft. The updraft area could have been defined as the area covered by data points containing the maximum reflectivity. However, the sampling problems inherent in radar observations and in transposing from polar to cartesian coordinates made the use of such a restrictive definition unwise. Instead, the two remaining possibilities for the definition of an updraft were used. The first definition assumed the updraft area to be that area having reflectivities of the maximum value or one decibel less than the maximum value. The second definition assumed the updraft area to be that area having reflectivities of the maximum value or one or two decibels less than the maximum value. Both of these definitions are consistent with the rule used to separate the cells in that neither allows the updrafts of neighboring cells to overlap.

Figure 3.4 shows how the process worked. Two cores, each having a maximum reflectivity of 48 dBZ, have been identified and are shown inside squares. Note that they cannot be connected without passing through a point where the reflectivity is three or more decibels less than the maxima. The updraft areas based on the first definition are contained within solid lines. In the upper cell part of this area is not contiguous with the reflectivity core. This is probably a result of the noisy nature of the data. Peculiarities of this sort appeared often in the radar data

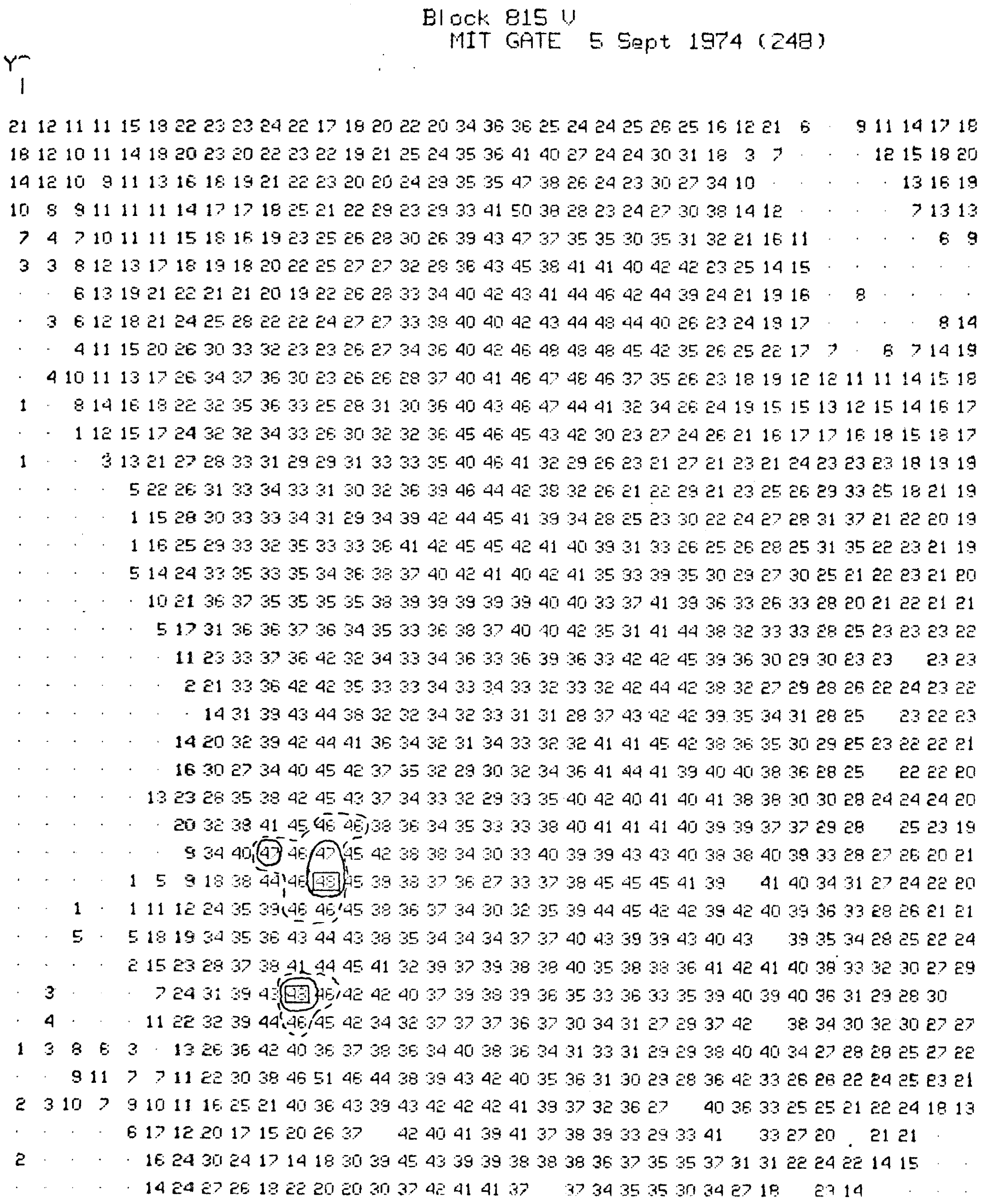

```
                              Block 815 V
                                MIT GATE  5 Sept 1974 (248)
Y^
|

21 12 11 11 15 18 22 23 23 24 22 17 18 20 22 20 34 36 36 25 24 24 25 26 25 16 12 21  6  ·  9 11 14 17 18
18 12 10 11 14 19 20 23 20 22 23 22 19 21 25 24 35 36 41 40 27 24 24 30 31 18  3  7  ·  ·  · 12 15 18 20
14 12 10  9 11 13 16 18 19 21 22 23 20 20 24 29 35 35 47 38 26 24 23 30 27 34 10  ·  ·  ·  ·  · 13 16 19
10  8  9 11 11 11 14 17 17 18 25 21 22 29 23 29 33 41 50 38 28 23 24 27 30 38 14 12  ·  ·  ·  ·  7 13 13
 7  4  7 10 11 11 15 18 16 19 23 25 26 28 30 26 39 43 47 37 35 35 30 35 31 32 21 16 11  ·  ·  ·  ·  6  9
 3  3  8 12 13 17 18 19 18 20 22 25 27 27 32 28 36 43 45 38 41 41 40 42 42 23 25 14 15  ·  ·  ·  ·  ·  ·
 ·  ·  6 13 19 21 22 21 21 20 19 22 26 28 33 34 40 42 43 41 44 46 42 44 39 24 21 19 16  ·  8  ·  ·  ·  ·
 ·  3  6 12 18 21 24 25 28 22 22 24 27 27 33 38 40 40 42 43 44 48 44 40 26 23 24 19 17  ·  ·  ·  ·  8 14
 ·  ·  4 11 15 20 26 30 33 32 23 23 26 27 34 36 40 42 46 48 48 48 45 42 35 26 25 22 17  7  ·  6  7 14 19
 ·  4 10 11 13 17 26 34 37 36 30 23 26 26 28 37 40 41 46 47 48 46 37 35 26 23 18 19 12 12 11 11 14 15 18
 1  ·  8 14 16 18 22 32 35 36 33 25 28 31 30 36 40 43 46 47 44 41 32 34 26 24 19 15 15 13 12 15 14 16 17
 ·  ·  1 12 15 17 24 32 32 34 33 26 30 32 32 36 45 46 45 43 42 30 23 27 24 26 21 16 17 17 16 18 15 18 17
 1  ·  ·  3 13 21 27 28 33 31 29 29 31 33 33 35 40 46 41 32 29 26 23 21 27 21 23 21 24 23 23 23 18 19 19
 ·  ·  ·  ·  5 22 26 31 33 34 33 31 30 32 36 39 46 44 42 38 32 26 21 22 29 21 23 25 26 29 33 25 18 21 19
 ·  ·  ·  ·  1 15 28 30 33 33 34 31 29 34 39 42 44 45 41 39 34 28 25 23 30 22 24 27 28 31 37 21 22 20 19
 ·  ·  ·  ·  1 16 25 29 33 32 35 33 33 36 41 42 45 45 42 41 40 39 31 33 26 25 26 28 25 31 35 22 23 21 19
 ·  ·  ·  ·  5 14 24 33 35 33 35 34 36 38 37 40 42 41 40 42 41 35 33 39 35 30 29 27 30 25 21 22 23 21 20
 ·  ·  ·  ·  · 10 21 36 37 35 35 35 35 38 39 39 39 39 39 40 40 33 37 41 39 36 33 26 33 28 20 21 22 21 21
 ·  ·  ·  ·  ·  5 17 31 36 36 37 36 34 35 33 36 38 37 40 40 42 35 31 41 44 38 32 33 33 28 25 23 23 23 22
 ·  ·  ·  ·  ·  · 11 23 33 37 36 42 32 34 33 34 36 33 36 39 36 33 42 42 45 39 36 30 29 30 23 23    23 23
 ·  ·  ·  ·  ·  ·  2 21 33 36 42 42 35 33 33 34 33 34 33 32 33 32 42 44 42 38 32 27 29 28 26 22 24 23 22
 ·  ·  ·  ·  ·  ·  · 14 31 39 43 44 38 32 32 34 32 33 31 31 28 37 43 42 42 39 35 34 31 28 25    23 22 23
 ·  ·  ·  ·  ·  · 14 20 32 39 42 44 41 36 34 32 31 34 33 32 32 41 41 45 42 38 36 35 30 29 25 23 22 22 21
 ·  ·  ·  ·  ·  · 16 30 27 34 40 45 42 37 35 32 29 30 32 34 36 41 44 41 39 40 40 38 36 28 25    22 22 20
 ·  ·  ·  ·  · 13 23 28 35 38 42 45 43 37 34 33 32 29 33 35 40 42 40 41 40 41 38 38 30 30 28 24 24 24 20
 ·  ·  ·  ·  ·  · 20 32 38 41 45 46 46 38 36 34 35 33 33 38 40 41 41 41 40 39 39 37 37 29 28    25 23 19
 ·  ·  ·  ·  ·  ·  9 34 40 47 46 47 45 42 38 38 34 30 33 40 39 39 43 43 40 38 38 40 38 33 28 27 26 20 21
 ·  ·  ·  ·  1  5  9 18 38 44 46 48 45 39 38 37 36 27 33 37 38 45 45 45 41 39    41 40 34 31 27 24 22 20
 ·  ·  1  ·  1 11 12 24 35 39 46 46 45 38 36 37 34 30 32 35 39 44 45 42 42 39 42 40 39 36 33 28 26 21 21
 ·  ·  5  ·  5 18 19 34 35 36 43 44 43 38 35 34 34 34 37 37 40 43 39 39 43 40 43    39 35 34 28 25 22 24
 ·  ·  ·  ·  2 15 23 28 37 38 41 44 45 41 32 39 37 39 38 38 40 35 38 38 36 41 42 41 40 38 33 32 30 27 29
 ·  3  ·  ·  ·  7 24 31 39 43 48 46 42 42 40 37 39 38 39 36 35 33 36 33 35 39 40 39 40 36 31 29 28 30
 ·  4  ·  ·  · 11 22 32 39 44 46 45 42 34 32 37 37 37 36 37 30 34 31 27 29 37 42    38 34 30 32 30 27 27
 1  3  8  6  3  · 13 26 36 42 40 36 37 38 36 34 40 38 36 34 31 33 31 29 29 38 40 40 34 27 28 28 25 27 22
 ·  ·  9 11  7  7 11 22 30 38 46 51 46 44 38 39 43 42 40 35 36 31 30 29 28 36 42 33 26 28 22 24 25 23 21
 2  3 10  7  9 10 11 16 25 21 40 36 43 39 43 42 42 42 41 39 37 32 36 27    40 36 33 25 25 21 22 24 18 13
 ·  ·  ·  ·  6 17 12 20 17 15 20 26 37    42 40 41 39 41 37 38 39 33 29 33 41    33 27 20  . 21 21  ·
 2  ·  ·  ·  · 16 24 30 24 17 14 18 30 39 45 43 39 39 38 38 38 36 37 35 35 37 31 31 22 24 22 14 15  ·  ·
 ·  ·  ·  ·  · 14 24 27 26 18 22 20 20 30 37 42 41 41 37    37 34 35 35 30 34 27 18    23 14     ·  ·  ·
```

Figure 3. 4. Example of the use of a CAPPI radar map to identify cells and define their updraft areas. See text for explanation.

and had to be dealt with by objectively applying specific, subjectively-determined rules. The areas based on the second definition are contained within dashed lines. Note that in spite of the fact that the cells have the same maximum reflectivity, their updraft areas (as defined) differ considerably. Since the map has a horizontal resolution of 1 km, the updraft areas can be found by simply counting the blocks within the outlined regions.

3.3.4 Idealization

A close inspection of the radar data in Figure 3.4 reveals a substantial variability in cell characteristics. This type of variability was present in all the radar data for the line and the cluster. It is not clear whether it was due to actual differences in cell characteristics or arose from sampling similar cells at different times in their life histories. In any case, this variability posed problems both in selecting appropriate input variables for the model and in making comparisons between observed and modeled cells.

In order to determine suitable input variables, the features (i.e. the line and cluster of cells) were idealized into geometrically simple combinations of "representative" cells. The idealized features had the same number of cells as the observed features, but the representative cells in the idealized features were identical with each other and geometrically compatible with the model (i.e. they were composed of an inner cylinder which was the active core or updraft region of the cell, and an outer cylinder which was the "environment" or area where compensating motions take place. This idealization process is described in section 3.3.4.1.

Since the model would be simulating a "representative" cell, it was also necessary to determine representative values of the characteristics of the observed cells with which to compare model cells. The process for determining representative characteristics for comparison is presented in section 3.3.4.2.

3.1.4.1 Determination of Input Variables

Although the idealization processes for the cluster and the line were not identical, they had some common features which will be discussed in this section. The features peculiar to the idealization processes for the line and the cluster will be discussed in sections 4.1.2.1 and 5.1.2.1, respectively.

Because it was necessary to build some rather arbitrary definitions into the idealization process, some flexibility was also built into the process. As a result of this flexibility, the idealization process will produce a number of sets of input variables from which a choice of the most realistic values of the variables may be made based on intuitive judgment, theoretical reasoning, and field observations of these variables.

The first step in the idealization process was to determine which cells would be used in the process. The method of identifying cells on a CAPPI radar map was given in section 3.3.3. For the two CAPPI's nearest the ground, the cells were identified and their maximum reflectivity factors were recorded. Cells were then said to "exist" for the purpose of the idealization if they met certain criteria. The criteria varied (this variation provided some of the flexibility built into the process), but in all cases required that an identified cell exist in both of the lower layers and that the maximum reflectivities exceed given thresholds in one or both layers. These criteria will be referred to as the E (for existence) criteria. The E will be followed by two subscripts. The first subscript will prescribe the minimum reflectivity required in one layer and the second will prescribe the minimum reflectivity required in the other layer in order for a cell to be included in the idealization process. For example, $E_{30,1}$ will refer to the criterion requiring that a cell with a reflectivity of at least 30 dBZ will exist in one layer and some cell exist in the other layer. Similarly, $E_{40,40}$ will refer to the criterion requiring that cells with reflectivities of at least 40 dBZ exist in both layers. It was also required that the cells in the two layers exist in reasonable geographical proximity.

The method, described in section 3.3.3, for determining the areas of updrafts involved counting the data points surrounding a core of maximum reflectivity which had reflectivities within a given range of the maximum. The two ranges used in this study form the A (for "area") criteria. A_1 will refer to an updraft area determined from data points having the maximum reflectivity or reflectivities one decibel less than the maximum. Similarly, A_2 will refer to an updraft area determined from data points having the maximum reflectivity or reflectivities one or two decibels less than the maximum.

Updraft areas based on both A_1 and A_2 criteria were determined from the CAPPI's for the lowest two layers. Although the updraft area in the model is constant with height, the updraft areas determined from the radar data were seldom the same for both layers. Thus, methods were devised to combine the data from the two layers into one area. The two devised methods form the C (for "combination") criteria. C_{avg} will refer to the updraft area determined by averaging the areas of the updrafts in the two layers while C_{max} will refer to the updraft area determined by using the maximum area of the two layers.

The idealization processes for the line and the cluster employed different E criteria (i.e. the concept was the same but the subscripts were different). Both, however, used the same A and C criteria. The downdraft area of the cells in the cluster were determined by an entirely different process than that used for the cells in the line; these processes will be described in the following chapters.

3.3.4.2 Determination of Cell Characteristics for Comparison of Observed with Model Cells

The model provides fine time- and height-resolution information on such processes and properties as entrainment, vertical velocity, condensation, water content, forcings, etc. However, little is known about these processes in real situations because they are so difficult to measure. The only property which was available from the model and which was observed in some useful resolution in the field was radar reflectivity (the model calculates radar reflectivity from the drop size distribution). The radar data had sufficient spatial resolution to deal with most precipitating convective elements. Unfortunately, while its time resolution (15 min) was sufficient for studying mesoscale and synoptic-scale precipitation features, it was too coarse to allow more than a single "snapshot" of a cell taken at a random time in its life. It was possible, if the timing was right, for the same cell to appear on two consecutive radar maps. However, it was rarely possible to identify these as the same cell because of the confusion created by neighboring cells. Therefore, while the model produced a life history of the reflectivities within the modeled cells, no corresponding life history of observed cells was available. The problem, then, was to devise methods by which fine time- and height-resolution reflectivity data from a single cell simulated by the model could be compared to somewhat coarser height-resolution reflectivity data from instantaneous samples collected by the radar at random times in the lives of a number of cells. To address this problem, three cell characteristics were chosen: the maximum height, the maximum reflectivity, and the height of the maximum reflectivity.

Maximum Height

In vigorous convective situations ice crystals are usually found in the upper portions of the cells. These slowly-falling particles may blow off as an anvil or remain as debris after the intense lower portions of cells have rained out. In any case, they remain aloft for relatively long periods of time, so that when a number of cells occur in the same area, they tend to form a precipitation canopy over the area. The height of the canopy is not as time-dependent as the features of the individual cells and thus serves as a good indicator of the height which the more vigorous cells attained. Not all cells, of course, reach the height of the canopy, and occasionally very vigorous cells will penetrate it. However, it will be assumed in this study that the height of the canopy corresponds to the vertical extent of the representative cells. Maximum-tops radar charts were used to determine heights of cells in this study.

Maximum Reflectivity

During the cell-idealization process, the maximum reflectivity of each observed cell in the lowest two CAPPI's was determined. This allowed the construction of the distribution of maximum reflectivities in the updrafts of the observed cells. The model output allowed the determination of the distribution with time of the maximum reflectivity in the model cell updraft. These distributions were compared. However, it is important to notice that the comparison was made between the time spectrum of maximum reflectivity for a single modeled cell and the spectrum of instantaneous maximum reflectivity for a large number of observed cells. In order for such a comparison to be meaningful, it must be assumed that the observed cells were sampled at random times during their lifetimes. Furthermore, since the observed cells had varying degrees of representativeness, this comparison must be viewed as a somewhat subjective indication of the model's ability to simulate the observed cells.

Height of Maximum Reflectivity

The approach applied to comparing maximum reflectivities, described in the previous paragraph, was also applied to comparing the height of the maximum reflectivity in the cell updrafts. The model output provided these heights throughout the life of the cell. For the cluster of cells considered in Chapter 5, the cell population and organization was such that the heights could be determined by manual inspection of the CAPPI's. However, because of the large number of cells and the nature of their relationships with each other, the application of this manual inspection technique was not feasible for the line. Instead, a computer program was written which searched up each column in the 3-D radar charts for the line and recorded the height at which the maximum reflectivity occurred and that maximum value. The distribution of height versus the number of columns with maximum reflectivities at that height was then found for reflectivities above given thresholds. There were two drawbacks to this automated approach. First, except for the highest thresholds, the distributions probably included data from some columns which were not actually located in the cell updrafts. Secondly, any tilting of the updrafts which occurred might permit more than one maximum height to be recorded for a single updraft and thus tend to spread the distribution. These drawbacks increased the subjectivity, already alluded to in the previous paragraph, of this comparison scheme.

3.4 Upper Air Data

3.4.1 Source

The upper air data used in this study is described in Acheson (1976). It was gathered by rawinsonde ascents launched every three hours from the seven ships in the B-scale array. It consisted of temperature, humidity, wind, and height data every 5 mb.

3.4.2 Handling

Temperature and relative humidity data were to be loaded into the model at 500 m increments from the surface to 15 km. Thus the extremely fine vertical resolution of the data was unnecessary and somewhat of a nuisance. The observed temperature and relative humidity data were converted to a form more consistent with the model requirements by taking centered averages of the data from 250 m below to 250 m above the heights at which data would be loaded into the model. These mean temperatures and relative humidities were then plotted against a linear height scale extending from the surface to 15 km.

3.4.3 Idealization

Although there were no soundings taken in the midst of the line or cluster, there were numerous soundings available from their general vicinities. These profiles of temperature and relative humidity, while having major characteristics in common, varied enough over space and time to make difficult the determination of the actual environment in which the convection was taking place. To avoid this difficulty, idealized profiles, based on a number of soundings, were constructed in such a way as to retain the general characteristics of the actual soundings while ignoring the minor variations. The first step in this idealization process was to identify the important characteristics -- dry or moist layers, points where gradients changed suddenly, etc. Since all profiles did not have the same characteristics, it was necessary in some cases to identify more than one type of profile. The properties of the major characteristics (thickness, height, maximum or minimum value, etc.) were then averaged to produce information from which an idealized sounding could be constructed for each type of profile. The temporal and spatial distributions of the idealized soundings were then investigated to determine which would provide the most realistic initialization for the model. The specifics of the idealization process are given in the following chapters.

CHAPTER FOUR

SIMULATION OF CONVECTIVE CELLS IN A LINE

A line of convective showers, well documented by radar observations, entered the GATE B-scale array on the morning of 5 September, 1974. In this chapter, the line and its environment are described. Complex variations in the cells and the environment are eliminated through an idealization process which produced "representative" cells in a "representative" environment. Three sets of experiments are run with the idealized input, and their results are compared to observed data to determine how well the model simulated the cells.

4.1 The Line and its Environment -- Observed and Idealized

4.1.1 Description of the Line and its Environment

Marks and Raub (1978), using radar maps composited from four ships in the B-scale array, identified three distinct types of mesoscale features associated with the passage of easterly waves during phase III of GATE. The first type of feature was long, broad, slow-moving bands of deep convection associated with the wave trough. The second was the "squall lines" -- fast moving (11-18 m $\sec^{-1}$) lines of deep convection which moved toward the southwest and exhibited a behavior somewhat independent of the synoptic-scale waves. The third type of feature was long, thin, east-west oriented lines which move in the northerly flow ahead of the troughs at speeds of 4-6 m $\sec^{-1}$. The line considered in this chapter is an example of this third type of feature.

The origin of the line was evident from satellite pictures from the previous day which showed an extremely long (> 2000 km), narrow string of clouds approaching the array from the north-northwest. At about 2200Z on 4 September, shortly after it moved within radar range of the array, loosely-spaced cells of moderate intensity developed along the string of clouds. The cells formed a line about 200 km long and 20 km wide. At this time, the array was in wave sector 2. The line of cells expanded in the westerly direction and intensified so that by the time the line entered the array at 0300Z it had grown to be 500 km long and 50 km wide. Figure 4.1 shows the line at 0830Z (delineated by arrows) as seen by the radar aboard the Gilliss. By this time, the wave had progressed far enough west to place the B-scale array in wave sector 3. The line continued to move south for the next few hours, eventually losing its identity in the broad band of precipitation associated with the trough. The center of wave sector 4 (marking the trough) passed over the B-scale array at about 1800Z.

It appears that this convective line was associated with the interaction between a convergence line embedded in the northerly flow ahead of the trough and the dynamics of the trough itself. The first feature was able to produce only a line of clouds. However, when the features got close enough to compound their effects, the narrow line of clouds blossomed into full-scale deep convection.

4.1.2 Idealization of the Line and its Environment

4.1.2.1 Idealization of the Line

Three-dimensional radar charts showing the line at 0815Z and 0830Z

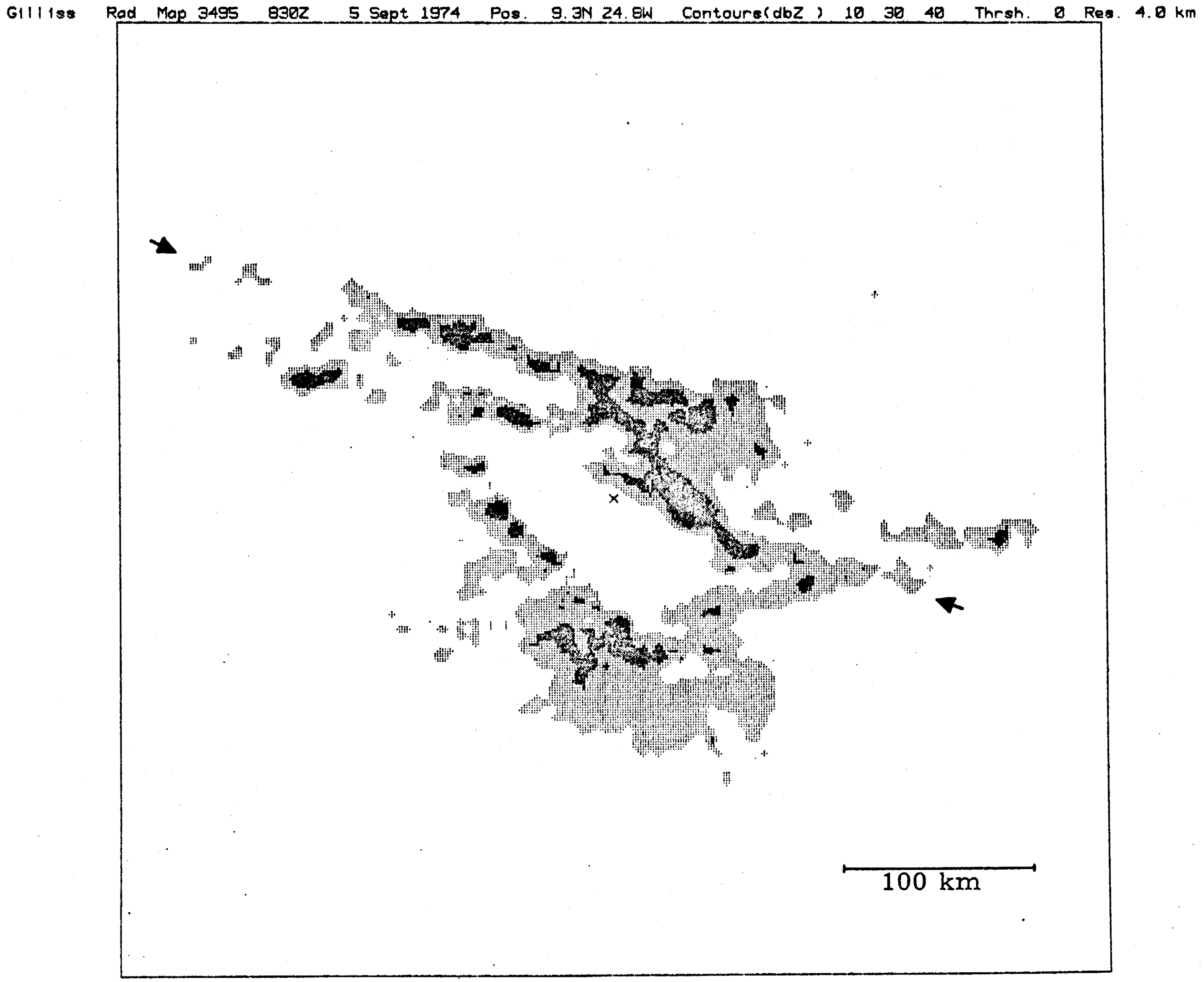

Figure 4. 1. Convective line at 0830Z as seen by radar aboard the Gilliss. Contours are 10, 30, 40, dBZ.

were constructed as described in section 3.3.2. Cores of maximum reflectivity were identified and their updraft areas were determined on the lowest two CAPPI's (0-2 and 2-4 km) using the A_1 and A_2 criteria (i.e., the areas extended 1dB and 2dB respectively down from the reflectivity maximum -- see section 3.3.4.1). The cores were then designated to represent or not to represent cells based on the following existence criteria:

$E_{1,1}$: a core had to appear in both layers;

$E_{40,1}$: a core had to appear in both layers and the core in at least one layer had to have a maximum reflectivity of 40dBZ or greater;

$E_{40,40}$: a core with a maximum reflectivity of at least 40dBZ had to appear in both layers.

This choice of existence criteria allowed investigation of all the cells ($E_{1,1}$), the moderately strong and strong cells ($E_{40,1}$), or just the strongest cells ($E_{40,40}$) appearing in the line at the given times. Each criterion yielded a different number of cells in the line. The updraft area of each cell was then determined in two ways: by averaging the updraft areas of the two layers (combination criterion C_{avg}) and by using the maximum area of the two layers (C_{max}).

The objective of this process was to produce an idealized line composed of identical "representative" cells. The updraft area of the representative cells was determined by averaging the updraft areas of the observed cells for each set of criteria. The existence criteria determined three sets of cells whose areas were averaged. For each set of cells, there were four different sets of areas resulting from the two area criteria and the two combination criteria. Thus, twelve different representative cell updraft areas were determined. Since the representative cells were assumed to be geometrically compatible with the model, the updrafts were assumed to be cylindrical and an updraft radius was calculated from each of the twelve updraft areas.

The last step in the idealization process was to determine the radius of the outer cylinder of the representative cells. Toward this objective, lines were drawn from cell to cell, connecting all the cells in the line by the shortest route (this was done for each E criterion). This continuous, but crooked, line was measured to give the length of the idealized line. It was then assumed that the representative cells were equally spaced along the line and that the outer cylinders of the adjacent cells just touched, but did not overlap (thus making the line continuous but precluding, as in the model, interaction between cells). The geometry of the idealized line then allowed calculation of the outer cylinder radius R from

$$R = \frac{\ell}{2(n-1)}$$

where ℓ is the length of the idealized line and n is the cell population. The process is shown schematically in Figure 4.2. (a) shows the line after the areas of the updrafts (shown dark) have been found. The cells have been connected by a line of length ℓ. (b) shows the idealized line. The cells are equally spaced along the length ℓ. The updrafts are the same size, having areas equal to the average of the areas of the updrafts in (a). The outer cylinders are also equal in size and touch but do not overlap.

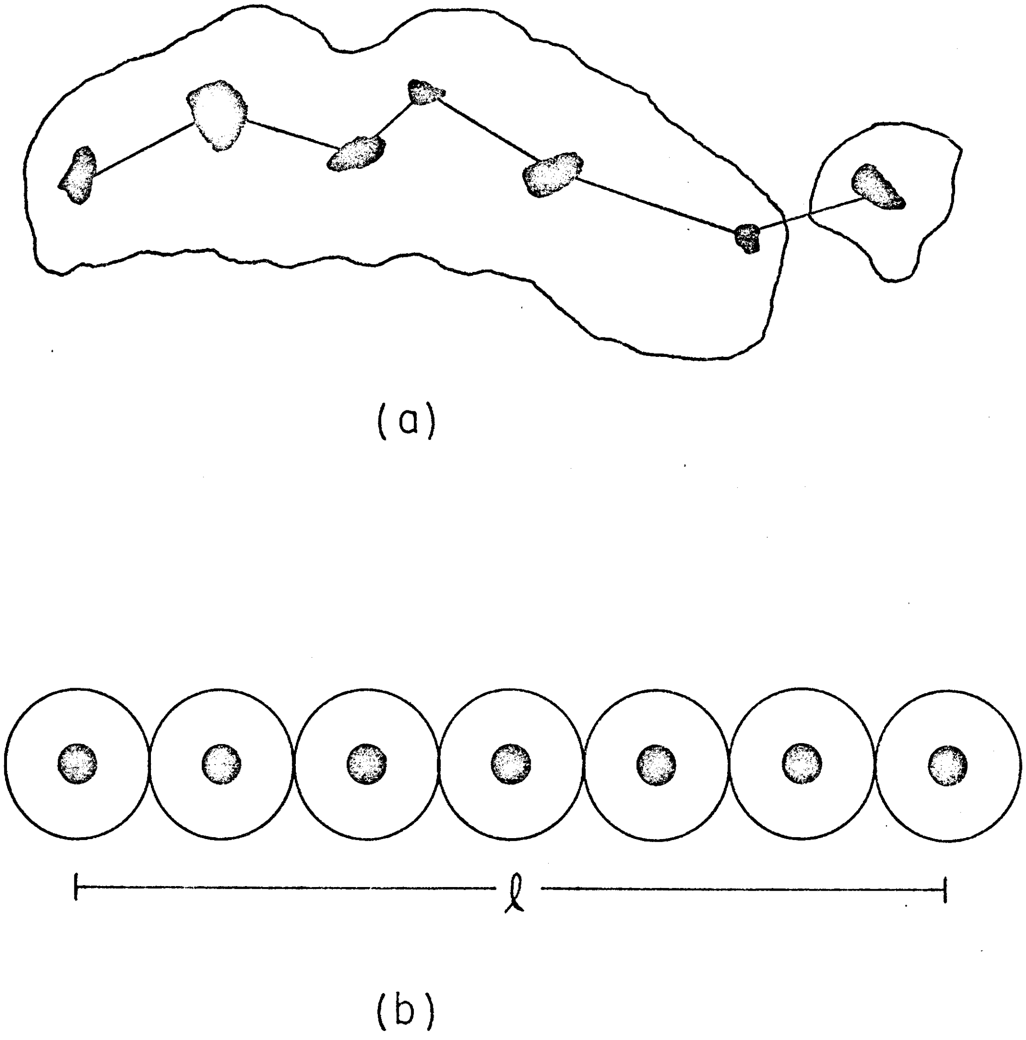

Figure 4. 2. Schematic representation of the idealization process for the line. (a), observed; (b), idealized.

Table 4.1 presents the results of the idealization process for all combinations of criteria for the line at 0815Z and 0830Z.

It is interesting to compare the data in Table 4.1 for the two times. The line is slightly longer at 0830Z, but contains fewer cells. Furthermore, the updraft radii are consistently larger (by about 10%) at 0830Z. However, the fact that the 0830Z line is longer and has fewer cells more than compensates for the larger updraft radii, so that the resulting σ's are smaller than at 0815Z.

As should be expected from the definition of the criteria, r and σ are smaller for the A_1 cases than for the corresponding A_2 cases, and are also smaller for the C_{avg} cases than for the corresponding C_{max} cases.

Since $E_{1,1}$, $E_{40,1}$, and $E_{40,40}$ represent increasing average cell strength, it is possible to investigate whether the results of Yau's sensitivity tests on σ are reflected in the results of the idealization process. Since for a given A and C criterion the updraft radius changes by only a few percent, the changes in σ as cell strength increases can be compared. This comparison shows a tendency, more obvious in the 0830Z data than in the 0815Z data, for σ to decrease as the cells get stronger. This is precisely what the model predicts will happen. However, this effect is probably a result of the fact that the areas of the cells eliminated by the adoption of more exclusive existence criteria effectively becomes part of the downdraft areas of the remaining cells. Since the elimination of cells does not appreciably change the average updraft area, the increase in the downdraft area forces σ to decrease. Nevertheless, both the model sensitivity tests and the idealization indicate that stronger cells have a larger surrounding area of downdraft.

Table 4.1. Results of the idealization of the line. See text for definition of criteria. Part a: 0815Z.

Time (Z)	Existence Criterion	Area Criterion	Combination Criterion	Length of line, ℓ (km)	Number of cells, n	Average Area of Updraft, $\bar{a}$ (km^2)	Radius of Average Updraft, r (km)	Radius of Average Downdraft, R (km)	$\sigma = \frac{r}{R}$
0815	$E_{1,1}$	A_1	C_{max}	315	38	2.78	.94	4.26	.22
			C_{avg}	315	38	2.43	.88	4.26	.21
		A_2	C_{max}	315	38	4.97	1.26	4.26	.30
			C_{avg}	315	38	4.11	1.14	4.26	.27
	$E_{40,1}$	A_1	C_{max}	261	32	2.68	.92	4.21	.22
			C_{avg}	261	32	2.32	.86	4.21	.20
		A_2	C_{max}	261	32	5.00	1.26	4.21	.30
			C_{avg}	261	32	4.16	1.15	4.21	.27
	$E_{40,40}$	A_1	C_{max}	233	27	2.70	.93	4.48	.21
			C_{avg}	233	27	2.33	.86	4.48	.19
		A_2	C_{max}	233	27	4.89	1.25	4.48	.28
			C_{avg}	233	27	4.07	1.14	4.48	.25

Table 4.1. Results of the idealization of the line. See text for definition of criteria. Part b: 0830Z

Time (Z)	Existence Criterion	Area Criterion	Combination Criterion	Length of Line, ℓ (km)	Number of Cells, n	Average Area of Updraft, $\bar{a}$ (km^2)	Radius of Average Updraft, r (km)	Radius of Average Downdraft, R (km)	$\sigma = \frac{r}{R}$
0830	$E_{1,1}$	A_1	C_{max}	369	36	3.36	1.03	5.27	.20
			C_{avg}	369	36	2.86	.95	5.27	.18
		A_2	C_{max}	369	36	6.03	1.39	5.27	.26
			C_{avg}	369	36	5.06	1.27	5.27	.24
	$E_{40,1}$	A_1	C_{max}	322	29	3.24	1.02	5.75	.18
			C_{avg}	322	29	2.69	.93	5.75	.16
		A_2	C_{max}	322	29	5.52	1.33	5.75	.23
			C_{avg}	322	29	4.48	1.19	5.75	.21
	$E_{40,40}$	A_1	C_{max}	293	24	3.25	1.02	6.37	.16
			C_{avg}	293	24	2.71	.93	6.37	.15
		A_2	C_{max}	293	24	5.75	1.35	6.37	.21
			C_{avg}	293	24	4.67	1.22	6.37	.19

Although the criteria used for idealization are admittedly arbitrary, they yielded fairly realistic values for updraft dimensions. Simpson and Wiggert (1969), using photogrametric techniques and aircraft penetrations, found updraft radii of oceanic cells near Puerto Rico ranging from 0.50 to 1.15 km. In later studies Simpson and Wiggert (1971) used photogrametric techniques alone to derive updraft radii of 0.65 to 1.30 km for Florida cells. Braham (1952) used data from aircraft penetrations during the Thunderstorm Project to determine likely radii of .55 to .75 km for Florida and Ohio thunderstorms.

Yau adopted the hypothesis of Asai and Kasahara (1967) that σ would take on a value such that vertical heat transport would be maximized. His calculations showed that the value of σ which maximized vertical heat transport varied with the updraft radius and the lapse rate, but generally fell between 0.3 and 0.4. The values of σ from the idealization were consistently smaller. This discrepancy might stem from improper assumptions in the idealization scheme. On the other hand, it is possible that the cells were not operating at peak efficiency.

It appears from the above considerations that the most reasonable combination of r and σ comes from the A_2 criterion for determining updraft size.

4.1.2.2 Idealization of the Environment

To determine a representative sounding with which to initialize the model, 123 soundings of temperature and relative humidity for 2 and 5 September from the B-scale ships were plotted as described in section 3.4.2. The 2 September data were used to beef up the sample and were selected because the situation on that day, at first glance, appeared to be similar to that on 5 September. The distribution of the soundings by day and by wave sector is given in Table 4.2.

Table 4.2. Distribution of soundings by wave sector and day.

Wave Sector	2 Sep	5 Sep	Total
2	6	10	16
3	10	16	26
4	17	23	40
5	17	23	40
6	1	0	1
	51	72	123

Relative Humidity

A perusal of the relative humidity soundings made it obvious that there were two characteristic profiles. In the first, there was a moist layer several kilometers deep near the surface, a sharp dry layer a few kilometers deep above the surface moist layer, and a moderately moist layer above the dry layer. The second also had a moist layer several kilometers deep near the surface, above which there was a gradual decrease in relative humidity. The amount of the decrease varied so greatly (from as little as 10% to as much as 60%) that it was difficult to combine these profiles into a single category. Consequently, they were grouped into two types, one relatively moist aloft and the other dryer aloft. Thus, three relative humidity profile types were defined as follows:

Type I:	Moist at low levels, sharply dryer at middle levels, moderately moist at upper levels;
Type II:	Moist at low levels with a moderate decrease in humidity in middle and upper levels;
Type III:	Moist at low levels with a strong decrease in humidity in middle and upper levels.

The division between Types II and III soundings was made at an average upper-level relative humidity of 54%, which corresponded to a "weak spot" in the distribution of that variable. Each sounding was classified by type, and the depth and average relative humidity of each of its layers was determined. For Type I soundings, the height and value of the minimum relative humidity in the dry layer was found, and for Type II and III soundings the minimum relative humidity in the upper layer was determined. Averages of these characteristics for each type of sounding were calculated. The results -- based on 43 Type I, 44 Type II, and 36 Type III soundings -- are given in Table 4.3.

Idealized relative humidity profiles for each type were then constructed to reflect the average characteristics. These profiles are shown in Figure 4.3.

In order to determine when these types tended to occur, their distribution by wave sector was found. This distribution is shown in Table 4.4, in which (a) is for 2 September and (b) is for 5 September, and the numbers in the parentheses are the percentage of the soundings of all the given type which occurred during the given sector.

Table 4.3. Mean values of characteristic features of relative humidity profiles. Range of values is shown in parentheses.

Type	Low Layer $\overline{RH}$ (%)	Low Layer ΔH (km)	Mid Layer $\overline{RH}$ (%)	Mid Layer ΔH (km)	Mid Layer RH_{min} (%)	Mid Layer RH_{min} Height (km)	Upper Layer $\overline{RH}$ (%)	Upper Layer RH_{min} (%)
I	83 (73-93)	5.8 (3.0-8.0)	35 (18-65)	2.6 (1.0-6.0)	20 (3-56)	7.2 (4.5-10.5)	57 (35-79)	--
II	88 (75-97)	5.4 (3.0-8.0)	--	--	--	--	65 (55-86)	48 (30-74)
III	85 (73-97)	5.4 (1.5-8.0)	--	--	--	--	44 (27-53)	25 (3-42)

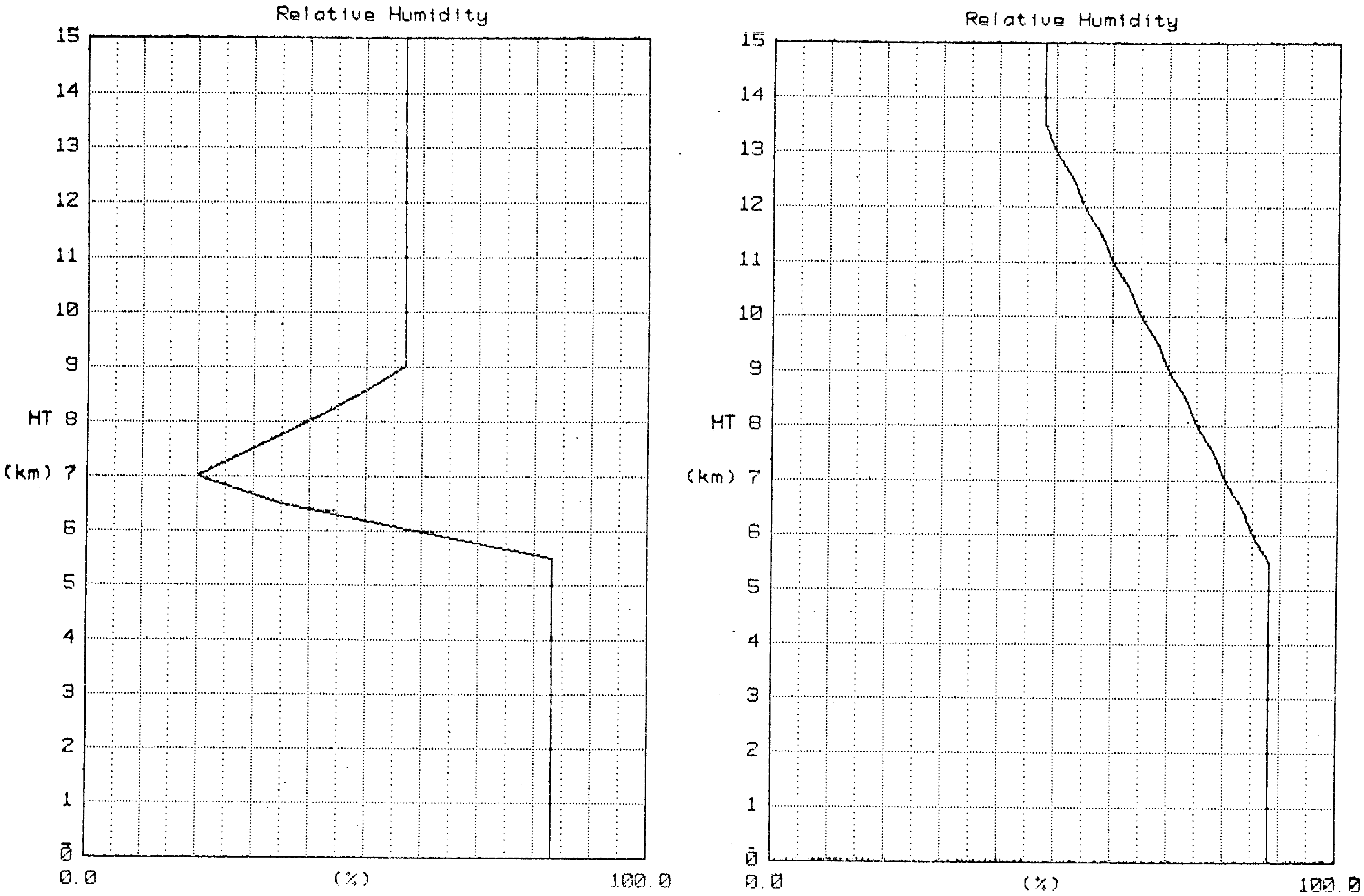

Figure 4. 3. Idealized relative humidity soundings for the line. Left, type I; right, type II.

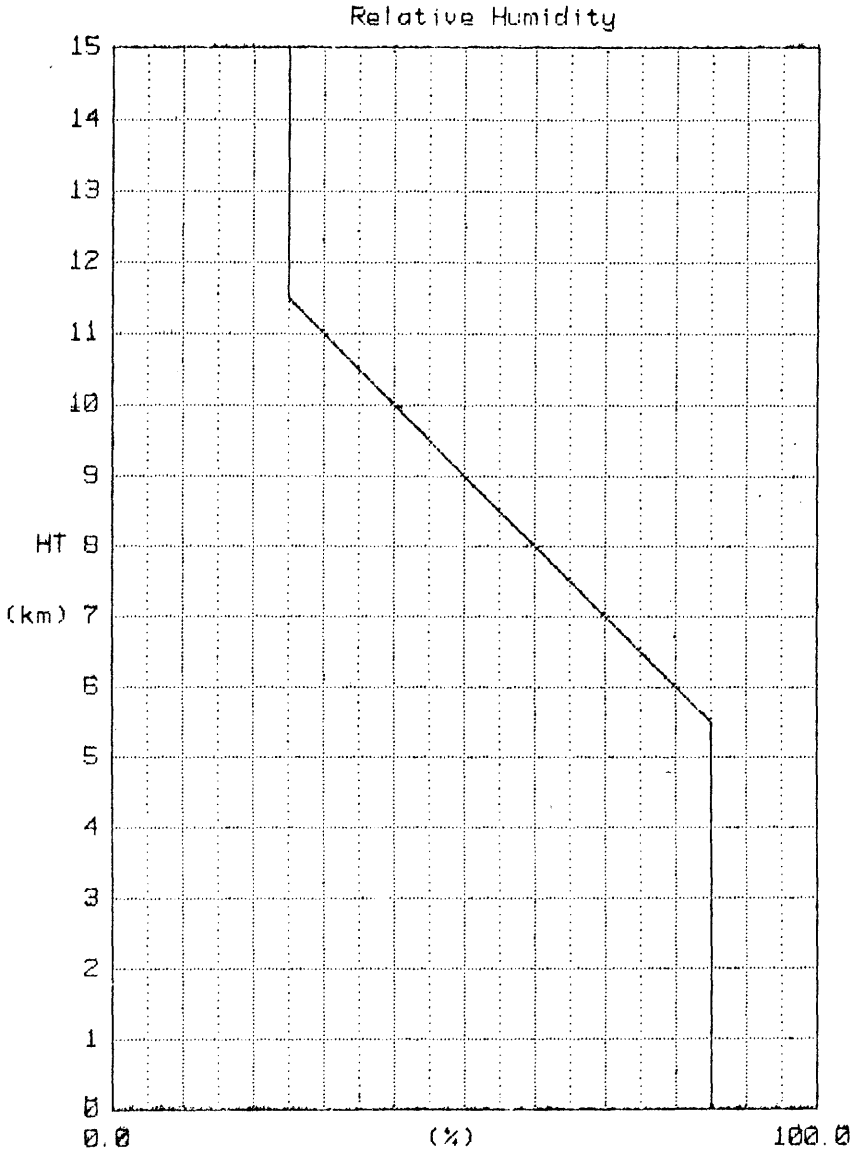

Figure 4.3. (con'd) Idealized relative humidity soundings for the line. Type III.

Table 4.4. Distribution of relative humidity sounding types by wave sector. Numbers in parentheses are percentage of soundings of given type which occurred in given sector.

	(a) 2 September						(b) 5 September					
	Wave Sector						Wave Sector					
Type	2	3	4	5	6	All	2	3	4	5	6	All
I	2	0	0	2	0	4	18	10	18	3	0	39
	(33)	(0)	(0)	(11)	(0)	(8)	(80)	(63)	(78)	(13)	(0)	(54)
II	4	8	7	14	1	34	1	1	4	4	0	10
	(67)	(80)	(41)	(82)	(100)	(67)	(10)	(6)	(17)	(17)	(0)	(14)
III	0	2	10	1	0	13	1	5	4	70	0	23
	(0)	(20)	(59)	(6)	(0)	(25)	(10)	(31)	(4)	(70)	(0)	(32)
All	6	10	17	17	1	51	10	16	23	23	0	72

The difference between the two days is immediately obvious. The Type II sounding dominated on 2 September, and there were few Type I soundings, while on 5 September the Type I sounding dominated and there were few Type II soundings. The sector distribution shows that on 2 September, Type II is strongly preferred in all sectors shown except sector 4, where it finishes a strong second to Type III. On 5 September Type I dominates all sectors except 5, where Type III is preferred.

Temperature

Aside from slight variations near the surface and an occasional hint of the tropopause at 15 km, the temperature profiles were strikingly similar. There was a temptation to average a handful of them and use that average as the idealized temperature profile. However, the temperature soundings were idealized using a method conceptually similar to that used in the relative humidity idealization.

The obvious common characteristic of the temperature soundings was a smaller lapse rate in the lower levels than in the upper levels. An increase with height in the lapse rate occurred between 6 and 9 km above the ground in each sounding. The change was sometimes abrupt, but more often it was gradual. Above and below the change the lapse rates were reasonably constant. Since this characteristic could be expected to affect the growth of cumulus cells, it was chosen as the characteristic on which to base the idealization. The object of the idealization was to construct a temperature-versus-height profile composed of two straight lines -- obviously a simplification, but more realistic than assuming a constant lapse rate as Yau did in his tests.

Toward this objective, the following three characteristics were determined for 109 temperature soundings (14 of the soundings used in the relative humidity idealization had insufficient temperature data):

1) the height of the point at which the lapse rate changed;
2) the lapse rate below that height; and
3) the overall (0-15 km) decrease in the temperature.

Because the change in the lapse rate was often gradual, taking place over two or three kilometers, the determination of the height at which it occurred was somewhat subjective. An attempt was made to choose the best point at which to break the temperature profile into two straight lines. There were some soundings in which there was a sudden decrease in the lapse rate near 15 km, presumably caused by the proximity of the tropopause. For these soundings, the lapse rate below this region was extended to 15 km in an attempt to avoid having the effect of the tropopause reflected in the lapse rate of the entire upper half of the troposphere.

The average values of the three characteristics for soundings grouped according to date, wave sector, and humidity type are given in Tables 4.5-4.7. In Table 4.5 (a), which shows the distribution of the mean height of the change in the lapse rate by wave sector, there is no evidence of a consistent pattern of change. Table 4.5 (b) shows an overall tendency for the height to increase from humidity Type I to Type II to Type III. However, the subjective nature of the determination of the heights and the fact that they were determined to the nearest kilometer make the significance of such minor variations questionable. In the 5

Table 4.5. Mean heights, in km, of the change in lapse rate for different wave sectors (a) and humidity types (b).

(a) Wave Sector							(b) Relative Humidity Type			
	2	3	4	5	6	All	I	II	III	All
2 Sep	6.8	7.2	7.7	7.7	8.0	7.5	7.0	7.6	7.4	7.5
5 Sep	7.9	7.9	7.5	7.8	--	7.7	7.6	7.8	8.0	7.7
All	7.4	7.7	7.5	7.8	8.0	7.6	7.5	7.6	7.8	7.6

Table 4.6. Mean low-level lapse rates, in °C km^{-1}, for different wave sectors (a) and relative humidity types (b).

(a) Wave Sector							(b) Relative Humidity Type			
	2	3	4	5	6	All	I	II	III	All
2 Sep	5.56	5.52	5.56	5.55	5.63	5.58	5.51	5.54	5.69	5.58
5 Sep	5.66	5.61	5.55	5.53	--	5.57	5.60	5.47	5.56	5.57
All	5.61	5.68	5.59	5.53	5.63	5.57	5.59	5.53	5.61	5.57

Table 4.7. Mean overall (0-15 km) temperature decrease, in °C, for different wave sectors (a) and relative humidity types (b).

(a) Wave Sector							(b) Relative Humidity Type			
	2	3	4	5	6	All	I	II	III	All
2 Sep	100.0	99.6	99.9	99.5	100.0	99.7	100.0	99.4	100.5	99.7
5 Sep	100.3	99.3	99.2	98.5	--	99.1	99.5	98.5	98.7	99.1
All	100.1	99.4	99.4	98.9	100.0	99.3	99.5	99.2	99.3	99.3

September data in Table 4.6 (a), there is evidence of a small but consistent decrease in low-level lapse rate as the wave approaches. The possible significance of this decrease will be discussed later. Table 4.6 (b) shows no pattern in the distribution of low-level lapse rate by humidity type. The only consistent pattern evident in Table 4.7 is a small drop in the overall temperature decrease as the wave approaches on 5 September. This is consistent with the decrease in the low-level lapse rate for the same day seen in Table 4.6 (a). The decrease in low-level lapse rate from sector 2 to sector 5 on 5 September was 0.13°C km^{-1}. Multiplying this by the mean height of the low layer for the same day gives a lapse rate decrease of 1.0°C per 7.7 km, approximately half the change in the overall lapse rate. Therefore, the decrease in the lapse rate is spread out over the entire 15 km. This result bears out the observations of Reed et al. (1977), who found relatively cold air at 850 mb below the trough and relatively warm air at 300 mb above the trough. Unfortunately, the 2 September data do not show the same effect.

In brief, except for the slight decrease in lapse rate as the wave approached on 5 September, there were no consistent patterns in the temperature profiles. Variations in the mean characteristics were so small as to be of questionable significance. It seems equally realistic to initialize the model with the overall idealization, the idealization based on a given day's data, the idealization based on the wave sector, or the idealization corresponding to the appropriate relative humidity profile.

4.2 Experiments

Three groups of experiments were conducted in an attempt to simulate the cells in the line. In the first group (X1-X7) values of the input variables suggested by the idealization were used, and each experiment was a separate entity. In the second group (X8-X12) an attempt was made to humidify the dry layer in the Type I relative humidity sounding by creating successive cells in the same atmosphere. Each experiment in this group was initialized using the final temperature and relative humidity profiles from the previous experiment. The third group of experiments (X13-X15) was an attempt to include mesoscale effects in the development of the cells.

Comparison of model cells with observed cells is made after all the experiments have been described. Table 4.9 summarizes the values of the important input variables. Some important characteristics of the resulting cells are given in Table 4.10.

4.2.1 Experiments 1-7, Simulation of Cells in the Line

Experiment 1 (X1)

The line of convective cells being simulated occurred while the array was in wave sector 3. Table 4.4 (b) shows that ten of sixteen sector 3 soundings from 5 September were Type I relative humidity soundings. For this reason, the Type I relative humidity sounding was chosen for this experiment. The characteristics of the idealized temperature soundings were practically the same for wave sector 3 and Type I situations. The chosen temperature profile had a low-level depth of 7.5 km, a low-level lapse rate of 5.6°C km^{-1}, and a 15-km temperature decrease of 100°C which yielded an upper-level lapse rate of 7.7°C km^{-1}. The resulting sounding, which employed the 0800Z surface temperature observation from the Gilliss, is plotted in Figure 4.4.

This first experiment was an attempt to model the average cell in the line. Thus, the inner-cylinder radius and σ were determined from the $E_{1,1}$ criterion which used data from all cells having maximum reflectivity cores in the lowest two CAPPI's. An inner-cylinder radius of 1.25 and a σ of 0.27 were determined by taking rough averages of the values of these variables for the A_2 criterion from both the 0815Z and 0830Z idealizations (see Table 4.1). The A_2 criterion was used in order to produce a large radius consistent with the idealization process.

Figure 4.5 is a time-height diagram of radar reflectivity factor (in dBZ) in the inner cylinder of the model. The cell was rather weak and attained a height of only 2.5 km. It would be ludicrous to suggest that this simulation resembles the average cell in the line. A number of reasons for this failure could be suggested, but further experiments will be presented before an attempt is made to explain the results of this experiment.

Experiment 2

It was expected that the dry layer in the Type I relative humidity profile would interfere with the growth of the convective cells. However, in X1, the precipitation reached a height of only 2.5 km, well below the dry layer. Experiment 2 was run in order to determine whether the dry layer played any role in that lack of development. The Type I relative humidity profile was altered to remove the dry layer by continuing the 83%

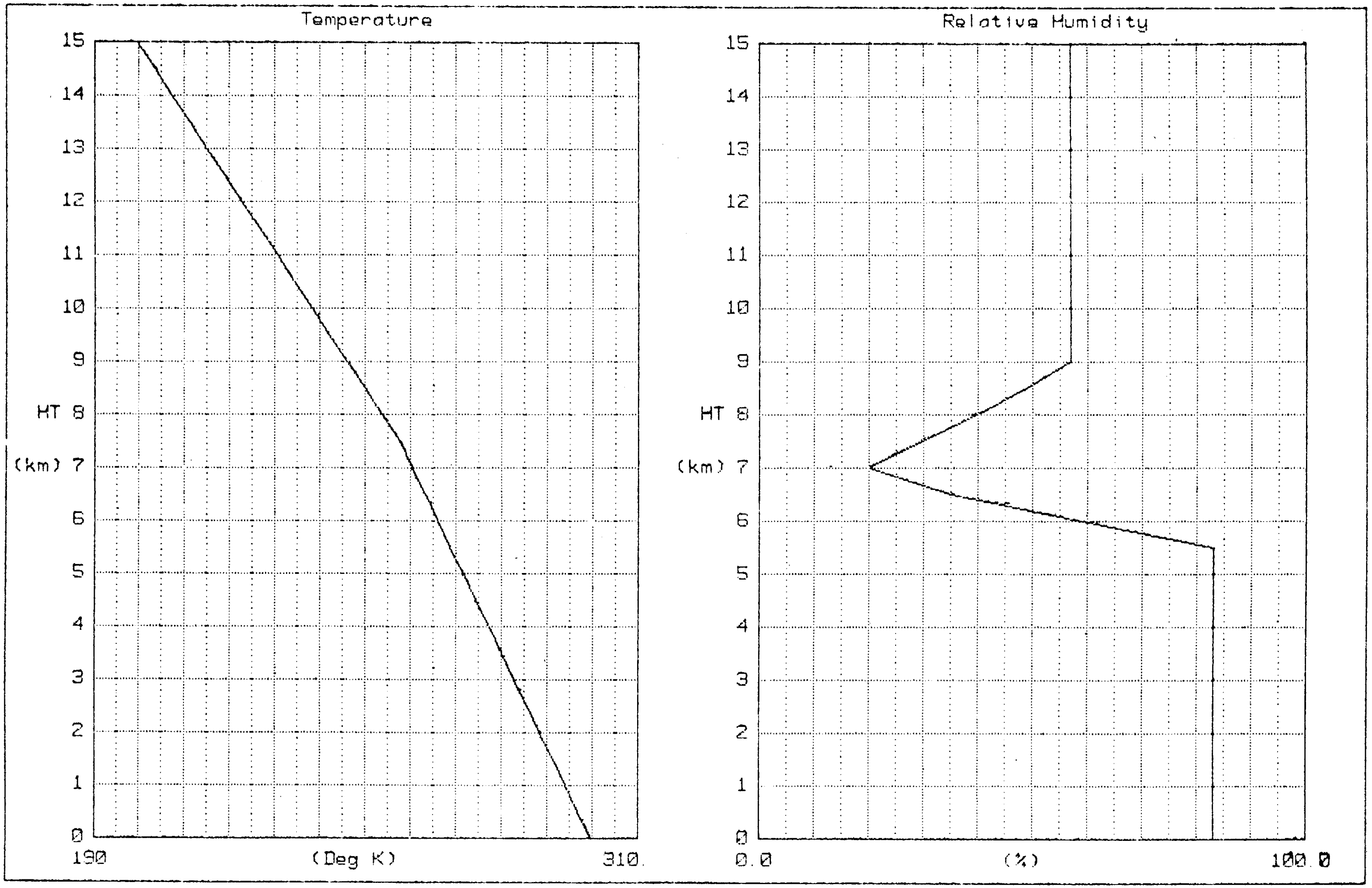

Figure 4.4. Sounding used in experiment 1.

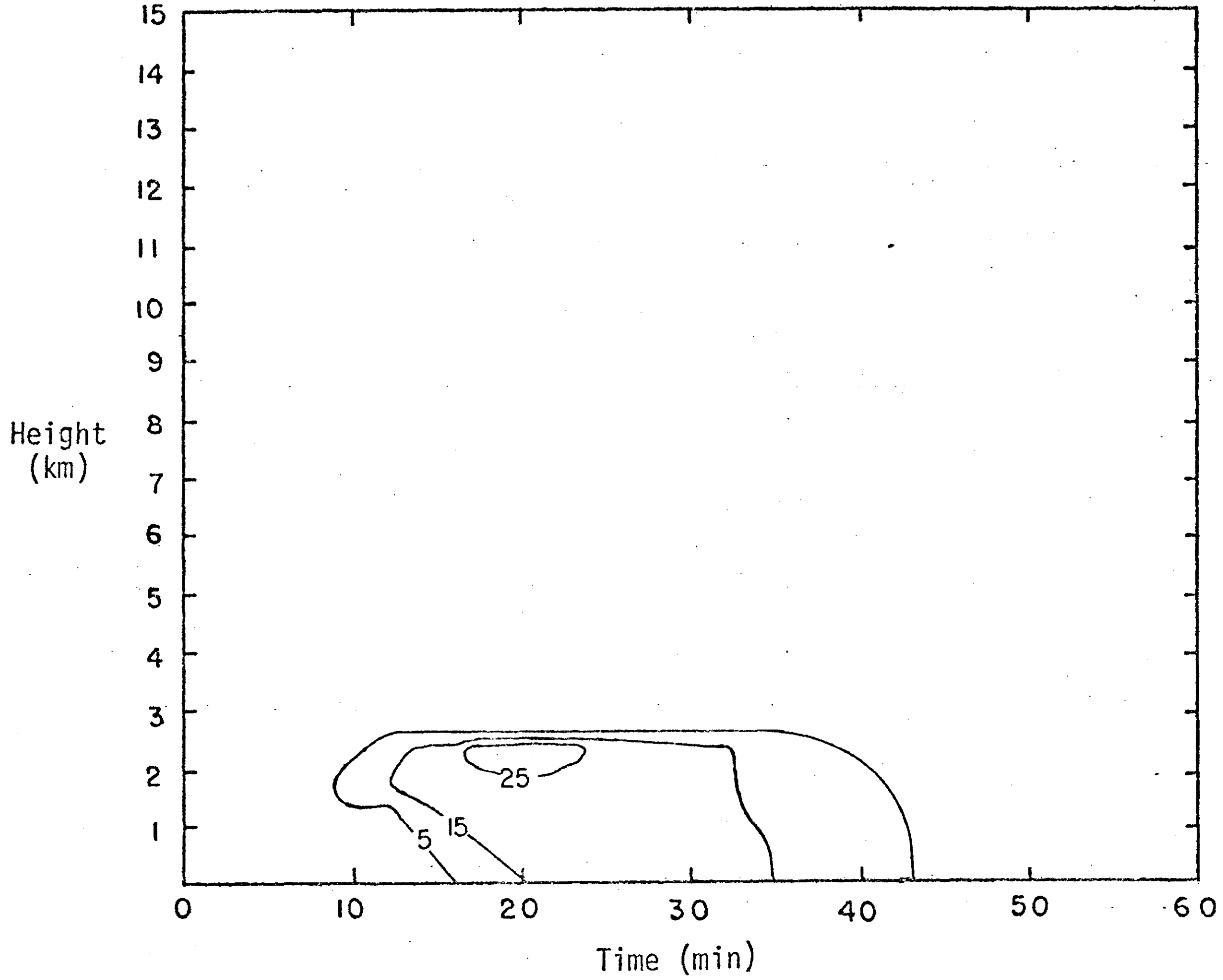

Figure 4.5. Time-height diagram of reflectivities for X1. Contours are in dBZ.

relative humidity characteristic of the low layer up to 8.5 km, the top of the dry layer. It was then decreased to 57%, the upper layer relative humidity.

The results of this experiment were, for all practical purposes, identical to the results of X1. This suggests that the dry layer was not responsible for the feebleness of the cell in X1. Apparently the 83% relative humidity was insufficient to support the condensation necessary to drive the updraft, and the resulting cell was able to reach only half a kilometer above the saturated velocity perturbation.

Experiment 3

X1 demonstrated that the model was unable to reproduce the deep convection characteristic of the line under the relative humidity conditions associated with the open atmosphere around the line. However, radar maps (see Figure 4.1) suggest that the Type I relative humidity profile may not be realistic. The individual cells were embedded in a broad band of precipitation. The synoptic situation suggests that the line probably existed in a region of synoptic-scale ascent associated with the approaching trough and a superimposed region of mesoscale ascent associated with the convergence line along which the convective line formed. It could be speculated that this reinforced ascent worked in concert with precipitation detrained from cells to produce the band of weak precipitation in which the thunderstorms were embedded. If this was the case, the cells could be occurring in a saturated or nearly saturated environment. X3 was conducted to investigate the effect of the environment being saturated. All input variables were the same as in X1 except that the relative humidity was 100% at all levels.

The result was the vigorous, deep convection shown in Figure 4.6, a time-height diagram of reflectivity for the inner cylinder. It is interesting to note that the cell continued to grow vertically after it had achieved its maximum reflectivity. This was probably caused by the sudden increase in lapse rate above 7.5 km.

Experiment 4

The first three experiments used values of r and σ which were determined from all the cells in the line. In this and the next experiment, an attempt was made to simulate just the strongest cells. The inner radius and σ were found by averaging the values for the $E_{40,40}$ A_2 criterion for both times. This included data from only those cells with a maximum intensity of at least 40 dBZ in both the lowest two CAPPI's. The resulting r was close enough to the 1.25 km used in the first three experiments to retain that value. The resulting σ was 0.23. All other input variables were the same as in X1.

The result, shown in Figure 4.7, differs only slightly from the result of X1 (see Figure 4.5). The cell is slightly more intense than that from X1, but certainly no more realistic.

Experiment 5

In X3, a respectable cell was produced by saturating the atmosphere in the situation from X1. In this experiment, the same thing is done for X4. Thus, a saturated atmosphere was assumed with $r = 1.25$ and $\sigma = 0.23$. The result, shown in Figure 4.8, was a cell similar to, but slightly stronger than the cell from X3.

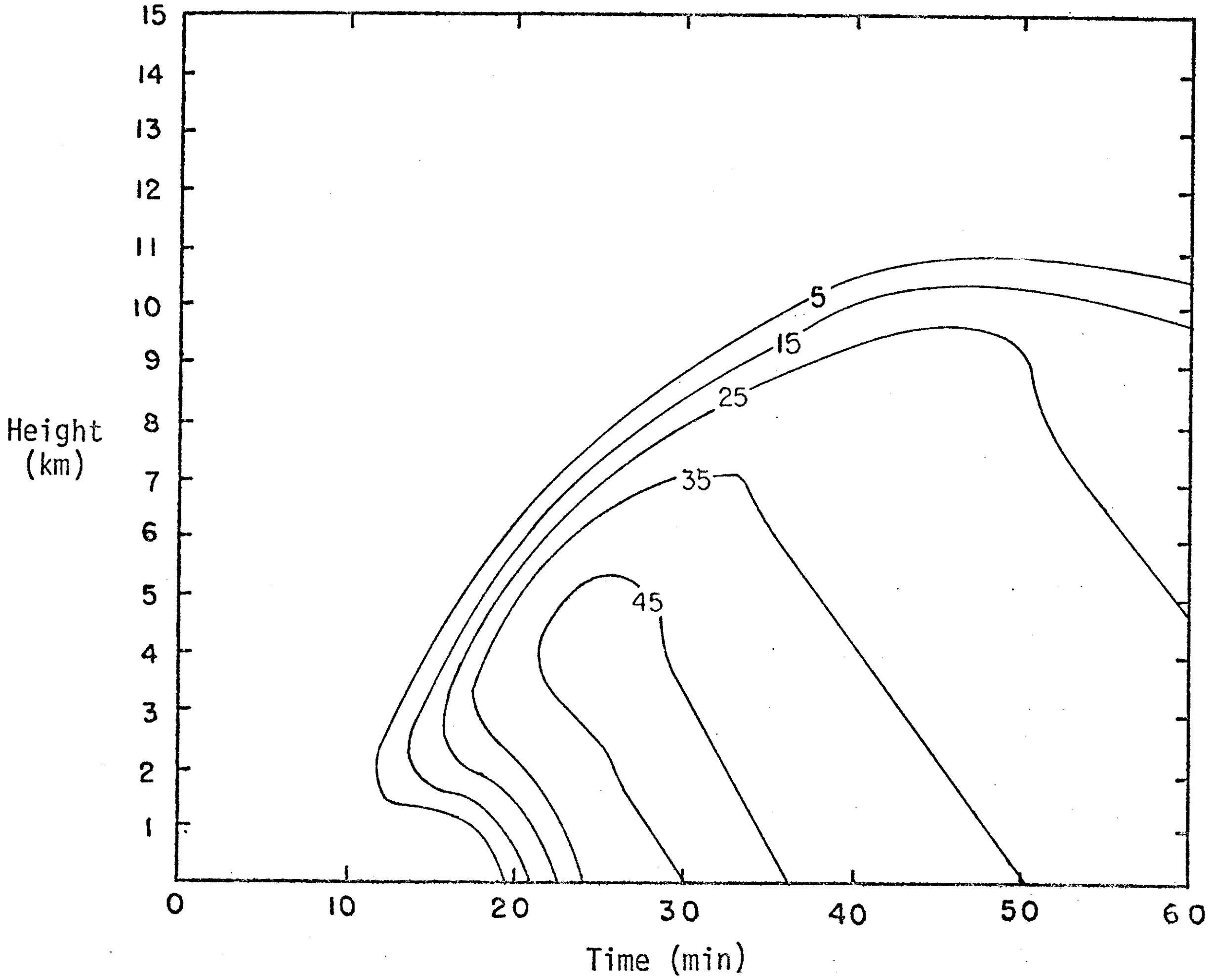

Figure 4. 6. Time-height diagram of reflectivities for X3. Contours are in dBZ.

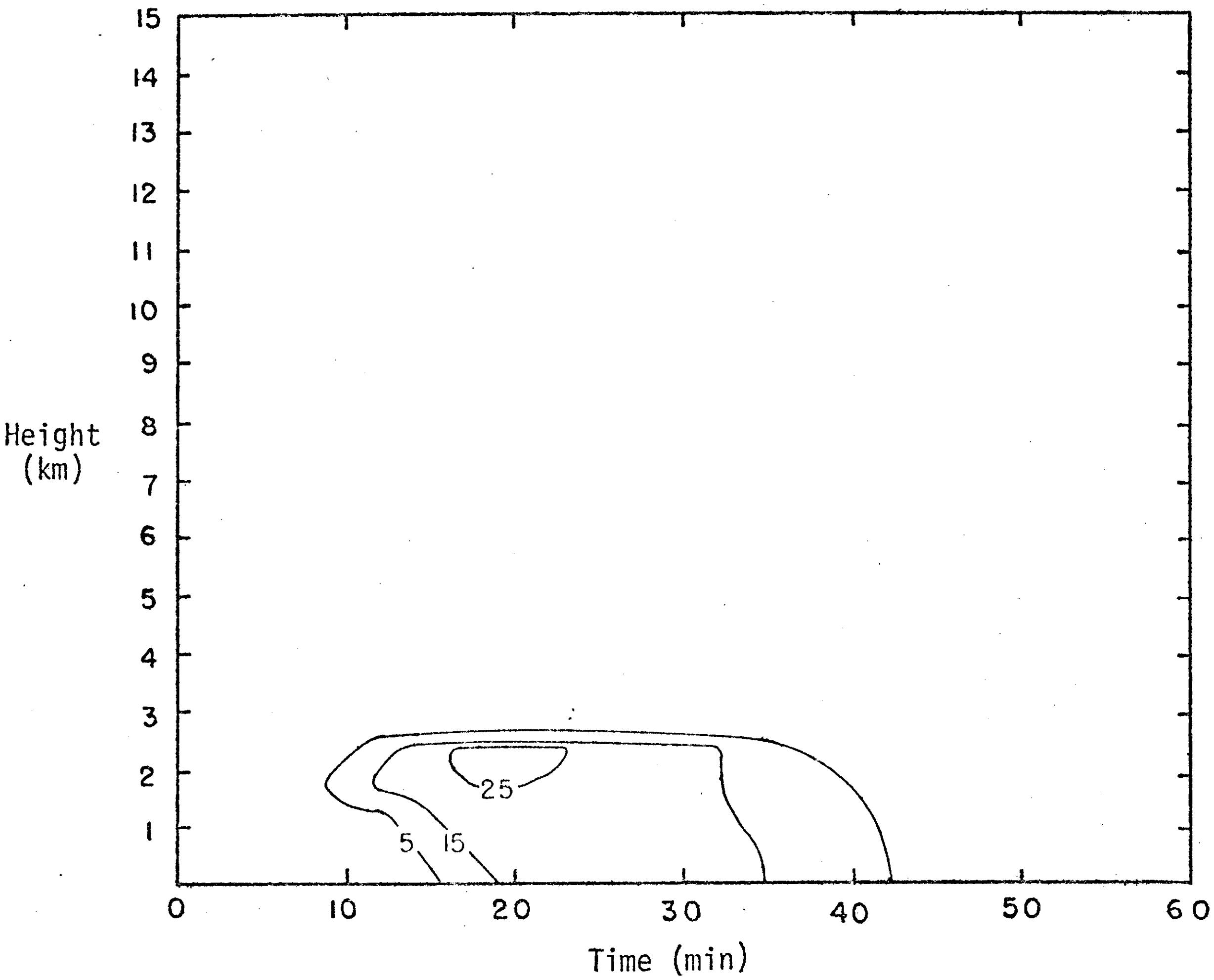

Figure 4.7. Time-height diagram of reflectivities for X4. Contours are in dBZ.

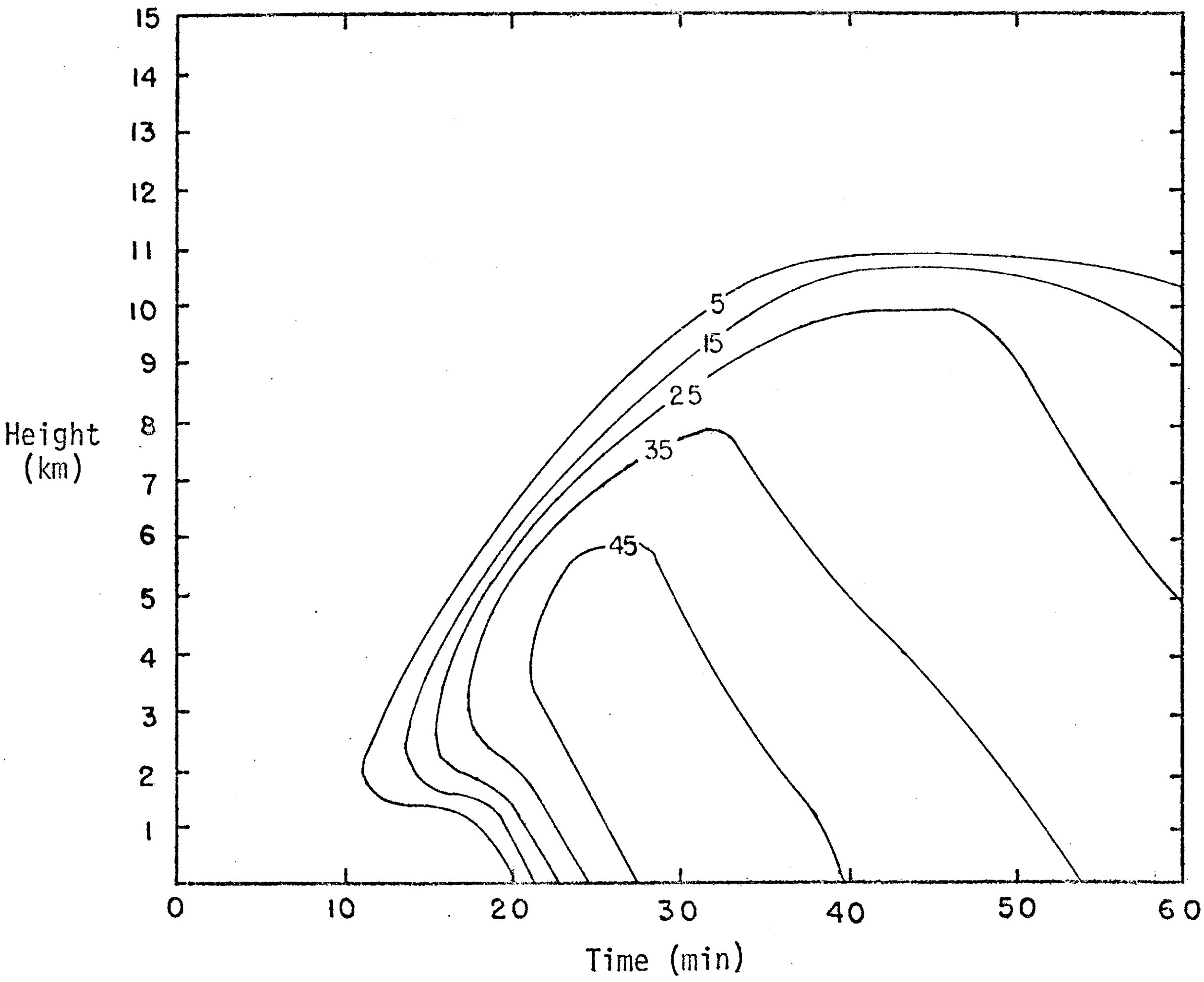

Figure 4.8. Time-height diagram of reflectivities for X5. Contours are in dBZ.

Experiment 6

It seems likely that the earlier convective cells assisted the presumed mesoscale updraft in humidifying the region around the line. If this was indeed the case, the regions toward the ends of the line, where the cells were more widely distributed in space and time, would be expected to be more humid than the surrounding environment (i.e., Type I sounding) but less humid than the region in the center of the line. This experiment was run to see what type of cell the model would produce in such a situation. The relative humidity was assumed to be 90% at all levels and the other input variables were the same as in X3.

Figure 4.9 is a time-height chart of radar reflectivity for the resulting cell. It grew only half as tall as the cell from X3 and had a maximum reflectivity of about 36 dBZ. Both the assumptions and the results of this experiment represent the "middle ground" between X1 and X3.

Experiment 7

In spite of the differences in σ, X3 and X5 produced cells of the same height. X7 was a deliberate attempt to produce a taller cell by changing the inner cylinder radius to 1.50 and σ to 0.17. Although the data show that neither of these values is unreasonable, they would not be expected to occur simultaneously because large inner radii are associated with large σ. Thus, this experiment was more contrived than realistic. All variables except r and σ were the same as in X3.

The result, shown in Figure 4.10, was a cell that was considerably more vigorous than that from X3, but only .5 km taller. These results seem to indicate that even with a saturated atmosphere and helpful hori-

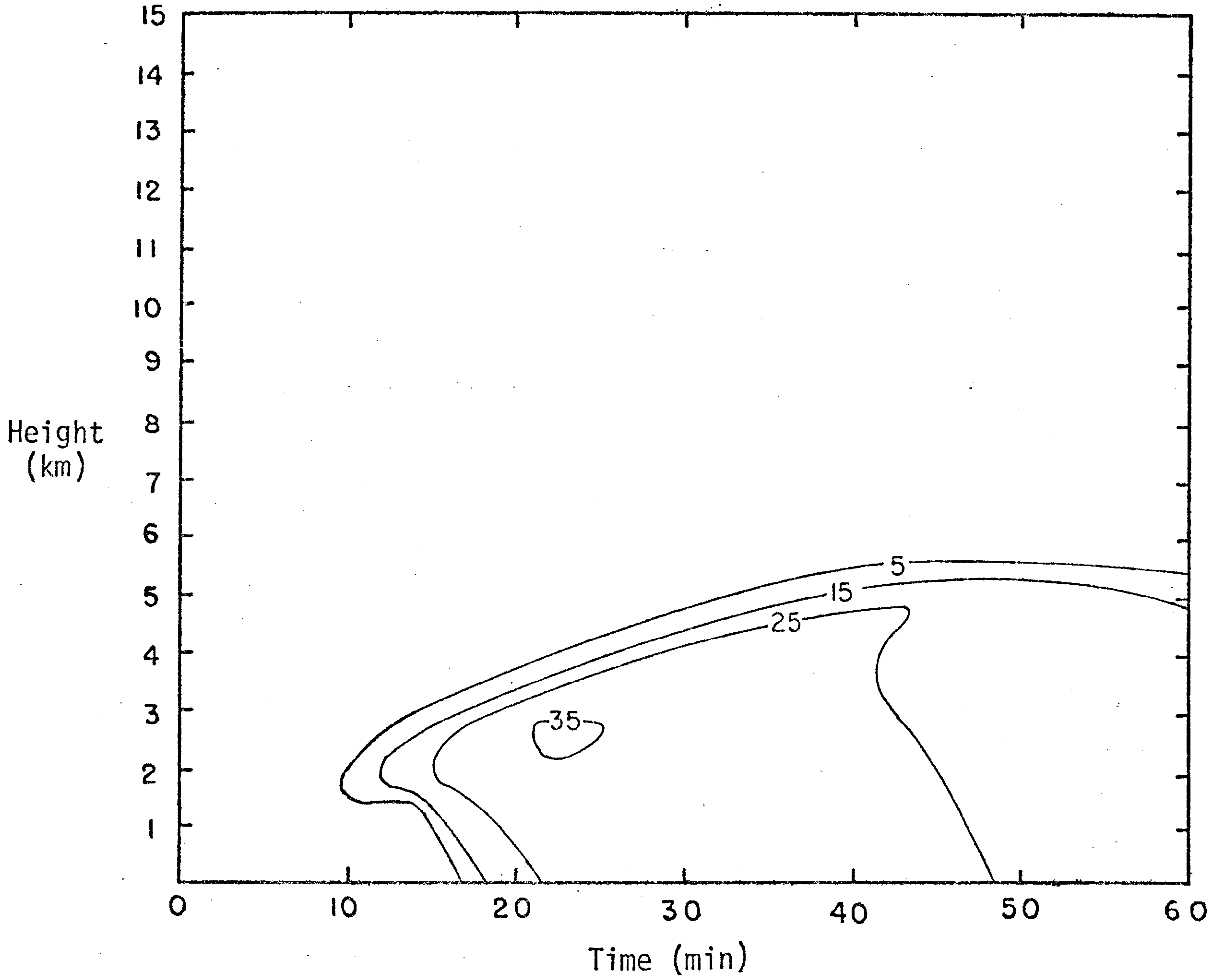

Figure 4.9. Time-height diagram of reflectivities for X6. Contours are in dBZ.

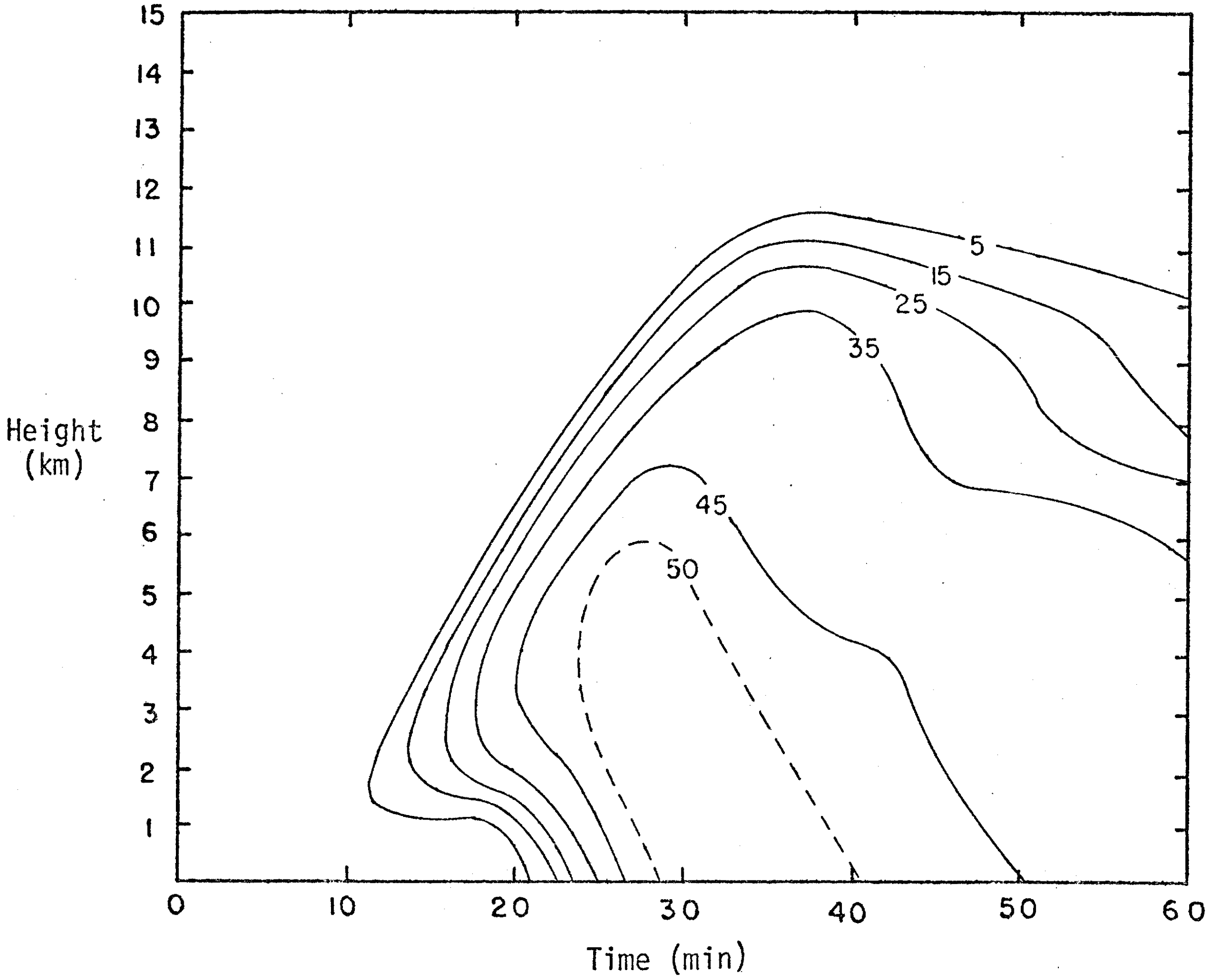

Figure 4.10. Time-height diagram of reflectivities for X7. Contours are in dBZ.

zontal dimensions, the model can produce cells no taller than about 11 km. It is possible that taller cells could be produced by increasing the lapse rate; however, because the vertical temperature profiles were so consistent in the situation being modeled, it would have been unrealistic to increase the lapse rate in order to try to produce taller cells.

4.2.2 Experiments 8-12, Humidification of Dry Layer by Convective Activity

An analysis of the moisture budget in X1 showed that the moisture perturbation added 21.1×10^9 g of water to the inner cylinder while only 1.4×10^9 g rained out of both cylinders combined. Thus, considerable moistening of the atmosphere took place. It seemed possible that if the final atmosphere from X1 was used as the initial atmosphere for another cell, further humidification would take place. If so, perhaps the atmosphere would be moistened sufficiently to produce a fairly strong cell by repeating this process a number of times. Experiments 8-12 tested this hypothesis. Area-weighted means of the final temperatures and relative humidities from X1 were used to initialize X8. The results of X8 were used to initialize X9, and so on.

Table 4.8 gives the moisture added in the impulse, the rainfall from both cylinders during the course of the integration, the maximum reflectivity, and the maximum height for experiments 1 and 8-12. In X8-X12, precipitation was still occurring at the end of an hour's integration. Had the integration been run longer, some of this precipitation would have evaporated to add more moisture to the atmosphere while the remainder would have rained out. In any case, it was lost to the process because the model does not allow for initialization with ongoing precipitation. The relative humidity profiles below 2 km in X8-X12 were similar enough that it was safe to assume that approximately the same amount of moisture was added in the moisture impulses.

Table 4.8. Results of X1 and X8-X12.

Experiment	Moisture Added (10^9 g)	Total Rainfall[1] (10^9 g)	Maximum Reflectivity (dBZ)	Maximum Height (km)
X1	21.1	1.4	27.8	2.5
X8	≈ 21-22	4.5+	33.1	4.0
X9	"	5.6+	33.2	4.5
X10	"	6.5+	33.4	5.0
X11	"	6.8+	33.3	5.5
X12	"	6.0+	32.5	5.5

Figure 4.11a shows relative humidity profiles before and after X1, and after X8 and X9. Figure 4.11b shows relative humidity profiles before X1 and after X10, X11, and X12. Most of the moisture from the first three cells goes to humidify the low layer. The last three cells carry much of their moisture into the dry layer. The final cell reached a height of 5.5 km.

At first glance, the process appears to be working, albeit slowly. However, there were some discouraging changes taking place in the stability of the atmosphere. Overall (i.e., throughout the depth of the model), the atmosphere was becoming less stable, a consequence of cooling due to dry adiabatic ascent in the upper regions of the model, coupled with heating

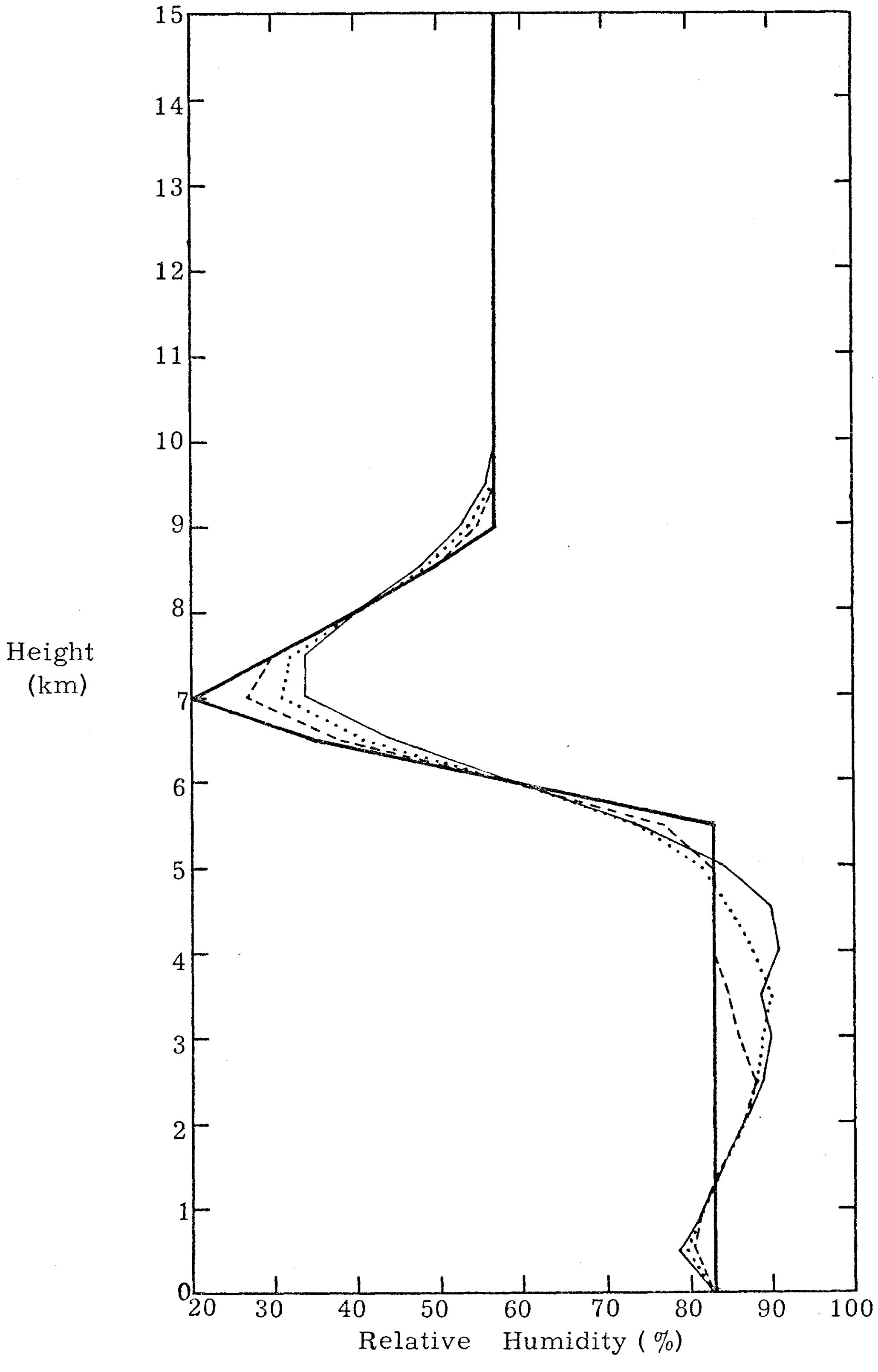

Figure 4.11(a). Successive relative humidity profiles. Before X1▬, after X1---, after X8·····, after X9—.

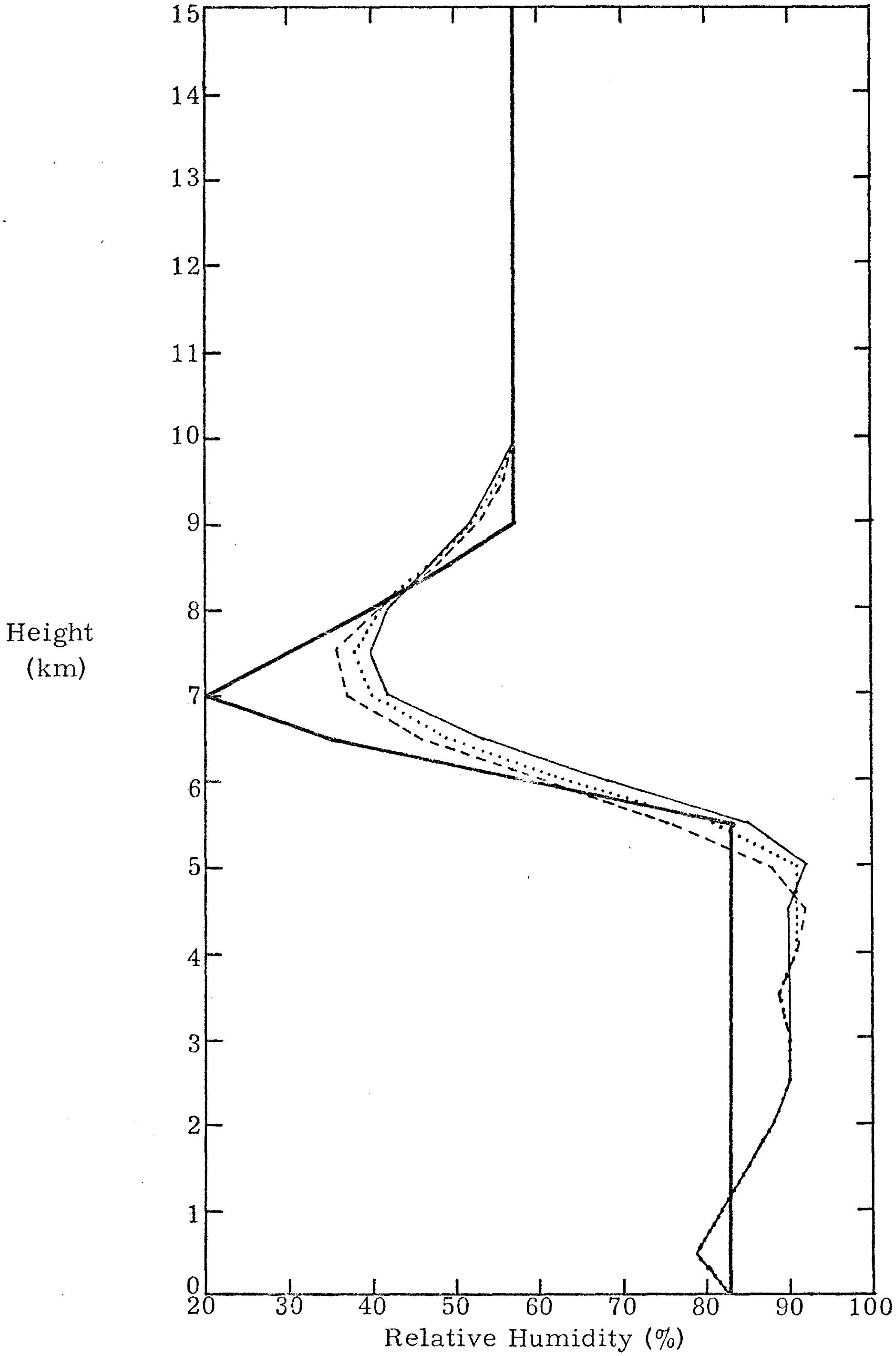

Figure 4.11(b). Successive relative humidity profiles. Before X1 ▬ , after X10---, after X11·····, after X12— .

due to condensation in the lower regions. This increased instability, however, was not available to the cells because the lack of moisture above 6 km cut off their growth. In the region in which the cells were growing, an interesting sequence of changes in stability occurred. X1 provided latent heat to a thin layer near the ground. X8-X11 tapped this instability along with the added moisture to produce relatively strong reflectivities and large rain accumulations. However, the maximum reflectivities decreased after X10 and the rain accumulations started to decrease after X11. This seems to indicate that once the depth of the convection has more or less stabilized, the degree of instability in the region in which it is occurring decreases with each succeeding cell. This comes as no surprise -- convection exists just for this purpose. However, it does not encourage acceptance of the hypothesis that a relatively dry atmosphere may be humidified by initiating successive moist convective cells within it. It appears that continuing this process would result in further decreasing the instability of the layer in which the cells are occurring. This, in turn, would result in less vigorous cells whose assaults on the dry layer would become more feeble. It would be difficult, short of expending a great deal of computer time, to determine where this process would lead. However, it is unlikely that sufficient time would exist to carry it through to possible fruition without some interaction with larger-scale processes taking place.

4.2.3. Experiments 13-15, Simulation of a Mesoscale Process

The model formulation does not allow any explicit inclusion of mesoscale processes. Some mesoscale processes, however, may be included implicitly in the choice of input variables. X3 and X5 are examples of implicit inclusion of mesoscale effects. In those experiments the atmosphere was assumed to be saturated, while any synoptic and mesoscale motions which might have contributed to the saturation were, by necessity, ignored. In experiments 13-15 an effort is made to deal implicitly with these motions.

An updraft is weakened in two ways by descent in the outer cylinder -- the air that is entrained carries downward momentum and has been dried by adiabatic descent. However, because the areas of outer cylinders are larger than areas of inner cylinders, the compensatory motions in the outer cylinders are generally weak. Mesoscale ascent assumed in the region of the line will work against the descent in an outer cylinder tending to minimize it and its effects on the updraft. To simulate the effect of a mesoscale updraft counteracting the convectively driven downdraft in an outer cylinder, σ may be given a very small value. This produces an extremely large outer cylinder and reduces vertical motions in that cylinder to near zero, but does not directly affect the inner cylinder. This approach will be tested in X13-X15.

Experiment 13

In this experiment, the input variables were the same as in X1 except that σ was set to 0.01. The resulting cell is shown in Figure 4.12. In this experiment, much less downward momentum was entrained from the outer cylinder than was entrained in X1. However, the size of the outer cylinder made it a continual source of relatively dry air for entrainment -- the detrained moisture was simply swallowed up by the outer cylinder.

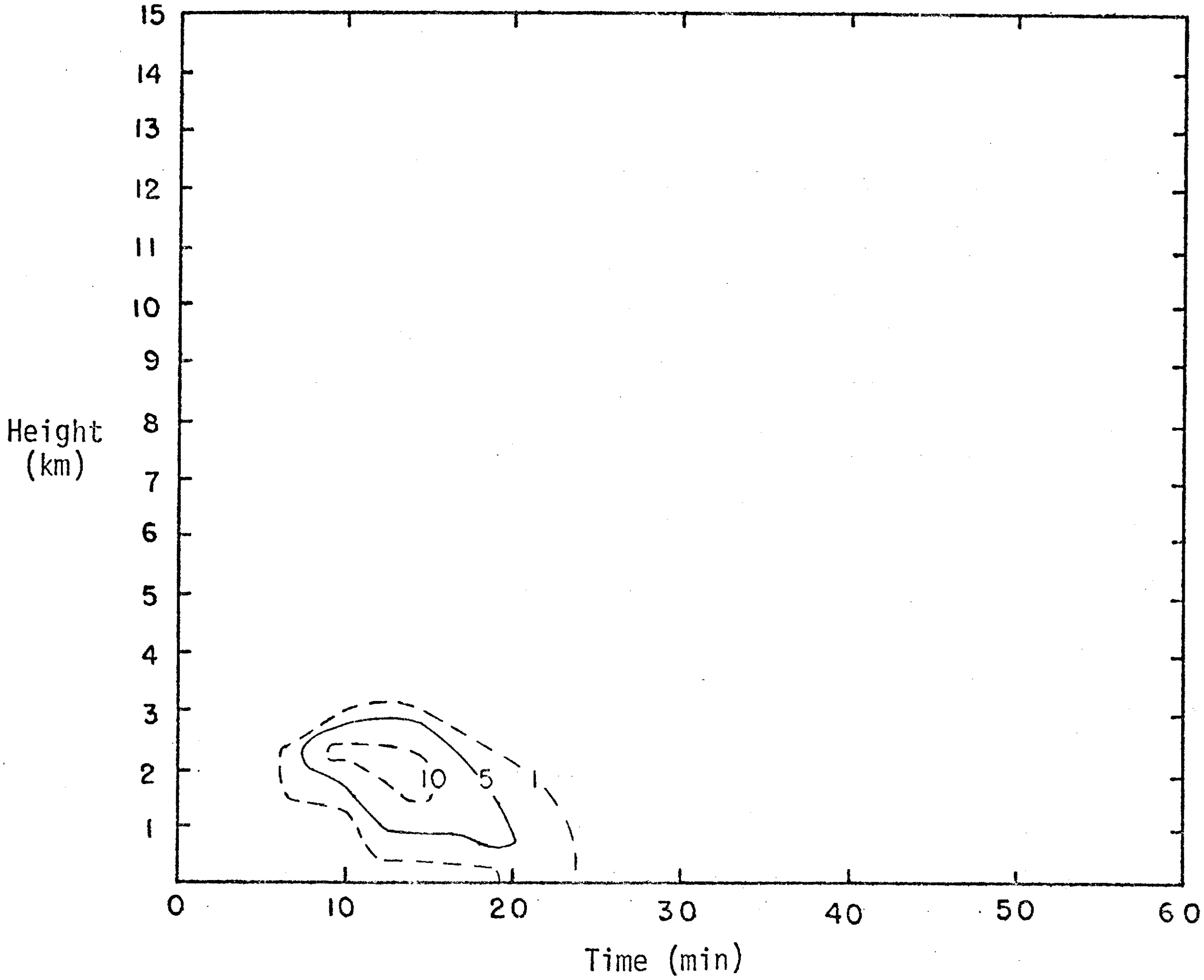

Figure 4.12. Time-height diagram of reflectivities for X13. Contours are in dBZ.

This dry air weakened the cell and shortened its life.

Experiment 14

To avoid the problem of the outer cylinder being an almost unlimited moisture sink, the atmosphere was saturated in X14. Otherwise, the input variables were the same as in X13. The result, shown in Figure 4.13, was the most vigorous cell generated thus far. It had an unrealistically high maximum reflectivity of over 57 dBZ and reached a height of 12 km. The dual effects of a continuous supply of saturated air and no downward momentum to entrain produced a cell of unrealistic vigor.

Experiment 15

In an effort to "tone down" the cell generated in X14, the relative humidity throughout the atmosphere was lowered to 90% in X15. The resulting cell, shown in Figure 4.14, was surprisingly weak. X6, by comparison, employed all the same input variables except $\sigma = 0.27$ and was noticeably more vigorous. The reason for this is that in the most vigorous portion of the updraft where the turbulent entrainment is greatest, the updraft in X6 had humidified the environment to well above 90% relative humidity, while in X15 the environmental relative humidity did not change from the initial 90%. Apparently, this moisture effect was more important than the counteracting momentum effect.

It can be concluded from this last series of experiments that the effects of reducing the downdraft to near zero by making σ very small, are secondary to the effects, also brought about by making σ small, of

Table 4.9. Important input variables for X1-X15.

Experiment #	Inner Radius (km)	σ	Relative Humidity Profile	Temperature Profile
X1	1.25	.27	Type I (see Fig. 4.4)	corresponding to Type II relative humidity profile (see Fig. 4.4)
X2	1.25	.27	83% up to 8.5 km 57% above 8.5 km	"
X3	1.25	.27	Saturated throughout	"
X4	1.25	.23	Type I	"
X5	1.25	.23	Saturated throughout	"
X6	1.25	.27	90% throughout	"
X7	1.50	.17	Saturated throughout	"
X8	1.25	.27	Result of X1 (see Fig. 4.9a)	Result of X1
X9	1.25	.27	Result of X8 (see Fig. 4.9a)	Result of X8
X10	1.25	.27	Result of X9 (see Fig. 4.9a)	Result of X9
X11	1.25	.27	Result of X10 (see Fig. 4.9b)	Result of X10
X12	1.25	.27	Result of X11 (see Fig. 4.9b)	Result of X11
X13	1.25	.01	Type I	As in X1
X14	1.25	.01	Saturated throughout	"
X15	1.25	.01	90% throughout	"

Table 4.10. Characteristics of model cells from X1-X15. All results are from inner cylinder.

Experiment #	Max Top (km)	Maximum Reflectivity dBZ	time (min)	height (km)	Maximum Rainfall Rate (mm hr^{-1})	time (min)	Cumulative Rainfall (cm)
X1	2.5	27.8	19	2.25	0.7	27	0.02
X2	2.5	27.8	19	2.25	0.7	27	0.02
X3	11.0	46.9	24	4.25	48.6	34	1.31+
X4	2.5	28.2	18	2.25	0.8	22	0.02
X5	11.0	48.6	26	3.75	68.4	32	1.77+
X6	5.5	35.9	23	2.75	6.1	33	0.20+
X7	11.5	53.3	29	3.75	121.5	34	3.24+
X8	4.0	33.1	21	2.75	2.9	28	0.06+
X9	4.5	33.2	21	2.75	3.2	30	0.08+
X10	5.0	33.4	21	2.75	3.2	30	0.09+
X11	5.5	33.3	21	2.75	3.3	30	0.10+
X12	5.5	32.5	22	2.75	2.8	29	0.09+
X13	3.0	14.2	11	2.25	0.04	21	0.0006
X14	12.0	57.6	31	3.25	173.0	35	4.81+
X15	4.0	29.6	17	3.25	1.6	26	0.03

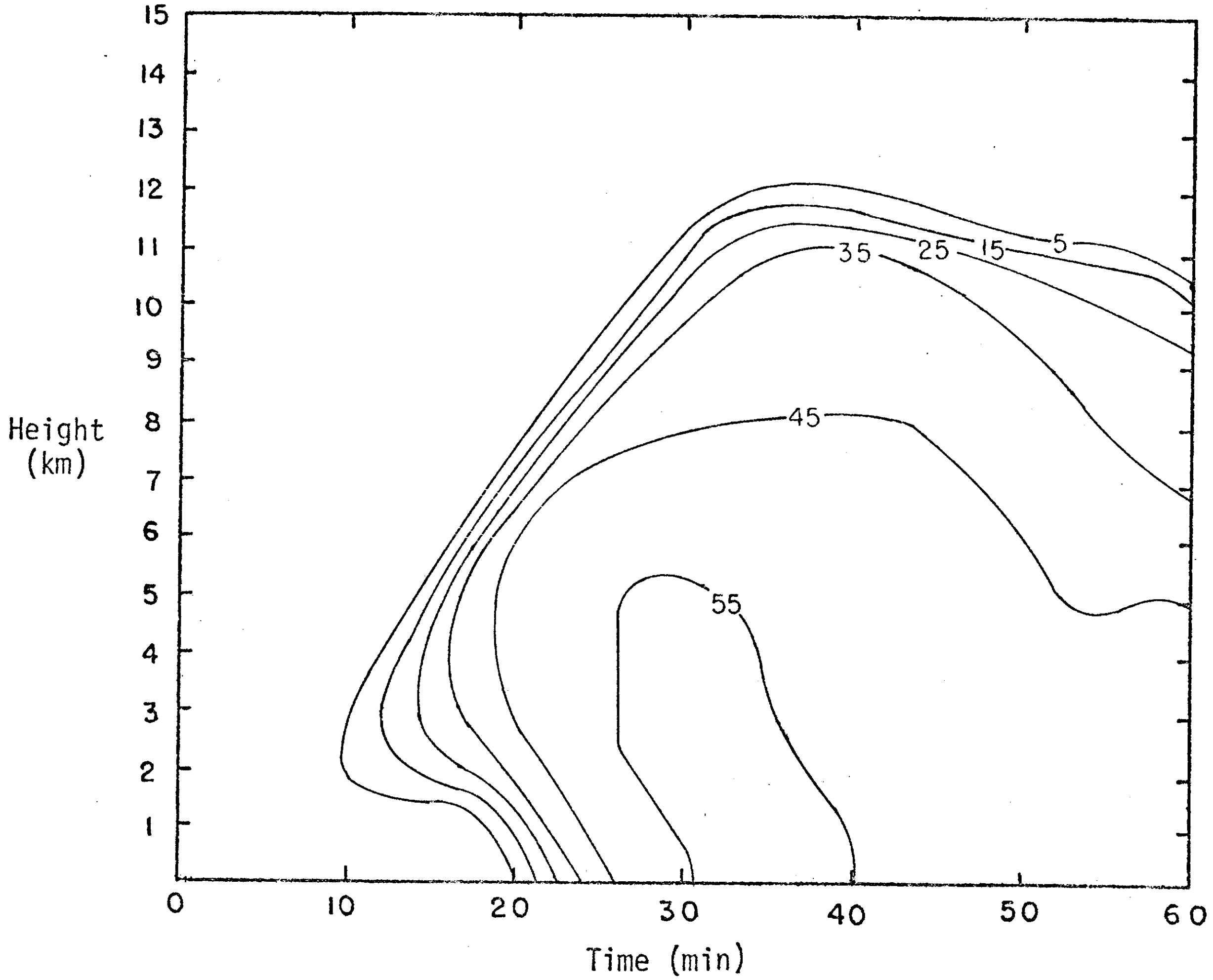

Figure 4.13. Time-height diagram of reflectivities for X14. Contours are in dBZ.

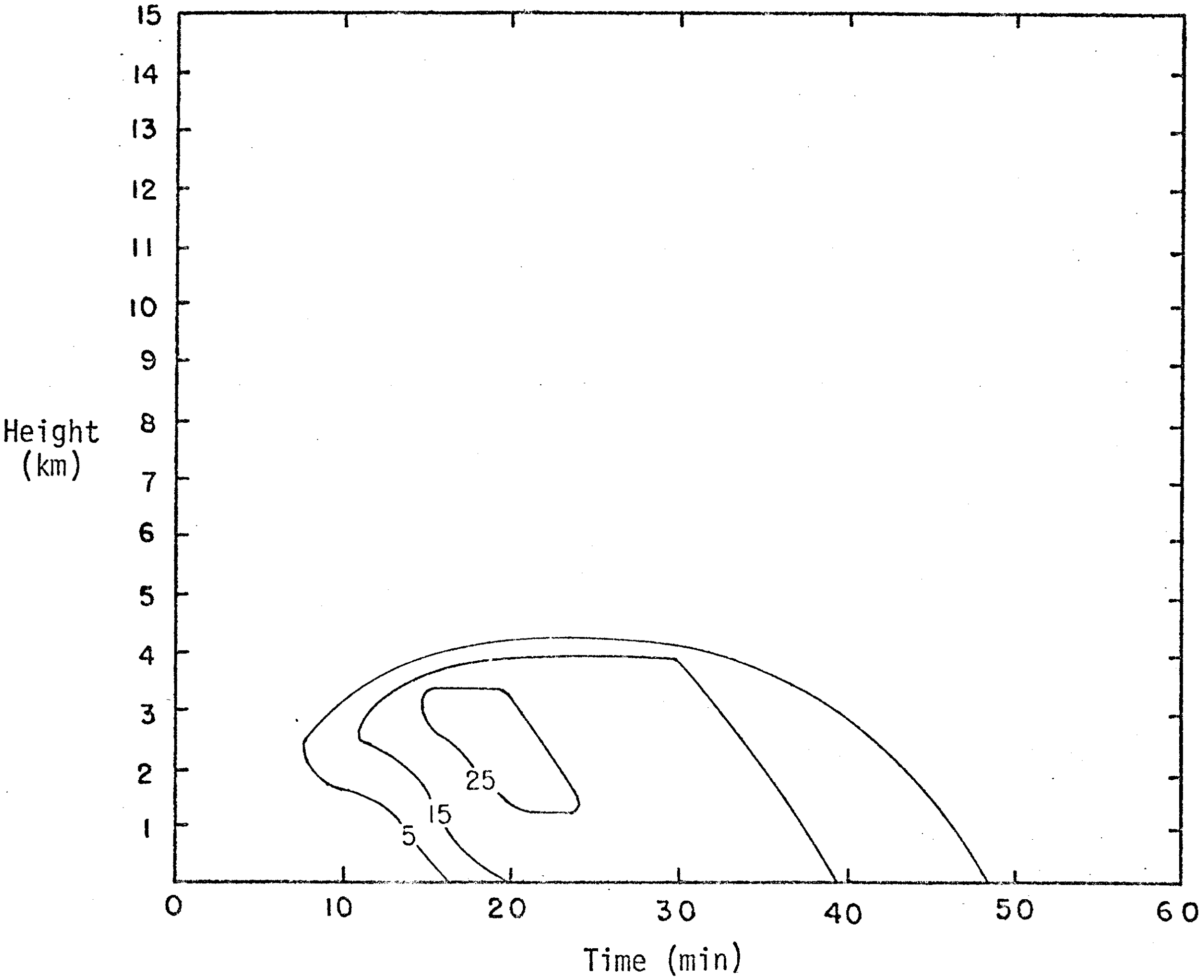

Figure 4.14. Time-height diagram of reflectivities for X15. Contours are in dBZ.

averaging detrained moisture over an extremely large outer cylinder. Since the purpose of making σ small was to simulate the effects of mesoscale motion in counteracting the downdraft in the outer cylinder, these results indicate that the simulation was not effective.

4.2.4. Comparison of Model Output to Observed Data

Preliminary investigation indicated that the cells produced in experiments 3 and 5 were the most likely to compare favorably with observed cells. Although cells from other experiments will be mentioned occasionally, these two experiments will bear the bulk of the comparison, which will be made in accordance with the procedures suggested in section 3.1.4.2.

Maximum tops

Digital radar maps displaying maximum tops of echoes to the nearest kilometer were constructed from Gilliss radar data at 15-minute intervals from 0630Z to 1001Z. From these maps, it was possible to determine the trends in the height of the precipitation canopy lying over the line. Figure 4.15 is an analog max-tops map for 0830Z which may be compared with Figure 4.1, the corresponding map of low-level reflectivities. In Figure 4.15 light gray represents max-tops of 6 to 9 km, dark gray represents max tops of 10 to 12 km, and black represents max tops of 13 km. This map, which is reasonably representative of all the max-tops maps, shows that in the regions of most active convection, tops are generally 10-12 km with some towers to 13 km. Tops are generally lower toward the ends of the line where cells are more widely separated (probably in both space and time) and the convection is less vigorous. Even in these areas, the cells sometimes reached heights of 10-11 km, but apparently their sparsity precluded

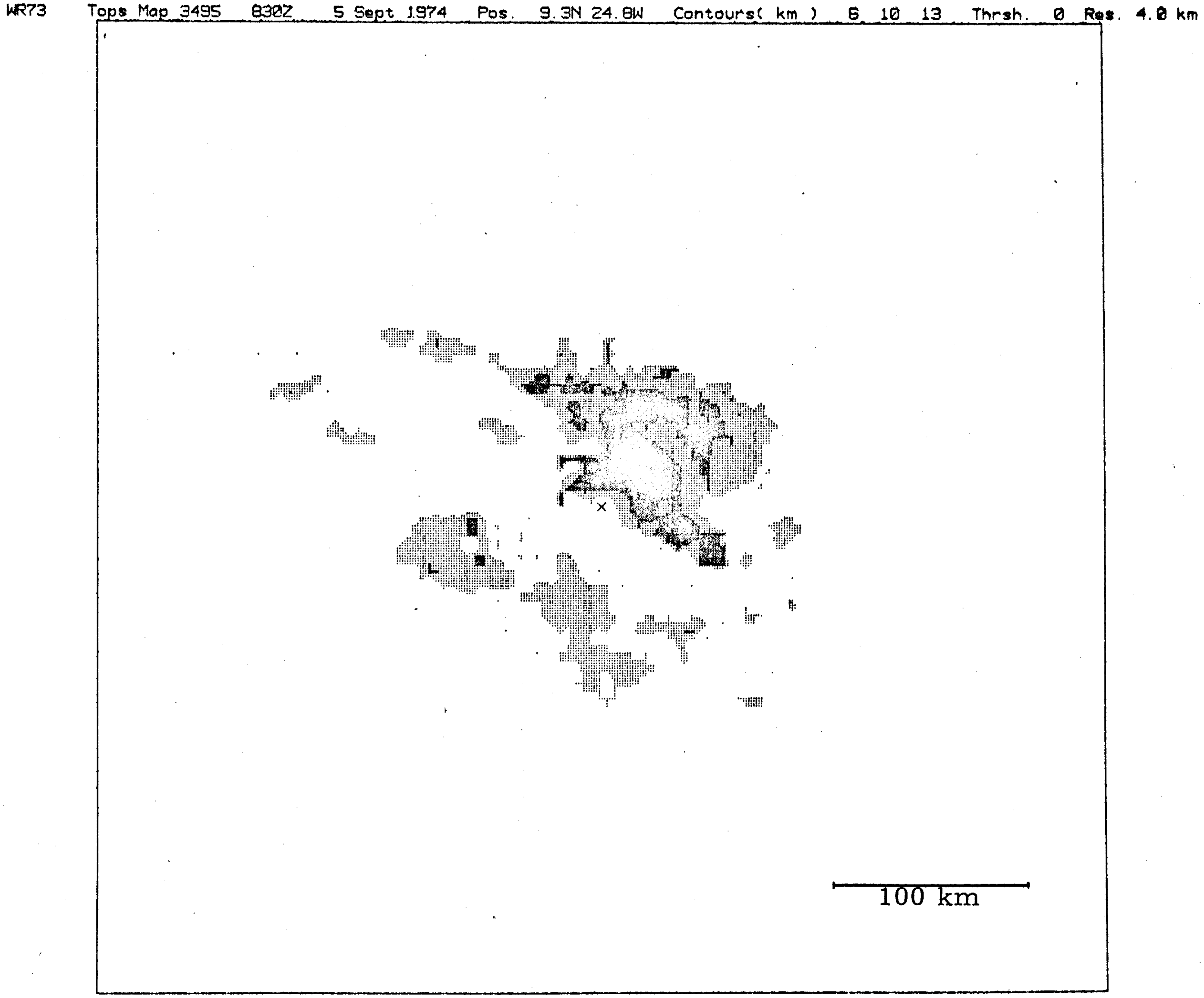

Figure 4.15. Max-tops radar map of line at 0830Z. Contours are 6, 10, and 13 km.

the formation of a canopy. It appears that the 11 km height achieved in X3 and X5 was fairly realistic. However, the model failed to simulate those cells with tops to 13 km. X7, which used questionable input variables in an attempt to produce a taller cell, produced a cell that reached only 11.5 km. The cell from X14 was 12 km high, but was presumed to be unrealistic because of its exceptionally high reflectivity. The failure of the realistic cells to reach 13 km might be attributed to the loss of the latent heat of fusion in this version of the model which does not include the ice phase. Experiments by Yau (1977) which included the ice phase suggested that its inclusion would cause model cells to grow slightly taller.

Maximum Reflectivity

The spectrum of observed maximum reflectivity of the cells in the convective line is plotted in Figure 4.16 in the solid line. This spectrum includes all cells used in the idealization process for the $E_{1,1}$ existence criterion for 0815Z and 0830Z combined -- a total of 74 cells. The dashed line in the same figure is the time spectrum of maximum reflectivity from X3 for the 34 minutes during which its maximum reflectivity was within the range of values given on the graph. The numbers in the time spectrum were multiplied by a constant to make its sample size the same as that of the observed data. Both spectra were determined from data below 4 km averaged over a 2 km depth (i.e. for 0-2 and 2-4 km).

Even if the model simulated the representative cell perfectly, these two spectra would not be expected to be identical. Thus, it is difficult to decide how much of the discrepancy between the spectra is

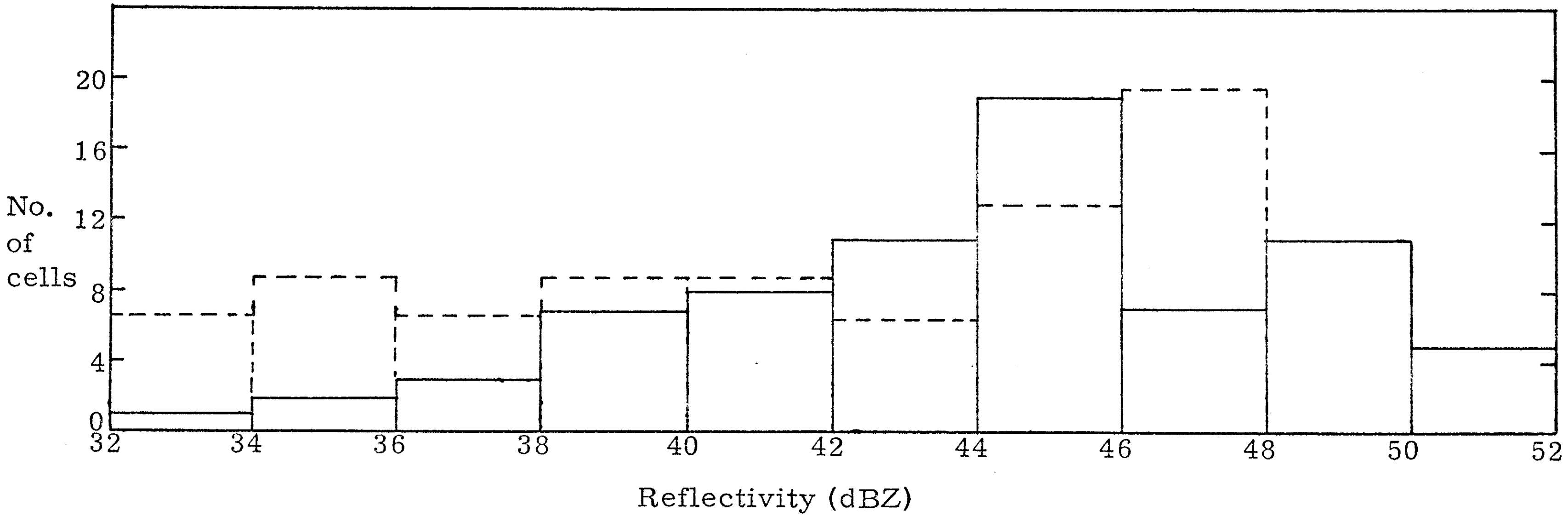

Figure 4.16. Model and observed spectra of maximum reflectivity. Observed ($E_{1,1}$ criterion) ——, model (X3)--- . See text.

attributable to variations in the observed cells and how much of it should be blamed on the model's inability to simulate the representative cell. The differences in the two highest reflectivity categories can probably be attributed to variations in the observed cells. The differences in the lower categories could be caused by observed cells being masked by the general precipitation. In any case, considering the myriad assumptions and approximations made to determine the input variables for the experiment and the inherent weaknesses in the model, the similarity of the spectra is encouraging.

Height of Maximum Reflectivity

The distribution of observed heights of reflectivity for the convective line was found by the method given in section 3.3.4.2. This distribution included data from 0815Z and 0830Z combined and was determined for thresholds of 30 and 40 dBZ. For comparison, the output from X3 was investigated to determine during what part of its lifetime its maximum reflectivity was greater than or equal to the same thresholds. The distribution of the height of the maximum reflectivity during this portion of the life cycle was then found. The results are shown in Table 4.11.

The agreement between the distributions for the 40 dBZ threshold is fairly good. The distributions for the 30dBZ do not agree quite so well. A possible reason for this may be seen in Figure 4.16. Although the input variables for X3 were determined using cells with reflectivity maxima as low as 32 dBZ, the contribution by cells with maxima below 40 dBZ was small. Thus, we should expect better agreement for the comparison employing the 40 dBZ threshold.

Table 4.11. Distribution of radar-observed and model (X3) heights of maximum reflectivity. For radar: % of columns in which reflectivity maximum was at given height for given thresholds. For model: % of time during which the reflectivity maximum exceeded the threshold that the maximum was located at the given height.

	Threshold(dBZ)	Height (km)			
		0-2	2-4	4-6	6-8
Radar	30	56	34	9	1
	40	49	40	11	0
Model (X3)	30	68	24	8	0
	40	54	32	14	0

Although this evaluation is subjective, it seems to indicate that the model did a reasonable job of locating the height of the maximum reflectivity when a suitably strong threshold was employed. Since the inner-cylinder maximum reflectivity, when it is stationary or rising, generally corresponds to the maximum updraft and, when descending, usually occurs just below the maximum downdraft, it may be inferred that the model is doing a reasonable job of locating the most vigorous vertical motion.

Rainfall Rate

Surface rainfall was measured as the convective line passed over the *Gilliss* at about 1000Z. Five cumulative rainfall measurements allowed the estimation of rainfall rates at four times by finite differencing. The observed rainfall rate, estimated from the rates at the four times, is plotted in Figure 4.17 in a solid line. In the same figure, rainfall rates from X3 (dashed) and X5 (dotted) were plotted such that their maxima coincided with the maximum for the observed rate. The similarity in the shapes of the curves is striking, especially when one considers that the observed data were taken as a cell passed over the ship while the model data were calculated at the base of the inner cylinder throughout the life of the model. Since it is not known how representative the cell that passed over the ship was, where it was in its life cycle, or what portion of it passed over the ship, this comparison is crude at best. It indicates merely that the observed and the model rainfall rates are in the same ballpark,

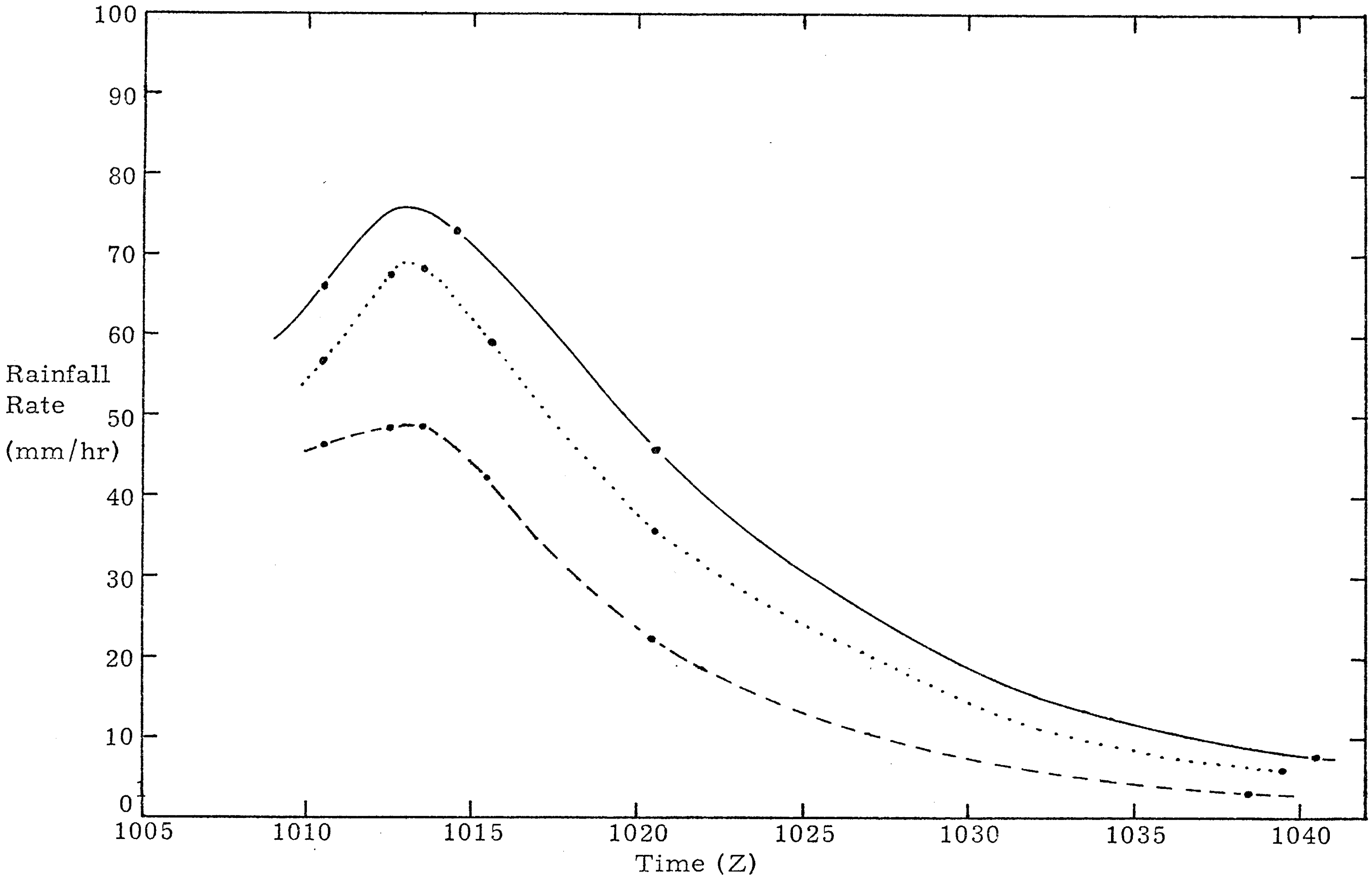

Figure 4.17. Observed and model rainfall rates. Observed——, X3---, X5·····.

4.3 Summary

The cells in the 5 September GATE line have been modeled using input variables determined by idealizing the line and its environment. The moisture in the open atmosphere around the line was found to be insufficient to support deep convection in the model. Model cells which compared favorably with observed cells were produced by assuming that the atmosphere within the line was saturated. An attempt was made to humidify the dry layer in the Type I relative humidity sounding by initiating successive cells in the same environment, permitting each of them to modify it. Although the moisture impulses did add a considerable amount of moisture to the atmosphere, the process was slow and seemed to be decreasing the available instability. Finally, σ was assumed to be very small in an attmept to simulate the effects of mesoscale ascent counteracting the convectively driven downdraft in the outer cylinder. The assumption caused the outer cylinder to become an almost unlimited source or sink of moisture, which made the model extremely sensitive to humidity and masked the desired momentum effects.

CHAPTER FIVE

SIMULATION OF CELLS IN A CLUSTER

A small cluster of convective cells developed near the Gilliss on the afternoon of 1 September 1974. In this chapter, the cluster and its environment are described and idealized. Two sets of experiments are run using idealized input, and their results are compared to observed data to determine how well the model simulated the cells.

5.1 The Cluster and Its Environment -- Observed and Idealized

5.1.1 Description of the Cluster and Its Environment

Marks and Raub (1978) found that there was little organization in the precipitation patterns near the ridges (wave sectors 1, 7, and 8) during GATE phase III. During the afternoon of 1 September the B-scale array was experiencing weak northeasterly flow characteristic of wave sector 1, and clusters of convective cells were scattered randomly about the array. The cluster under consideration in this chapter, shown circled in Figure 5.1, appeared at about 1430Z 30 km south of the Gilliss. It persisted for about three hours, moving toward the southeast at about 3 m sec^{-1}. At 1445Z it covered an area of only 30 km^2 but grew to nearly 150 km^2 by 1614Z, and was composed of from one to five identifiable cells at any given time during its life. Because its scale was small compared to the spacing of observations, there was no evidence of synoptic or mesoscale features having any effect on the cluster.

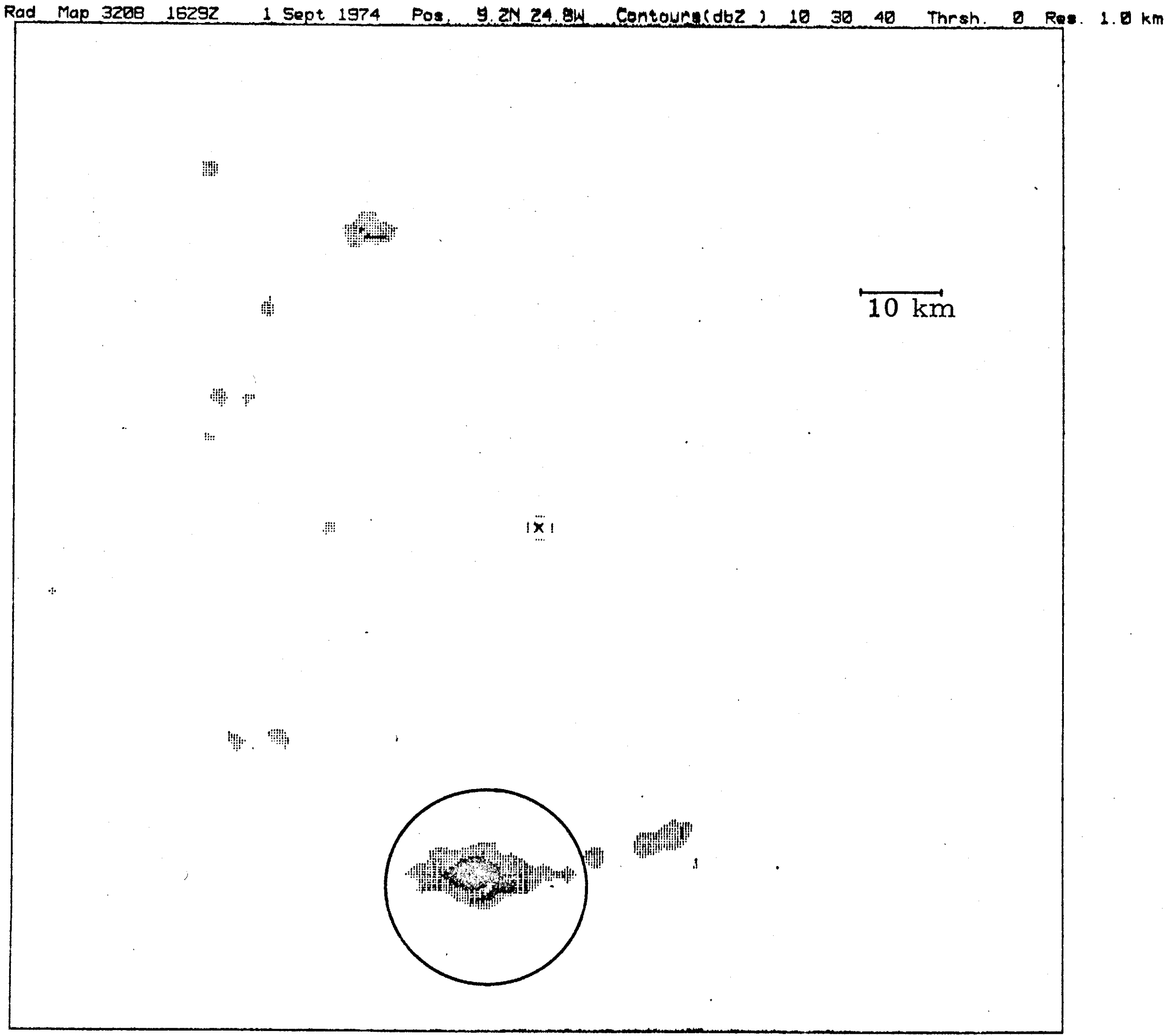

Figure 5.1. Cluster at 1629Z as seen by radar aboard the <u>Gilliss</u>. Contours are 10, 30, 40 dBZ.

5.1.2 Idealization of the Cluster and Its Environment

5.1.2.1 Idealization of the Cluster

Three-dimensional radar charts showing the cluster at 15 to 30 minute intervals between 1445Z and 1715Z were constructed as described in section 3.3.2. These charts had a horizontal and vertical resolution of 1 km. Cores of maximum reflectivity were identified and their respective updraft areas were determined on the two lowest CAPPI's(0-1 and 1-2 km) using the A_1 and A_2 criteria for determining updraft areas (see section 3.3.3). The cores were determined to represent or not to represent cells based on five existence criteria. Each criterion required that a core exist in both layers, and the following additional requirements on maximum reflectivities of the cores were made:

$E_{1,1}$: no additional requirement;
$E_{30,1}$: at least 30 dBZ in at least one layer;
$E_{30,30}$: at least 30 dBZ in both layers;
$E_{40,30}$: at least 40 dBZ in one layer, 30 dBZ in the other;
$E_{40,40}$: at least 40 dBZ in both layers.

These criteria are progressively more exclusive, allowing investigation of all cells, or just those cells above a given intensity. The updraft area of each cell was then determined by averaging the updraft areas in the two lowest layers (combination criteria C_{avg}) and by using the maximum of the areas in the two layers (C_{max}).

The objective of this process was to produce an idealized cluster composed of identical "representative" cells. The updraft area of the representative cells was determined by averaging the updraft areas of the observed cells. The existence criteria designated five sets of cells whose areas were averaged. For each set of cells, the two area and two combination criteria defined four sets of updraft areas to be averaged. Thus, 20 different representative cell updraft areas were determined.

For the line considered in Chapter 4, the size of the outer cylinder of the representative cell was determined from the geometry of the line. This approach would not work for the cluster because its geometry was so ill-defined. Instead, the size of the outer cylinder was determined directly from the radar data on the assumption that the precipitation surrounding the updrafts was detrained from the updrafts and that its outer edge marked the "circumference" of an irregularly shaped outer "cylinder". On the CAPPI's for the two lowest layers, the total area of precipitation echo associated with the cluster was divided into portions such that each core had a separate surrounding area. The divisions were made along the minimum reflectivity between cores. The area of the downdraft of each cell was then assumed to be its surrounding precipitation area. This area varied depending on which A criterion was used. The A_1 criterion produced a smaller updraft and hence a larger downdraft than the A_2 criterion. The downdraft areas were then averaged in the same manner as were the updraft areas to produce 20 corresponding representative cell downdraft areas.

There is a fundamental difference between this process for determining the downdraft size for cells in the cluster and the process employed for cells in the line. When more exclusive existence criteria eliminated cells from the line, the method for determining the downdraft size had the effect of making the eliminated cells and the areas surrounding them become part of the downdraft of the remaining cells. In the process for the cluster, when a cell was eliminated by the adoption of a more exclusive existence criterion, its updraft and downdraft areas were discarded and did not affect the areas assigned to the remaining cells.

Because no more than five cells existed in the cluster at any time, the data from ten times between 1445Z and 1715Z were combined to form a sample of 25 cells for the $E_{1,1}$ criterion. The sample size, of course, decreased as E criteria became more exclusive. To make the representative cells geometrically compatible with the model, the updrafts were assumed to be cylindrical, the downdrafts were assumed to be concentrically cylindrical, and the radius of each was calculated from their areas. This yielded an inner cylinder radius r and a ratio of radii σ for the representative cells.

A schematic representation of the idealization process is shown in Figure 5.2. (a) shows the cluster after the cells have been identified and the associated precipitation divided into surrounding areas for each updraft. (b) shows the idealized cluster composed of the same number of cells, each with the average updraft and downdraft area. The results of the idealization process are presented in Table 5.1.

The most interesting feature in the data in Table 5.1 is the way the values of r and σ change as the E criterion changes because the E criteria define the strength of the cells used in the idealization process. The model predicts that larger radii lead to stronger cells. Except for the increase in r associated with the $E_{40,40}$ criterion, this effect is not

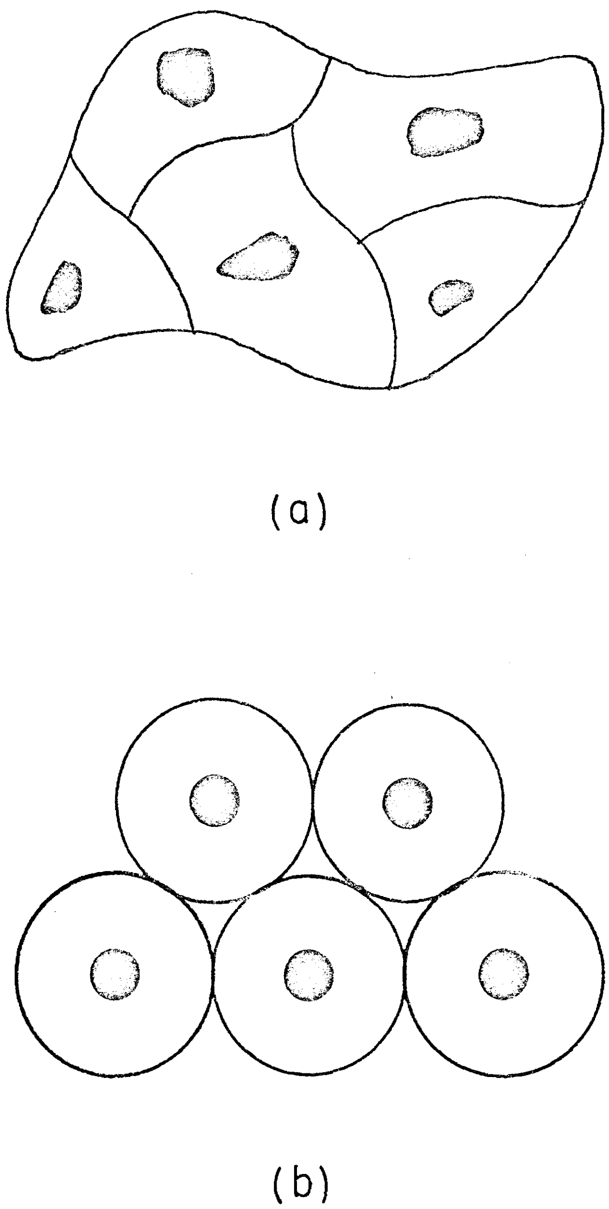

Figure 5. 2. Schematic representation of the idealization process for the cluster. (a), observed; (b), idealized.

evident from the data. The variation in the strength of the cells must be attributed to some other effect. The relation between the value of σ and cell intensity can be investigated by observing the dependence of σ on the E criterion. The model predicts that for the same r, a decrease in σ will result in a stronger cell. This is indeed reflected in the data. A similar effect was evident in the data from the idealization of the line, but in that case it was thought to be a fortuitous by-product of the method used to determine the size of the downdraft areas. In the case of the cluster, on the other hand, the effect reflected in the results is more likely to be real because of the fundamental difference, cited earlier, between the two methods used for determining the downdraft areas. It is interesting to note further that σ shows almost no change between $E_{40,30}$ and $E_{40,40}$ criteria. This relationship suggests that the sudden increase in r (which, for the other E criteria had remained fairly constant while σ changed) caused the cells to be stronger. However, because of the small sample size, this must be regarded as speculation.

The inner cylinders for the cluster were smaller than those for the line, but did fall within the range of values of updraft radii observed by Simpson and Wiggert (1969, 1971). The values of σ for the cells in the cluster were within the range of values found for the cells in the line.

5.1.2.2 Idealization of the Environment

To determine a representative sounding with which to initialize the model, 27 soundings from the B-scale ships were plotted as described in section 3.4.2. The soundings, taken every three hours, spanned the

Table 5.1. Results of idealization of cluster.

Existence Criterion	Area Criterion	Combination Criterion	Number of Cells	Average Area of Updraft (km^2)	Radius of Average Updraft, r (km)	Average Area of Downdraft (km^2)	Radius of Average Downdraft, R (km)	$\sigma = \frac{r}{R}$
$E_{1,1}$	A_1	C_{max}	25	1.64	.72	19.00	2.56	.28
		C_{avg}	"	1.40	.67	19.42	2.57	.26
	A_2	C_{max}	"	2.00	.80	19.74	2.63	.30
		C_{avg}	"	1.68	.73	19.16	2.58	.28
$E_{30,1}$	A_1	C_{max}	16	1.56	.71	24.63	2.89	.24
		C_{avg}	"	1.34	.65	25.03	2.90	.23
	A_2	C_{max}	"	2.06	.81	25.75	2.98	.27
		C_{avg}	"	1.72	.74	24.59	2.89	.26
$E_{30,30}$	A_1	C_{max}	10	1.50	.69	32.40	3.29	.21
		C_{avg}	"	1.30	.64	33.75	3.34	.19
	A_2	C_{max}	"	2.10	.82	34.40	3.41	.24
		C_{avg}	"	1.75	.75	33.30	3.40	.22
$E_{40,30}$	A_1	C_{max}	5	1.40	.67	37.40	3.51	.19
		C_{avg}	"	1.20	.62	41.60	3.69	.17
	A_2	C_{max}	"	2.00	.80	43.60	3.81	.21
		C_{avg}	"	1.60	.71	41.20	3.69	.19
$E_{40,40}$	A_1	C_{max}	3	1.67	.73	45.00	3.85	.19
		C_{avg}	"	1.33	.65	52.00	4.12	.16
	A_2	C_{max}	"	2.67	.92	55.33	4.30	.21
		C_{avg}	"	2.00	.80	51.33	4.12	.19

period from 0600Z to 1800Z on 1 September. The first few hours of the period were from sector 8 of the previous wave, but the bulk of the data were from sector 1 of the approaching wave. Because the soundings were not distributed over a number of wave sectors, no attempt was made to categorize them by sector. Instead, they were categorized by time to allow investigation of temporal variability and construction of the best possible idealized sounding for the time when the cluster occurred.

Relative Humidity

All 27 relative humidity soundings were moist at low levels with a strong decrease in humidity in the middle and upper levels and could have been classified as Type III soundings. Within the Type III regime, however, the soundings had strikingly similar characteristics. Each was composed of six layers, alternately moist and dry, which covered approximately the lowest 10 km. Above the sixth layer, the relative humidity was higher than in the sixth layer and reasonably constant.

To develop idealized soundings, each layer was characterized by its height and relative humidity and averages of these quantities were calculated for each time and for all the data combined. The moist layer immediately above the surface was defined by its surface relative humidity, the location and value of its maximum relative humidity, and the height and relative humidity at its top. The next five layers were defined by the location and value of the minimum (for the dry layers) or maximum (for the moist layers) relative humidity. The region above the sixth layer was defined by the height of its base and its mean relative humidity.

The results of this process are shown in Table 5.2. Figure 5.3,

Table 5.2. Mean values of characteristic features of the idealized relative humidity profiles.

Time (Z)	Sample Size	Surface Relative Humidity	Layer 1 Max R.H.		Layer 1 Top		Layer 2 Min R.H.		Layer 3 Max R.H.		Layer 4 Min R.H.		Layer 5 Max R.H.		Layer 6 Min R.H.		Top Layer	
			Hgt. (km)	R.H. (%)	Hgt. (km)	R.H. (%)	Hgt. (km)	R.H. (%)	Hgt. (km)	R.H. (%)	Hgt. (km)	R.H. (%)	Hgt. (km)	R.H. (%)	Hgt. (km)	R.H. (%)	Hgt. of Base	Mean R.H.
06	5	86	.5	96	1.5	92	3.5	54	5.0	80	7.0	25	8.0	57	9.5	14	11.0	29
09	6	82	.5	94	1.5	89	3.5	57	4.5	76	7.0	27	8.0	46	9.5	19	10.5	32
12	6	78	.5	94	1.5	90	3.5	61	5.0	76	7.0	32	8.0	44	9.0	21	10.5	39
15	5	79	.5	90	1.5	84	3.5	59	4.5	74	7.0	29	7.5	43	9.0	21	10.0	44
18	5	76	.5	91	1.0	79	2.5	60	4.5	82	7.5	30	8.5	58	10.0	32	10.5	55
06-18	27	80	.5	93	1.5	87	3.5	58	4.5	78	7.0	29	8.0	49	9.5	21	10.5	39

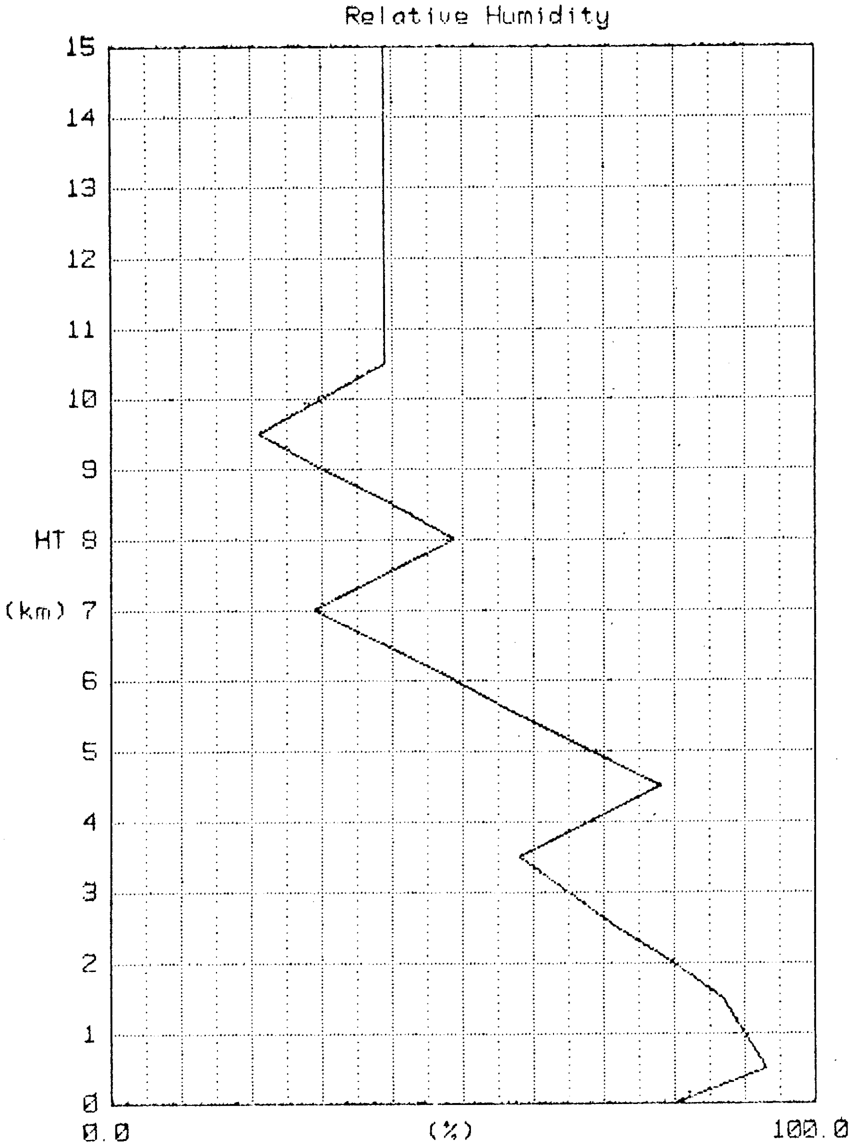

Figure 5.3. Relative humidity profile idealized from all the data for the cluster.

a plot of the idealized profile for all the data, shows the general shape of the profiles. Table 5.2 shows that the mean heights of the features were consistent from time to time, seldom varying by more than a half kilometer and never varying by more than one kilometer. The minimum relative humidity in each dry layer was less than that in the dry layer below it, and the same was true for the maximum relative humidities in the moist layers. As the day proceeded, the vertical variations in humidity became less sharp -- the dry layer minima increased and the moist layer maxima decreased. The top layer showed a significant increase in relative humidity throughout the 12-hour period.

Temperature

The temperature profiles associated with the cluster were similar to each other and displayed the same characteristics as those associated with the line: a stronger lapse rate aloft than near the surface and a point between 6 and 9 km where the change in the lapse rate occurred. Therefore, idealization of temperature profiles for the cluster was accomplished in the same manner as for the line (see section 4.1.2.2) except that the data were categorized by time instead of by wave sector and relative humidity type. The results, shown in Table 5.3, indicate that there was little variation in the temperature profile during the course of the day.

5.2 Experiments

Two groups of experiments were conducted in an attempt to simulate

Table 5.3. Mean values of characteristic features of temperature profiles for the cluster.

Time (Z)	Sample size	Height of change in lapse rate (km)	Low level lapse rate (°C/km)	Overall (0-15 km) temp decrease (°C)
06	5	6.5	5.56	99.40
09	6	6.5	5.66	98.83
12	6	6.0	5.56	98.75
15	5	7.0	5.75	98.20
18	5	7.0	5.78	99.00
06-18	27	6.5	5.66	98.84

the cells in the cluster. The general approach to these experiments was the same as the approach used in the experiments for the line, and most of the experiments in this chapter correspond to similar experiments in Chapter 4. The first group of experiments (X16-X19) employed values of the input variables suggested by the idealization. In the second group (X20-X23) an attempt was made to humidify a dry layer by initiating successive cells in the same atmosphere. Each experiment in this group was initialized using the final temperature and relative humidity profiles from the previous experiment. Table 5.5 summarizes the values of the important input variables in the experiments. Some important characteristics of the resulting cells are given in Table 5.6.

5.2.1 Experiments 16-19, Simulation of Cells in the Cluster

Experiment 16 (X16)

The temperature and relative humidity soundings with which X16 was initialized were the idealized profiles for 1500Z, the only time at which soundings were taken during the life of the cluster. The temperature profile employed the surface air temperature from the 1500Z Gilliss observation. The sounding is plotted in Figure 5.4.

This experiment was an attempt to model the average cell in the cluster. Thus, the inner cylinder radius and σ were determined from the $E_{1,1}$ criterion which used data from all cells having reflectivity cores in the lowest two CAPPI's. A relatively large radius was chosen by using the A_2 C_{max} criteria which yielded a radius of 0.8 km and a σ of 0.30 (see Table 5.1).

Figure 5.5 is a time-height diagram of the resulting radar reflec-

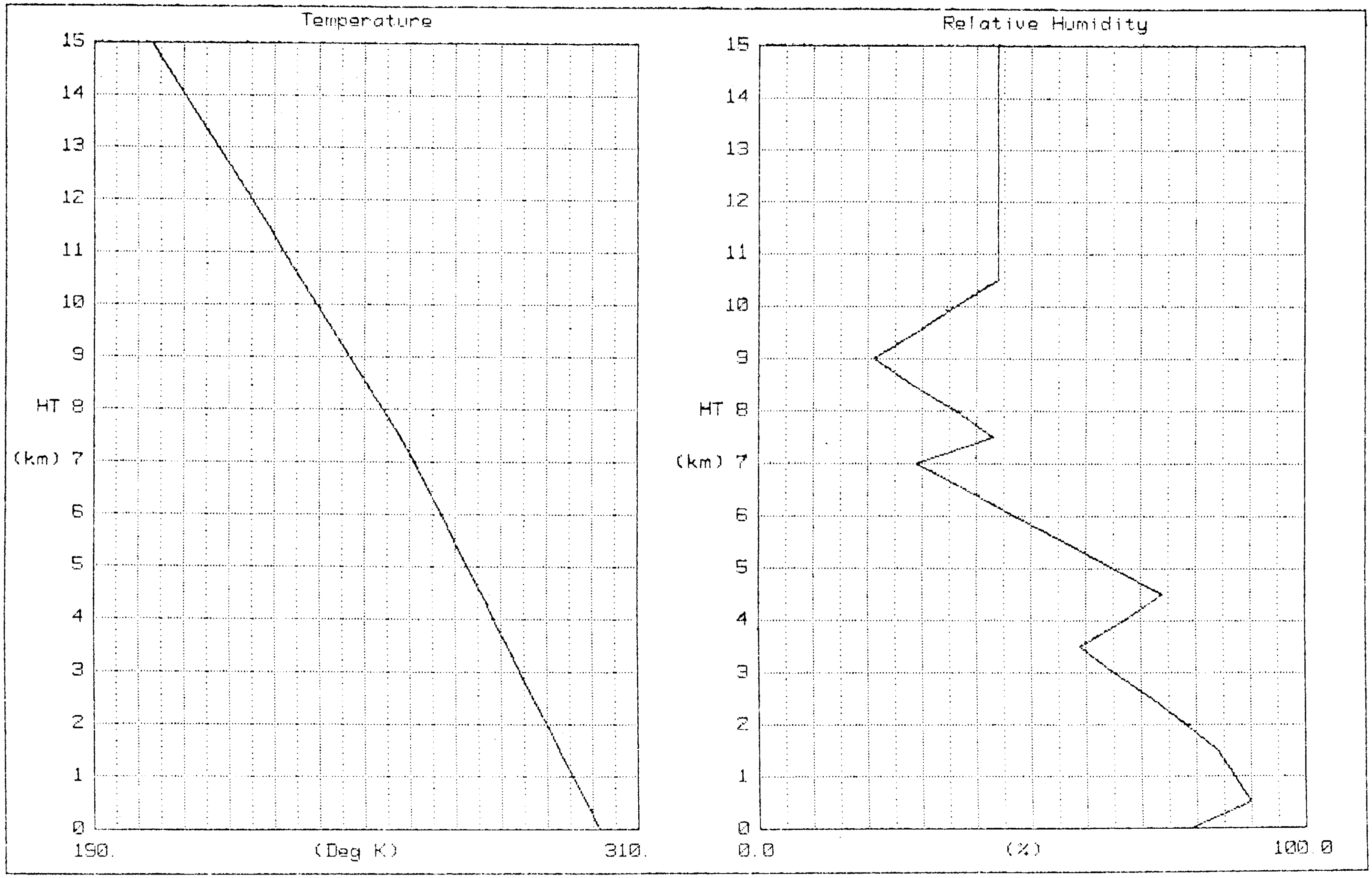

Figure 5.4. Sounding used in experiment 16.

tivity factor (in dBZ) for the inner cylinder of the model. The cell was not very strong and attained a height of only 3 km. However, it should not be written off as unrealistic as was the cell from the corresponding experiment (X1) for the line because the cells in the cluster appeared to be quite different, in some respects, from the cells in the line.

Experiment 17

In this experiment the initial relative humidity throughout the atmosphere was set to 100% under the assumption that the environment had been saturated by previous convective activity and mesoscale ascent (when the assumption was applied in Chapter 4, the most realistic cells were produced). All other input variables were the same as in X16.

The resulting cell, shown in Figure 5.6, grew to a height of 10 km and had a maximum reflectivity of nearly 45 dBZ.

Experiment 18

The mesoscale effects associated with the cluster were probably weak and short-lived compared with those associated with the line. Furthermore, the convective activity had not been occurring for nearly so long a time. It is possible that although these effects worked to humidify the cluster environment, they were too weak and short-lived to saturate it. This experiment investigated the type of cell which would grow in a humidified, but not saturated, environment. The relative humidity was assumed to be 90% throughout the depth of the model and all other input variables were the same as in X17.

Figure 5.7 shows the resulting cell. It is essentially a scaled-

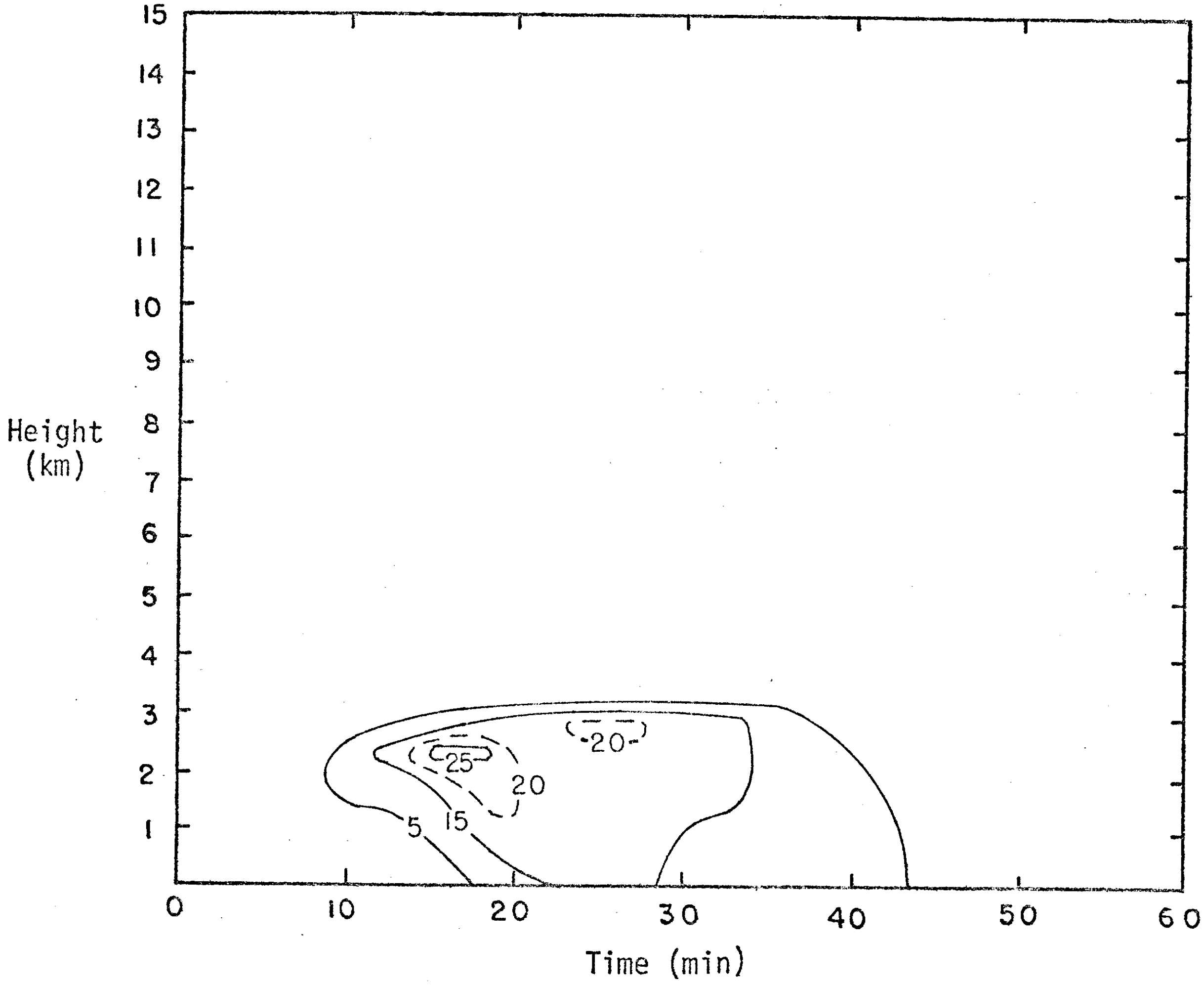

Figure 5.5. Time-height diagram of reflectivities for X16. Contours are in dBZ.

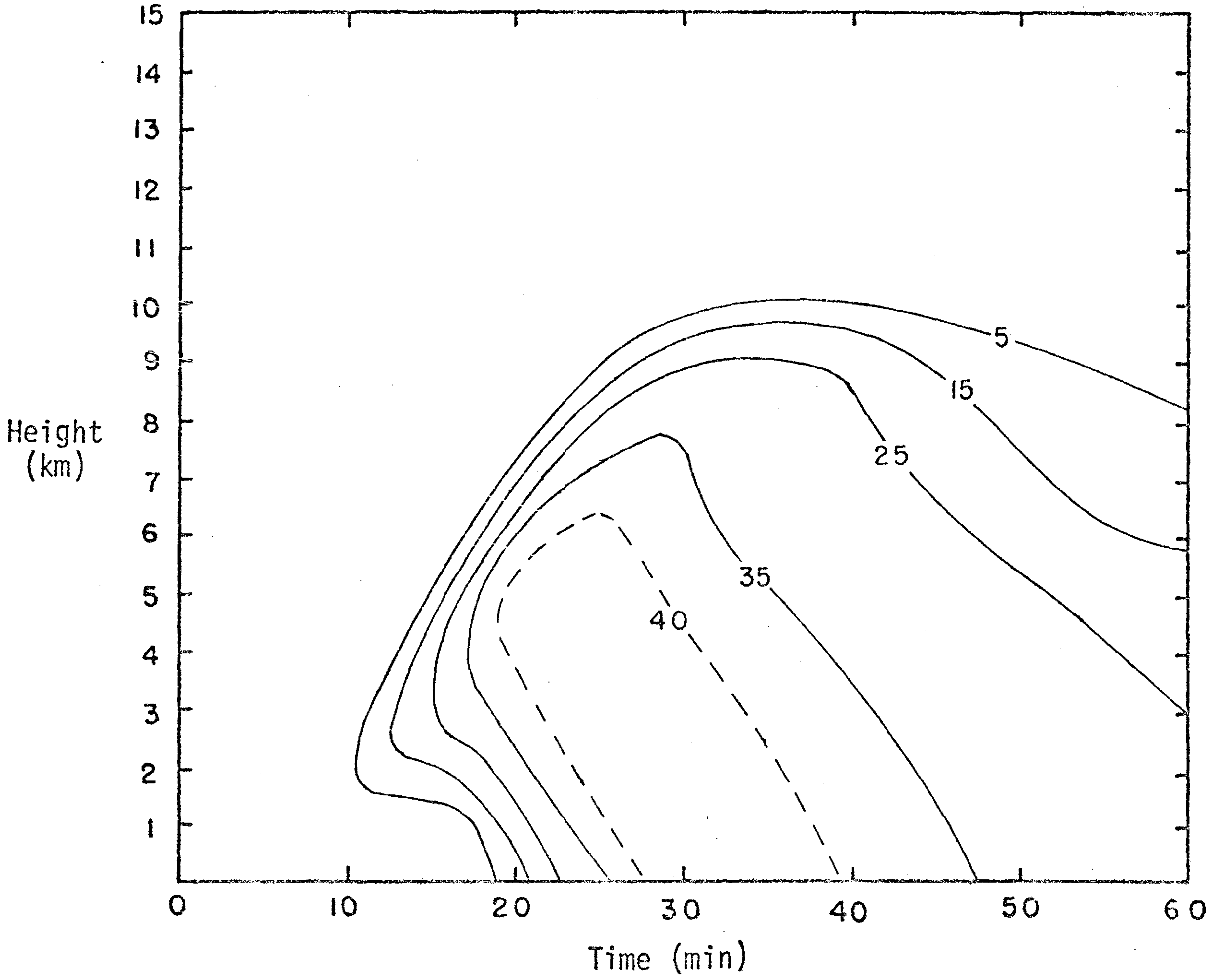

Figure 5. 6. Time-height diagram of reflectivities for X17. Contours are in dBZ.

down version of the cell from X17. It achieved a height of 6.5 km and a maximum reflectivity of 36.4 dBZ.

Experiment 19

Experiments 16-18 employed values of r and σ based on all the cells in the cluster. In this experiment, those variables were chosen from the $E_{40,40}$ A_2 C_{max} criteria ($r = 0.90$, $\sigma = 0.21$) to simulate the strongest cells. The relative humidity was assumed to be 90% throughout the atmosphere and the temperature profile was the same as that used in the previous experiments. Figure 5.8 is the time-height diagram of reflectivity for the resulting cell. The cell grew no taller than that from X17, but achieved a maximum reflectivity of nearly 40 dBZ.

5.2.2 Experiments 20-23, Humidification of Dry Layer by Convective Activity

In Chapter 4, a series of experiments was described that tested the hypothesis that successive cells initiated in the same environment would progressively humidify the environment and, in turn, would result in successively stronger cells. Although the hypothesis was not disproved, stability and time considerations made it questionable. The idealized relative humidity profile for the cluster was similar to that for the line in that both contained dry layers sufficiently close to the surface to prematurely disrupt the convective process. However, the profile for the cluster was dissimilar enough to warrant further evaluation of the hypothesis. The process used in this section was the same as that used in Chapter 4. Briefly, area-weighted averages of the final temperature and relative humidity profiles of both cylinders from X16 were used to initial-

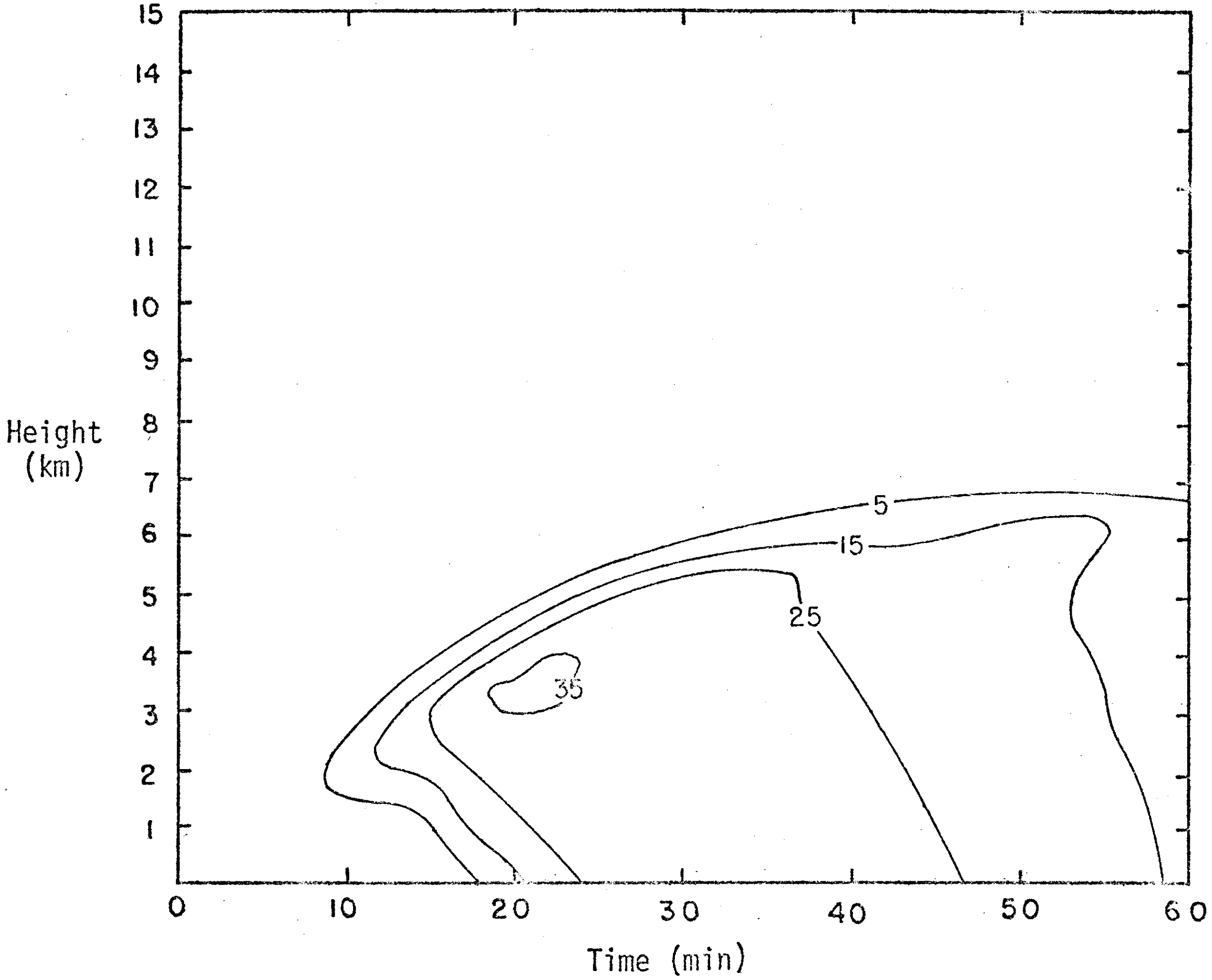

Figure 5.7. Time-height diagram of reflectivities for X18. Contours are in dBZ.

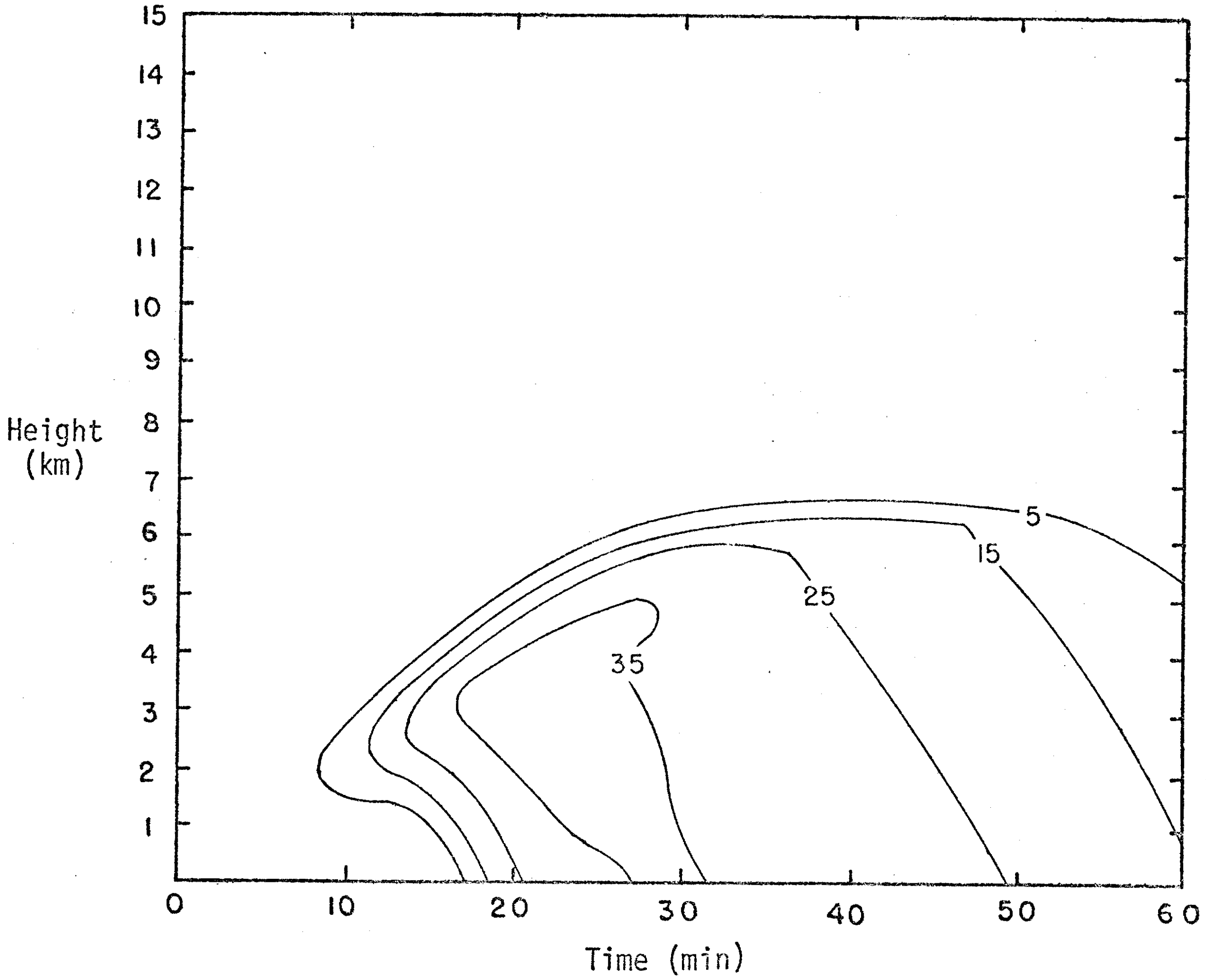

Figure 5.8. Time-height diagram of reflectivities for X 19. Contours are in dBZ.

ize X20, the averages from X20 were used to initialize X21, and so on.

Table 5.4 gives the moisture added in the impulse, the rainfall from both cylinders during the course of the integration, the maximum reflectivity, and the maximum height for experiments 16 and 20-23. It is obvious from a comparison of the moisture added and the total rainfall that the environment was being humidified. Figure 5.9 shows the successive relative humidity profiles.

Table 5.4. Results of X16 and X20-X23.

Experiment	Moisture (10^9 g)	Total Rainfall (10^8 g)	Maximum Reflectivity (dBZ)	Maximum Height (km)
X16	7.8	3.0	26.7	3.0
X20	9.7	4.4	29.3	3.5
X21	10.9	8.1	32.4	4.0
X22	11.7	12.7	33.3	4.5
X23	12.2	18.5	35.3	5.0

The process showed more promise for the cluster than it did for the line. In the line situation the dry layer was extremely sharp. The added moisture was insufficient to humidify it very rapidly with the result that the capped convection occurred continually within the same layer and began destroying its instability. The successive cells then became weaker, and it seemed unlikely that the process would lead to cells of the same strength and vertical extent as those actually observed in the line. In the idealized relative humidity profile for the cluster, the decrease in humidity in the dry layers was more gradual. The lowest dry

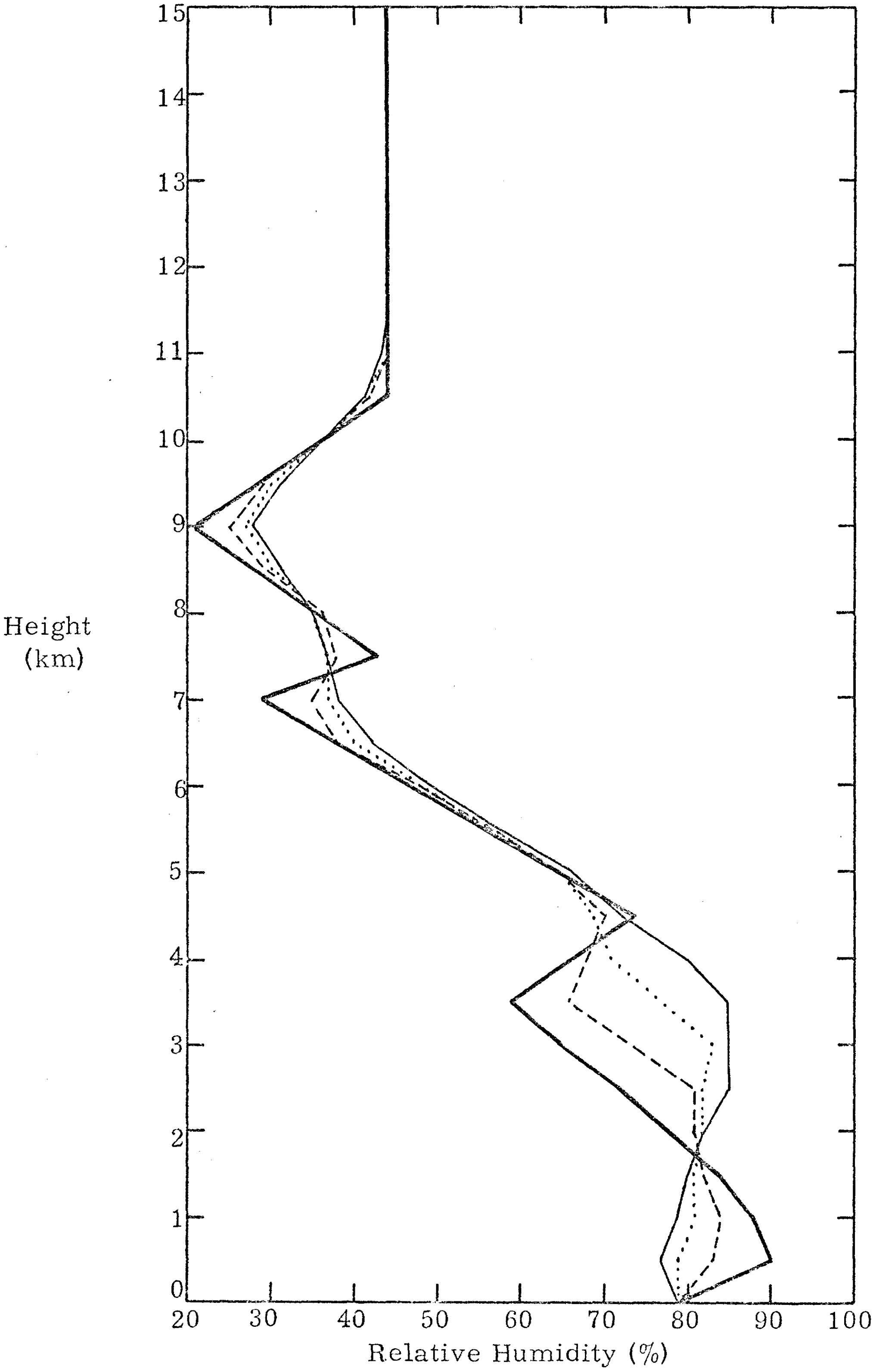

Figure 5.9(a). Successive relative humidity profiles. Before X16 ▬, after X16 - - -, after X20 ·····, after X21 —.

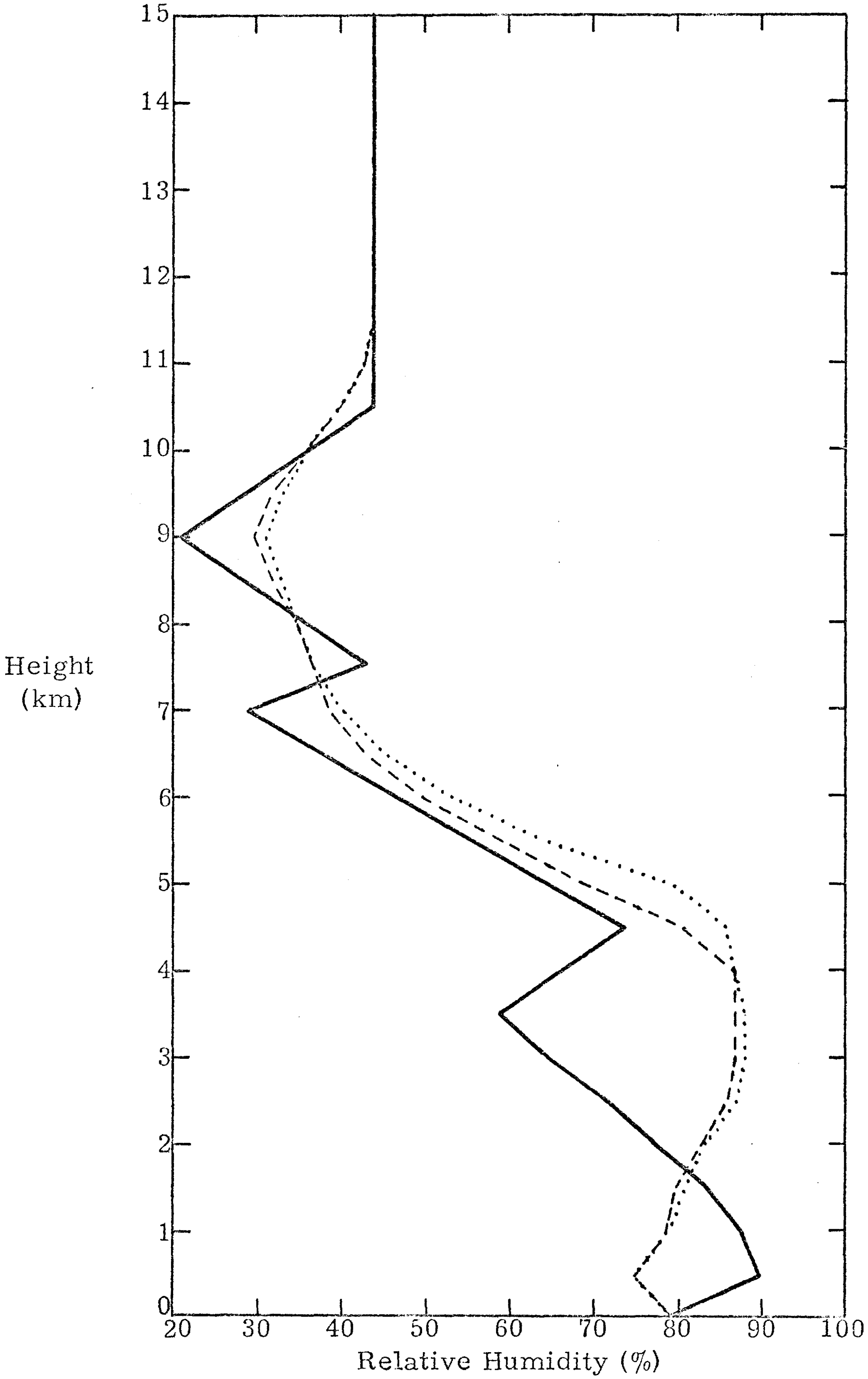

Figure 5.9(b). Successive relative humidity profiles. Before X16▬, after X22---, after X23····.

layer was quickly humidified by the first three cells and the last two cells raised the second dry layer a half kilometer. The cells were growing progressively stronger and taller. It is unlikely, however, that such progress would continue to be made because the process had produced a sharp dry layer similar to that encountered in the line situation (compare X10, Figure 4.11 (b) to X23, Figure 5.9 (b)). Thus, one might expect that the instability in the layer in which the convection was occurring would be weakened by the next few cells, and the process would suffer from the same problems which arose in the line situation. Why, then, did this process show more promise for the cluster than it showed for the line? There are two reasons. First, the relative humidity profile was such that the successive cells could grow steadily in height resulting in increasing instability from one cell to the next. This allowed successive cells to become more intense. Secondly, the cells observed in the cluster were, on the average, not nearly as tall or intense as the ones observed in the line. Thus, by the time the effects of the evolved sharp dry layer could be felt, the model cells had become fairly realistic.

One major drawback of the hypothesized process as a means for humidifying dry layers is that it proceeds too slowly, as seen in both the line and cluster situations. It is possible that a cell could be initiated before the previous cell had completely dissipated, allowing the process to run faster (the formulation of the model does not allow for the testing of this possibility). The stability problems, however, would remain.

Table 5.5. Important input variables for X16-X23.

Experiment #	Inner Radius (km)	σ	Relative Humidity Profile	Temperature Profile
X16	0.80	0.30	15Z (see Fig. 5.4)	15Z (see Fig. 5.4)
X17	0.80	0.30	100% throughout	"
X18	0.80	0.30	90% throughout	"
X19	0.90	0.21	"	"
X20	0.80	0.30	Result of X16 (see Fig. 5.9(a))	Result of X16
X21	0.80	0.30	Result of X20 (see Fig. 5.9(a))	Result of X20
X22	0.80	0.30	Result of X21 (see Fig. 5.9(a))	Result of X21
X23	0.80	0.30	Result of X22 (see Fig. 5.9(b))	Result of X22

Table 5.6. Characteristics of model cells from X16-X23. All results are for the inner cylinder.

Experiment #	Max Top (km)	Max Reflectivity dBZ	time (min)	height (km)	Max Rainfall Rate (mm hr^{-1})	time (min)	Cumulative Rainfall (cm)
X16	3.0	26.7	17	2.25	.4	25	.01
X17	10.0	44.9	24	4.25	41.0	32	.99
X18	6.5	36.4	20	3.25	6.9	29	.17
X19	6.5	39.4	20	3.25	11.7	29	.30
X20	3.5	29.3	18	2.75	.9	26	.02
X21	4.0	32.4	19	3.25	1.8	27	.03
X22	4.5	33.3	21	3.75	2.5	28	.04
X23	5.0	35.3	20	3.75	3.1	28	.06

5.2.3 Comparison of Model Output to Observed Data

The general approach to this comparison will be that described in section 3.3.4.2. However, an approach geared more toward individual cells than the broad statistical approach used in Chapter 4 will be applied to the cluster because the cells observed in the cluster were less numerous and easier to identify in all the CAPPI layers. Furthermore, these cells showed considerably greater variability than those in the line, thus making a more individualized approach to their comparison more meaningful.

Maximum Tops

The maximum tops of the cells in the cluster were not nearly as consistent as they were for the line, and there was little evidence of a precipitation canopy. Early in the life of the cluster, when the cells were weak, they generally reached 2-3 km. Later, when the cells had reached their maximum strength, they extended to 6-7 km. Initially, the observed tops were consistent with the results of X16. This suggests that the dry layers evident in the large-scale environment existed in the immediate vicinity of the cluster as it began to grow; i.e., there was probably no significant modification of the humidity profile prior to the onset of cell growth. The tops associated with the strongest observed cells were consistent with the results of X18 and X19, which suggests that the cell environment within the cluster had been humidified to some extent. The 10 km top produced in X17 was well in excess of observed tops, which suggests that the assumed 100% relative humidity was too high or was extended too high in the atmosphere.

Maximum Reflectivity

The spectrum of observed maximum reflectivity of cells in the cluster is plotted in Figure 5.10 in the solid line. This spectrum includes the 25 cells used in the idealization process of the $E_{1,1}$ existence criterion. The dashed line in the same figure is the time spectrum of maximum reflectivities from the cell produced in X18 for the 45 minutes during which its maximum reflectivity was within the range of values given on the graph. The numbers in the time spectrum were multiplied by a constant to make its sample size the same as that of the observed data. In the discussion in Chapter 4 it was noted that if it is assumed that the cells were observed at random times in their lives, the differences between these two types of spectra can be attributed to variations in the characteristics of the observed cells or to the inability of the model to simulate the "representative" cell. The reflectivity of the model cell did not exceed 35 dBZ, whereas over one-third of the observed cells had reflectivities greater than that value. This discrepancy is probably due to the large variation in the characteristics of the observed cells which, in turn, may reflect variations in their environments. One model cell simply could not be expected to embody the characteristics of such a wide variety of observed cells. To make the comparison somewhat more realistic, the observed cells having reflectivities greater than 35 dBZ were removed from the sample. The time spectrum, multiplied by a different constant to make its sample size agree with the new observed sample size, is shown in the dotted line. It agrees much better with the observed data than the first time spectrum. This result, rather than indicating a limitation of the model, points to a

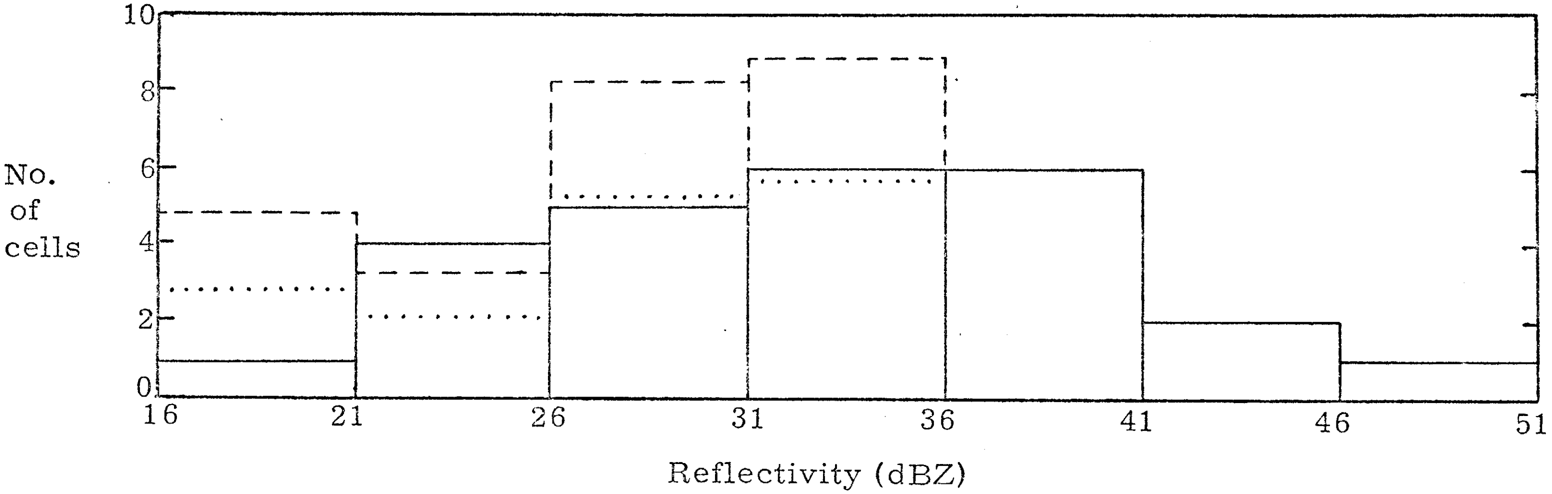

Figure 5.10. Model and observed spectra of maximum reflectivity. See text for explanation.

weakness in the idealization process: it is not reasonable to expect a "representative" cell to be very representative of a number of cells with highly variable characteristics.

A more subjective, individualized approach to comparing the maximum reflectivities of the observed and model cells suggests that the model cells were not unrealistic. The maximum reflectivity of the cell produced in X16 is similar to maximum reflectivities of cells observed early in the life of the cluster. The cells generated in X18 and X19 resembled cells observed later in maximum reflectivity in the same way that they resembled those cells in maximum height. This strengthens the suggestion made in the previous section that the cell environment within the cluster was humidified during the life of the cluster. Experiment 17 produced a maximum reflectivity of about 45 dBZ, representative of the strongest cells in the cluster. Its maximum top of 10 km was much higher than observed maximum tops; however, this feature could probably be controlled without significantly affecting the maximum reflectivity by decreasing the relative humidity above 7 km.

Height of Maximum Reflectivity

The simplicity of the radar data for the cluster allowed each cell to be identified in each CAPPI layer. Therefore, it was not necessary to resort to the statistical method described in section 3.3.4.2 to determine the distribution of heights of the reflectivity maxima. That distribution for the cell from X18 was found explicitly by first determining during what part of its life its maximum reflectivity exceeded 18 dBZ, the lowest maximum reflectivity of any cell in the cluster. Then the distribution of of the height of the model maximum reflectivity during this portion of the cell life was found. The observed and model distributions are shown in Table 5.7. No cell was observed to have its maximum reflectivity above 2 km, but the model cell had its maximum as high as 3-4 km. This could be attributed in part to the many observed cells which were not very tall and thus would tend to shift the distribution of maximum reflectivity heights toward lower values. However, there were enough strong cells that some higher values should have been observed if they had existed. Therefore, there seems to be a discrepancy between the model and observed cells in this respect.

Table 5.7. Distribution of radar-observed vs. model (X18) heights of maximum reflectivity. For radar: % of cells in which reflectivity maximum was located at the given height. For model: % of time during which the reflectivity maximum exceeded 18 dBZ that the maximum was located at the given height.

	Height (km)			
	0-1	1-2	2-3	3-4
Radar ($E_{1,1}$)	75	28	0	0
Model (X18)	62	7	17	14

5.3 Summary

The cells in a cluster which occurred on 1 September in the GATE B-scale array have been modeled using input variables determined by idealizing the cluster and its environment. The moisture in the open atmosphere around the cluster was found to be insufficient to support in the model the vigorous convection associated with the strongest cells observed in the cluster. However, the open-atmosphere moisture profile did produce model cells similar to those in the cluster at the beginning of its life when the convection was not as vigorous. The model produced cells which compared favorably with the more vigorous observed cells when the environment of the cluster was assumed to have been humidified to 90% relative humidity. An attempt was made to humidify the dry portions of the atmosphere near the ground by initiating successive cells in the same environment and allowing each to add moisture to it. Although this process was more successful for the cluster than it was for the line, time and stability considerations made it seem unlikely that the process could, working by itself, humidify a sufficient depth of the atmosphere rapidly enough to allow the model to produce cells having the strength and height of the more vigorous observed cells. It was recognized that the large variability of the cell characteristics in the cluster made the "representative" cell determined by the idealization process actually representative of only a small percentage of the cells in that cluster.

CHAPTER SIX

ASSESSMENT OF RESULTS

The model has been tested against cells observed in two situations. In the first, the cells occurred in a line which was well-developed and long-lived. This convective line occurred during a synoptically active period when an easterly wave was approaching the GATE B-scale array. The second situation, on the other hand, was relatively undisturbed; a synoptic-scale ridge was in the vicinity of the array. In this situation, the cells occurred in a cluster which was short-lived and poorly developed.

In order to initialize the model, it was necessary to specify the horizontal dimensions of the cell being modeled and the temperature and relative humidity profiles of the atmosphere in which it was occurring. Because of the variations observed in cell characteristics and the fact that the observed cells were geometrically more complex than the model formulation, it was necessary to idealize the numerous cells in the features to determine the dimensions of a "representative" cell. The idealization process was somewhat arbitrary, but produced updraft dimensions comparable with observed values and downdraft (i.e. outer cylinder) dimensions which seemed reasonable based on theoretical reasoning and intuitive judgment.

There were no soundings available from within the mesoscale features containing the cells. Soundings from the open atmosphere around those features had major characteristics in common, but were not identical. They were idealized to retain the major characteristics while smoothing out the minor variations. The relative humidity soundings fell into three idealized types, the distribution of which varied with the situation. On the other hand, there was only one type of temperature sounding, and the variations in its characteristics were insignificantly small and not systematic. The idealization process was important to the determination of a representative relative humidity profile because it retained the important characteristics which probably would have been lost or significantly altered in a mean relative humidity sounding. However, because of the lack of variation in the temperature profiles, a mean temperature sounding would probably have served as well as the idealized soundings used in the experiments.

In the case of the line, the model cells initialized with the relative humidity profile, idealized from open-atmosphere soundings around the line, were unrealistically weak. However, the model generated cells which were quite similar to the observed cells when some moisture was added to the atmosphere. The addition of moisture was justified on the assumption that the cells were growing in a mesoscale region which was more moist than the open atmosphere. The results of further experiments suggested that the additional humidity required for realistic model cells could not be added solely by the action of previous convective cells. Apparently, some mesoscale convergence and ascent was also needed.

In the case of the cluster, the model cell based on the open-atmosphere relative humidity did not compare favorably with the representative cell, but was similar to the cells which occurred early in the life of the cluster. As in the case of the line, it was necessary to add moisture to produce cells similar to the representative cell in the cluster. Although further calculations showed that previous convective activity could contribute significantly to the humidification of the atmosphere, this contribution was rather small and would require an unrealistically long time to humidify the environment to the point where representative cells could be produced. Once again, this result suggested that some mesoscale ascent was necessary.

The techniques for deducing representative cell dimensions from radar data appear to be satisfactory. However, in this study the process was accomplished by hand and was extremely tedious. If these techniques are to be applied in the future, their automation is clearly desirable.

The use of one cell to represent a group of cells with varying characteristics has an important drawback; as the variation in cell characteristics increases, the percentage of cells for which the "representative" cell is actually representative decreases. Since the cells in the line were similar, the model cells compared favorably with the observed cells. The greater variation of the cells in the cluster resulted in a less favorable comparison. The indication is that when cells have substantially different characteristics, they should be divided into sub-groups prior to idealization.

The results of this study suggest that the simple two-cylinder model, when appropriately initialized, can simulate many of the characteristics of observed cells remarkably well.

It appears that although horizontal cell dimensions are not unimportant, the effect of their variation within reasonable ranges is limited to minor changes in cell height and changes of several decibels in reflectivity. The variable exerting the greatest influence on the development of model cells was the relative humidity profile. Furthermore, the results pointed up the inadequacy of using relative humidity profiles determined from soundings taken in the open atmosphere. The use of such soundings is based on the unrealistic assumption that the cells are isolated in the larger-scale environment. Apparently, the effects of mesoscale processes must be taken into account.

One way to include the effects of mesoscale processes is to take soundings in the immediate vicinity of the cells, preferably in the weak precipitation surrounding the updrafts. This would be the best way to use the model in its present form, but it is highly impractical.

A second method would be to utilize assumptions which take into account the effects of mesoscale processes on the humidity profile (this method was applied in this study when the open-atmosphere relative humidity soundings were altered). The assumptions could be based on intuitive judgment, crude calculations of mesoscale effects, or trial-and-error. In any case, these approaches essentially force the atmosphere to simulate the model, whereas the opposite relationship is desired. Furthermore, it is questionable whether anything important could be learned about the effects of the cell on its environment if that environment has to be altered to produce the cell.

The best approach to including the effects of mesoscale processes in the model would be to include the cell model as an integral part of a mesoscale model. This, of course, is a problem of much larger scope; but, such a model would provide, in addition to more realistic simulation of cumulus cells, insights into cumulus-mesoscale interactions.

A further refinement, which should be incorporated into the larger-scale model discussed in the previous paragraph and could be incorporated into the present model, would be the addition of a realistic modeling of boundary-layer effects. There is reason to believe that much of the air that is drawn into the base of an updraft converges from the boundary layer surrounding the cell (see, e.g. Zipser, 1978). However, in the present model formulation, the air that enters the updraft near its base is entrained from the outer cylinder. It is unlikely that this air, which has subsided in the outer cylinder, bears much resemblance to boundary-layer air.

The addition of a boundary layer to the model should incorporate the formulation of a less artificial initiating impulse. The height of the impulse as well as its temperature and humidity should be geared to boundary layer structure and conditions. The experiments in which the final relative humidity from one cell was used to initialize a subsequent cell illustrated the possible contribution to the humidification of the atmosphere by the humidity impulse. In experiments of this nature, in which the long-term (relative to the cumulus time scale) effects of convection on the environment are investigated, it is imperative that the most realistic humidity perturbation attainable be employed. Further research is needed to determine realistic forms and magnitudes of the velocity perturbation, but these perturbations should be based on observed vertical velocity fluctuations in the boundary layer, reinforced, perhaps, by ascent from mesoscale convergence.

References

Acheson, D., 1976: Documentation for GATE B-scale rawinsondes. GATE Processed and Validated Data, 21 pp. *

Arakawa, A., and W.H. Schubert, 1974: Interaction of a cumulus cloud ensemble with the large-scale environment, Part 1. J. Atmos. Sci., 31, 674-701.

Asai, T., and A. Kasahara, 1967: A theoretical study of the compensating downward motions associated with cumulus clouds. J. Atmos. Sci., 24, 487-496.

Austin, P.M., 1976: Documentation for Gilliss radar raw digital data. GATE Processed and Validated Data, 50 pp. *

Austin, P.M., and R.A. Houze, Jr., 1973: A technique for computing vertical transports by precipitating cumuli. J. Atmos. Sci., 30, 1100-1111.

Braham, R.R. Jr., 1952: The water and energy budgets of the thunderstorm and their relationship to thunderstorm development. J. Meteor., 9, 227-242.

Brazier-Smith, P.R., S.G. Jennings, and J. Latham, 1973: Raindrop interactions and rainfall rates within clouds. Q.J.R.M.S., 99, 260-272.

Charney, J.G., and A. Eliassen, 1964: On the growth of the hurricane depression. J. Atmos. Sci., 21, 68-75.

Gray, W.M., 1973: Cumulus convection and larger-scale circulations: I. Broadscale and mesoscale considerations. Mon. Wea. Rev., 101, 839-855.

Hudlow, M.D., 1975: Collection and handling of GATE shipboard radar data. Proc. 16th Radar Meteor. Conf., AMS, Boston, Mass. 186-193.

Kessler, E., 1969: On the distribution and continuity of water substance in atmospheric circulation. Meteor. Monogr., 10, No. 32, 84 pp.

Kuettner, J.P., D.E. Parker, D.R. Rodenhuis, H. Hoeber, H. Kraus, and G. Philander, 1974: GATE: final international scientific plans. Bull. Amer. Met. Soc., 55, 711-744.

Marks, F.D., and W.A. Raub, Jr., 1978: Principal mesoscale precipitation features associated with passage of easterly waves during GATE. Proc. 18th Radar Meteor. Conf., AMS, Boston, Mass. 28-53.

Ogura, Y., and N.A. Phillips, 1962: A scale analysis of deep and shallow convection in the atmosphere. J. Atmos. Sci., 19, 173-179.

Orville, H.D. and K.J. Sloan, 1970: A numerical simulation of the life history of a rainstorm. J. Atmos. Sci., 27, 1148-1159.

Reed, R.J., D.C. Norquist, and E.E. Recker, 1977: The structure and properties of African wave disturbances as observed during Phase III of GATE. Mon. Wea. Rev., 105, 317-333.

Sax, R.I., 1969: The importance of natural glaciation on the modification of tropical maritime cumuli by silver iodide seeding. J. Appl. Meteor., 8, 92-104.

Simpson, J., and V. Wiggert, 1969: Models of precipitating cumulus tower. Mon. Wea. Rev., 97, 471-489.

__________, ____________, 1971: Florida cumulus seeding experiment: Numerical model and results. Mon. Wea. Rev., 99, 87-118.

Soong, S.-T. and Y. Ogura, 1976: A determination of the trade-wind cumuli population using BOMEX data and an axisymmetric cloud model. J. Atmos. Sci., 33, 992-1007.

Weinstein, A.I., 1970: A numerical model of cumulus dynamics and microphysics. J. Atmos. Sci., 27, 246-255.

Yau, M.K., 1977: Microphysical-dynamical processes and interactions in a precipitating cumulus cell model. Sc.D. Thesis, Department of Meteorology, Massachusetts Institute of Technology, Cambridge, Mass. 256 pp.

Zipser, E.J., 1978: Mesoscale and convective-scale downdrafts as distinct components of squall-line structure. Mon. Wea. Rev., 105, 1568-1589.

---

* Available from World Data Center-A, National Climatic Center, Asheville, North Carolina.